PhD-FSTM-2021-067

The Faculty of Science, Technology and Medicine

DISSERTATION

Presented on 20/09/2021 in Luxembourg

to obtain the degree of

DOCTEUR DE L'UNIVERSITE DU LUXEMBOURG
EN INFORMATIQUE

by

Oltjon Kodheli
Born on 14 September 1991 in Fier, Albania

Communication Algorithms for 5G Internet of Things Systems via Satellites

Dissertation defense committee

Dr. Symeon Chatzinotas, Dissertation Supervisor
Professor and Co-Head of SIGCOM, SnT, University of Luxembourg
Dr. Björn Ottersten, Chairman
Professor and Director of SnT, University of Luxembourg
Dr. Stefano Andrenacci, Vice-Chairman
Systems Development Engineer, SES S.A., Luxembourg
Dr. Alessandro Vanelli-Coralli
Professor, University of Bologna, Italy
Dr. Stefano Cioni
Telecommunication Systems Engineer, European Space Agency, Netherlands

Communication Algorithms for 5G Internet of Things Systems via Satellites

Oltjon Kodheli

Abstract

The Internet of things (IoT) via satellites is an attractive system architecture that has been identified as a key enabling technology to extend the IoT services on a global scale. Terrestrial-only IoT infrastructures are unable to cover a large portion of the Earth (e.g oceans, deserts, forests, etc.), while in other regions they represent a cost-inefficient solution (i.e. rural or remote areas). Furthermore, the potential tremendous number of IoT devices communicating in a network leads to large capacity demands. To this end, the role of the satellites to extend and complement the terrestrial IoT networks is unique and irreplaceable. Among several IoT technologies, Narrowband Internet of Things (NB-IoT) has been recognized as the leading one in addressing the machine type communication (MTC) traffic of the 5th generation of mobile communication systems (5G). Global-scale NB-IoT services hold a huge potential in opening up new market verticals and use cases for the future. However, the novel impairments caused by the signal propagation over the satellite channel compromise several procedures of the existing NB-IoT protocol.

In the above context of having NB-IoT connectivity via satellite links, the work carried out in this thesis mainly focuses on designing new communication algorithms which are capable of counteracting the impairments induced by the satellite channel. More specifically, the main objective of this work is to propose techniques that require minimal adaptations in the current standard, in order to have a fully functional NB-IoT network, either terrestrial or satellite-based. This approach is advantageous compared to designing a completely new satellite-specific protocol for several reasons. First, it relaxes the need for totally new network infrastructures and IoT chipsets. NB-IoT is being designed to co-exist and operate over cellular networks (4 & 5G) and the infrastructure is already in place. Second, it offers a capacity increase and flexibility of operation. Similar to terrestrial-only networks, relying on the satellite as the only mean of communication may lead to scarce capacity. Besides, in certain IoT applications (e.g. asset tracking) the devices are in a continuous movement in

various environments, thus requiring both terrestrial and satellite connectivity. Last but not least, adapting an already existing protocol so as to be satellite-compatible clearly leads to faster network deployment and management.

The first part of the thesis is focused on developing a user scheduling strategy for the uplink data transmission which mitigates the level of the differential Doppler experienced in a Low-Earth Orbit (LEO) satellite down to a limit supported by the NB-IoT devices. The performance of the proposed strategy is validated through numerical simulations and a link budget analysis is done, allowing then to derive the space segment requirements from the power budget perspective in order to have reliable NB-IoT communications via LEO satellites. In addition, we bring the user scheduling strategy one step further and propose an efficient resource allocation strategy, which not only is capable of counteracting the differential Doppler problem, but also takes into account the distinct user channel conditions and various data demands. Extensive numerical results are performed to evaluate different performance trade-offs of our LEO satellite-based NB-IoT system.

The second part of the thesis is devoted to the random access (RA) procedure of the NB-IoT, which is mainly utilized for achieving uplink synchronization among users. The challenges imposed by the increased delay in the communication link into the RA procedure are analyzed and novel solutions to overcome them are proposed. We validate our techniques in an experimental setup, consisting of a user and a base station implemented in open air interface (OAI), and a satellite channel implemented in hardware that emulates the signal propagation delay. The laboratory test-bed built in this last part of the thesis, not only enables us to validate various solutions, but also plays a crucial role in identifying novel challenges not previously treated in the literature. This work increases the technology readiness level (TRL) of satellite-based NB-IoT systems, demonstrating over a laboratory environment a successful RA procedure even in extreme values of delays experienced in a geostationary (GEO) satellite.

Acknowledgments

First of all, I would like to express my sincere gratitude to my supervisor, Prof. Symeon Chatzinotas, for his excellent guidance and for all the opportunities I was given to further develop on a professional and personal level. His consistent support and encouragement had a crucial role in the accomplishment of this thesis. Also, I am highly indebted to Dr. Nicola Maturo for his valuable technical guidance and his immediate feedback on my work. I would like to extend my deepest gratitude to Dr. Stefano Andrenacci and Frank Zimmer from the Société Europeenne des Satellites (SES), for their insightful suggestions and for helping me to understand several practical concepts of satellite communication systems.

I am also highly grateful to my CET committee member, Prof. Alessandro Vanelli-Coralli, from the University of Bologna, for the fruitful discussions we had during our meetings. He has been a substantial support throughout my whole research career, and I owe him a special acknowledgement for inspiring my interest in satellite communication systems and for his profound belief in my abilities. I very much appreciate Dr. Stefano Cioni, from the European Space Agency (ESA), for kindly accepting to participate in my dissertation committee, and Prof. Björn Ottersten for kindly accepting to serve as the Chairman of the defense.

I also had great pleasure of working with Dr. Jorge Querol, Abdelrahman Astro, Mohammad Gholamian and Sumit Kumar, during the implementation of my research work in the Lab. The completion of my dissertation would not have been possible without their valuable support. A special thanks go to all my current and past colleagues at SnT for creating such an amazing work environment.

Most importantly, I owe all my accomplishments to the support, trust and love of my family and friends. I dedicate this thesis to them.

Oltjon Kodheli

Luxembourg, 12 August 2021

Contents

List of Figures

List of Tables

Abbreviations

3GPP	3rd Generation Partnership Project
4G	Fourth Generation of Mobile Communications
5G	Fifth Generation of Mobile Communications
BLER	Block Error Rate
BPSK	Binary Phase-Shift Keying
BS	Base Station
CP	Cyclic Prefix
EIRP	Effective Isotropic Radiated Power
FEC	Forward Error Correcting
GEO	Geostationary Orbit
GNSS	Global Navigation Satellite System
GW	Gateway
GS-F	Group Scheduling in Frequency
GS-T	Group Scheduling in Time
HARQ	Hybrid Automatic Repetition Quest
ICI	Inter-carrier Interference
IoT	Internet of Things
ISL	Inter-Satellite Link
KPI	Key Performance Indicator
LEO	Low Earth Orbit
LPWAN	Low Power and Wide Area Network
LTE	Long Term Evolution
M2M	Machine-to-Machine
MAC	Medium Access Control Layer
MCS	Modulation and Coding Scheme

MIB	Master Information Block
MKP	Multiple Knapsack Problem
NB-IoT	Narrowband Internet of Things
NGSO	Non Geostationary Orbit
OAI	OpenAir Interface
OFDMA	Orthogonal Frequency Division Multiple Access
NPBCH	Narrowband Physical Broadcast Channel
NPDCCH	Narrowband Physical Downlink Control Channel
NPDSCH	Narrowband Physical Downlink Shared Channel
NPRACH	Narrowband Physical Random Access Channel
NPSS	Narrowband Primary Synchronization Signal
NPUSCH	Narrowband Physical Uplink Shared Channel
NR	New Radio
NSSS	Narrowband Secondary Synchronization Signal
NTN	Non-Terrestrial Network
PHY	Physical Layer
PRB	Physical Resource Block
QoS	Quality of Service
RA	Random Access
RAO	Random Access Opportunity
RAN	Radio Access Network
RAR	Random Access Response
RTT	Round Trip Time
RU	Resource Unit
SC-FDMA	Single Carrier Frequency Division Multiple Access
SCS	Subcarrier Spacing
SNR	Signal to Noise Ratio
TA	Timing Advance
TBS	Transmission Block Size
ToA	Time of Arrival
UE	User Equipment

Chapter 1

Introduction

By 2025, it is estimated by recent market studies that the number of connected devices in the world would reach 75.44 billion [1]. This tremendous growth is due to the inclusion of machines in the telecommunication domain, causing a paradigm shift from human-to-human (H2H) interaction to machine-to-machine (M2M) communications. Such machines include daily tech devices (e.g. smartphones, wearables, etc.), sensors or actuators in a smart home/office or smart city, as well as industrial devices (i.e. smart machines). The interconnection of these devices ("things") in a network allowing them to exchange data through the internet, creates the so-called Internet of Things (IoT) concept [2]. Through its large pool of applications and market vertical, including transportation, health care, smart grids, smart lighting, smart parking systems, etc., the IoT has the potential to revolutionize the way we live and work towards a more intelligent society [3,4]. To address such important applications and market verticals, the Narrowband-IoT (NB-IoT) protocol was designed as part of the terrestrial cellular networks, including the 4th and 5th generation (4 & 5G) of mobile communication systems [5,6]. NB-IoT, together with the LoRa [7] and Sigfox [8], are the leading technologies nowadays with the aim of providing low-power & wide-area network (LPWAN) connectivity.

1.1 Motivation

In order to express the motivation of the work carried out in this thesis, I would like to address the following three question: a) Why NB-IoT?; b) Why NB-IoT via satellites?; and c) Why new communication algorithms?

1.1.1 NB-IoT versus other technologies

As mentioned earlier, NB-IoT, LoRa and Sigfox have already been identified as the most promising technologies in the LPWAN category [9]. However, in this thesis, we keep our attention and deeply analyse the NB-IoT protocol due to the several advantages it brings compared to the other competitors. Let us elaborate on this idea in more detail considering a number of key requirements that a network should meet in order to satisfy the demands coming from typical IoT applications and services.

Easy network deployment and management in a large-scale

Since its conception, NB-IoT has been designed to be compatible with the 4G long term evolution (LTE) standard, which is developed by the 3rd Generation Partnership Project (3GPP) [10]. This means that the technical peculiarities in the Physical (PHY) and the Medium Access Control (MAC) layer would be the same as LTE, only with simplified procedures so as to meet the low-complexity and low-power requirement of the IoT devices [11]. Because of its potential, NB-IoT rapidly emerged as a class-leading LPWAN protocol and during the standardization of the 5G New Radio (NR) it was agreed to classify it as a 5G technology [12]. This was also enabled by the similarities among LTE and NR in the PHY and MAC layers. Compared to LTE, NR comes with more flexibility in the radio access network (RAN), allowing for various numerologies in the signal transmission [13]. Being part of the cellular network, either LTE or NR gives a huge advantage to NB-IoT because the network infrastructure is already in place, allowing for fast and large-scale network deployment. Furthermore, operating over a licensed spectrum makes the whole network easily manageable, especially from the interference point of view. On the contrary, LoRa and Sigfox are open protocols operating in an unlicensed spectrum. Although this brings a unique advantage in permitting almost anyone to build their own small-scale IoT network at a low cost, it makes the network difficult to manage once expanded on a large-scale [14].

High network capacity

The amount of traffic that a network is able to handle at any given time defines also its capacity. The NB-IoT intrinsically offers a higher capacity due to the orthogonal frequency division multiple access (OFDMA) scheme used in the MAC layer [15]. This allows several users to transmit simultaneously without inter-carrier interference (ICI) since the time-frequency re-

source allocation is orchestrated by the base station. Not only this but relying on the OFDMA signal for data transmission, which is recognized to have high spectral efficiency, enables data rates of up to 250 kb/s. Compared to the 50 kb/s in LoRa and 100 b/s in Sigfox [9], the NB-IoT peak data rate is significantly larger. To handle many users in the network, Sigfox utilizes the random frequency and time division multiple access (RFTDMA), while LoRa relies on the slotted ALOHA [16]. Because the uplink data transmission is initiated by the users and is based on a random selection of the time-frequency resources (among a range of allowed values), interference and packet collision may occur, limiting the capacity of these two technologies.

Extended coverage

To transmit over long distances, the Sigfox technology is based on an ultra narrowband (UNB) signal occupying a bandwidth of approximately 100 Hz. On the other hand, LoRa is based on Chirp Spread Spectrum (CSS) modulation [17]. Such PHY layer design enables LoRa and Sigfox to extend their coverage up to 15 km [18] and 50 km [19] respectively. In contrast, NB-IoT offers greater coverage of services, reaching values of up to 120 km [20]. This is done by introducing a repetition coding strategy to further extend the coverage, with the cost of losing in terms of data rate. The high achievable data rate of the OFDMA signal makes this strategy feasible.

1.1.2 The importance of NB-IoT via satellites

According to 3GPP specifications for 5G [21], the targeted connection density is 1,000,000 devices/km2 in urban areas. Taking into account the rapidly increasing trend in the number of IoT connections around the globe [1], the overall generated traffic by the IoT devices will undoubtedly have a significant impact on the cellular terrestrial network load. Besides, terrestrial-only networks fail to cover a large portion of the Earth (e.g oceans, deserts, forests, etc.), while in other regions (i.e. rural or remote areas) building a terrestrial infrastructure does not bring any economic advantage. In this context, satellite communication systems (SatComs) with their inherited feature of providing very wide coverage on Earth and short service deployment time, represent an irreplaceable solution to complement and extend the terrestrial networks [22]. The crucial role that the satellite can play for the future 5G NB-IoT systems in boosting the IoT services beyond the boundaries imposed by the current

terrestrial infrastructures, has been already recognized and discussed not only in the research domain [23–25], but also in the 3GPP standardization contributions [26,27]. More specifically, satellite-based NB-IoT systems can play a significant role in the following two uses cases, wide-area IoT and local-area IoT.

In the wide-area IoT type of services, the devices are scattered over a large geographical area (or moving around wide areas) and report/receive information to/from a central server. Typical applications in this category include transportation (e.g. fleet management, asset tracking, remote road alerts, map updates, traffic flow optimization), energy (e.g surveillance of oil/gas infrastructures) and agriculture (e.g. farming, livestock management). On the other hand, local-area IoT has to do with a group of sensors/actuators that collect local information and then report to a central server. Common applications in this category include smart buildings (e.g. smart offices, smart hospitals), or services to on-board moving platforms (e.g. containers on board a vessel, train or truck).

The above-mentioned services and applications are a clear indicator of the important role the satellite can play in many sectors, expanding the benefits brought by IoT also in geographical areas where it is not yet viable. Due to this, several start-ups have arisen in recent years intending to provide 5G NB-IoT connectivity on a global scale. OQ Technology [28] is one of them which has already launched their first satellite at low earth orbit (LEO) [29]. Furthermore, Sateliot [30] is another company that has recently signed a partnership agreement with GateHouse Telecom for delivering 5G IoT services from space [31, 32]. Last but not least, Mediatek [33] has successfully completed a field trial of 5G IoT connectivity utilizing the Inmarsat's Alphasat L-band satellite [34]. The above-mentioned examples are a shred of clear evidence that satellite-based technologies, able to be incorporated into the existing IoT terrestrial networks, are the way to go [35]. Notably, to provide global coverage of services, a constellation of LEO satellites and a network that can support multiple users at the same time is required. Nevertheless, such initial steps demonstrate that NB-IoT systems via satellites are not a futuristic concept anymore, but rather a reality.

1.1.3 The need for new communication algorithms

The current NB-IoT protocol specifications are being designed by taking into account the characteristic of terrestrial infrastructure. However, providing direct connectivity to the NB-IoT devices from a satellite link will impose novel impairments in the communication channel,

impacting the physical and link layer procedures of the protocol, and raising the need for new solutions. In fact, IoT communications via satellites have been a research topic of interest for many years now and new protocols that are satellite-specific have been proposed in the literature. More specifically, in [36] a new air interface suitable for IoT traffic over geostationary (GEO) satellites has been proposed while in [37] a survey of protocols based on random access transmission over the satellite link [38–41] has been provided. Furthermore, in [42] a new air interface for NB-IoT via LEO satellites based on Turbo-FSK modulation is investigated. The disadvantage of this line of research implementation-wise is that it requires building totally new infrastructures and IoT chipsets. Not only this but similar to terrestrial-only networks, relying on the satellite as the only mean of communication may lead to scarce capacity. In this context, having an integrated satellite-terrestrial protocol that can provide connectivity anytime and anywhere, regardless of the infrastructure utilized (either terrestrial or non-terrestrial), and regardless of the IoT user location, is certainly advantageous. To this aim, the main objective in this thesis is to propose novel communication algorithms that require minimal adaptations in the physical and link layer of the current NB-IoT standard, capable of counteracting the new impairments coming from the presence of the satellite channel. Other works exist in this direction, therefore we provide a detailed literature review in Section 2.3 where we highlight the gaps in the literature and the contributions of this work.

1.2 Thesis Outline

The thesis is organised as follows:

- Chapter 2 gives an overview of the NB-IoT protocol, mainly focused on the PHY and MAC layer characteristics. In addition, the main features of satellite communications are analysed, focusing on the ones that have an impact on the PHY and MAC layer procedures of the NB-IoT protocol. A literature review on the works related to satellite-based NB-IoT systems is provided and the contributions of this thesis in covering the literature gaps are highlighted.

- In Chapter 3 a user scheduling strategy for the uplink data transmission is proposed which mitigates the level of the differential Doppler experienced in a LEO satellite down to a limit supported by the NB-IoT devices. The performance of the proposed strategy is validated through numerical simulations and a link budget analysis is performed,

allowing then to derive the required Effective Isotropic Radiated Power (EIRP) and Antenna gain-to-noise-temperature (G/T) at the satellite for closing the link without touching the user terminal specifications.

- In Chapter 4 we bring the user scheduling strategy one step further and propose an efficient resource allocation strategy which not only is capable of counteracting the differential Doppler problem, but also takes into account the distinct user channel conditions and data demands. Extensive numerical results are performed to evaluate different performance trade-offs of our LEO satellite-based NB-IoT system.

- In Chapter 5 we deeply analyze the challenges imposed by the increased delay in the communication link into the RA procedure and propose novel solutions to overcome them. We validate our techniques in an experimental setup, consisting of a user and a base station implemented in open air interface (OAI), and a satellite channel implemented in hardware that emulates the signal propagation delay. Through the experimental implementation of our proposed solution, we achieve a successful RA procedure even in extreme values of delays experienced on a GEO satellite.

- Finally, in Chapter 6 the conclusions of the work performed in this thesis are highlighted, and the future research directions are discussed.

1.3 Publications included in the thesis

The work presented in this thesis has resulted in several peer-reviewed journal and conference papers, already published or accepted for publication , as well as in a book chapter. The publications that are fully or partially included in this thesis are listed here below. These publications are indicated in the text by J $\equiv$ Journal, C $\equiv$ Conference, and BC $\equiv$ Book Chapter.

Journals

- J1: O. Kodheli, S. Andrenacci, N. Maturo, S. Chatzinotas and F. Zimmer, "An Uplink UE Group-Based Scheduling Technique for 5G mMTC Systems Over LEO Satellite," *in IEEE Access*, vol. 7, pp. 67413-67427, 2019, *(published)*.

- J2: O. Kodheli, N. Maturo, S. Chatzinotas, S. Andrenacci, F. Zimmer, "NB-IoT via LEO satellite: An efficient resource allocation strategy for uplink data transmission, *in IEEE Internet of Things Journal*, 2021, *(accepted).*

- J3: O. Kodheli, A. Abdalla, J. Querol, M. Gholamian, S. Kumar, N. Maturo, S. Chatzinotas, "Random Access Procedure over NTN: From Theory to Practice, *in IEEE Access*, vol. 9, pp. 109130-109143, 2021, *(published).*

Conferences

- C1: O. Kodheli, S. Andrenacci, N. Maturo, S. Chatzinotas and F. Zimmer, "Resource Allocation Approach for Differential Doppler Reduction in NB-IoT over LEO Satellite," *2018 9th Advanced Satellite Multimedia Systems Conference and the 15th Signal Processing for Space Communications Workshop (ASMS/SPSC)*, 2018, pp. 1-8, *(published).*

- C2: O. Kodheli, N. Maturo, S. Andrenacci, S. Chatzinotas and F. Zimmer, "Link Budget Analysis for Satellite-Based Narrowband IoT Systems," *ADHOC-NOW 2019: Ad-Hoc, Mobile, and Wireless Networks*, pp. 257-271, *(published).*

- C3: O. Kodheli, N. Maturo, S. Chatzinotas, S. Andrenacci and F. Zimmer, "On the Random Access Procedure of NB-IoT Non-Terrestrial Networks," *2020 10th Advanced Satellite Multimedia Systems Conference and the 16th Signal Processing for Space Communications Workshop (ASMS/SPSC)*, *(published).*

Book Chapter

- BC1: O. Kodheli, S. Krishna and S. Chatzinotas, "Narrowband IoT Technologies for Smart City Applications," *in Communication technologies for networked smart cities*, IET 2021, *(published).*

1.4 Publications non included in the thesis

The following publications are not included in the thesis to keep it consistent. Nonetheless, they are still relevant to the work carried out during the PhD studies as they incorporate a broader overview of satellite communication systems.

- J1: O. Kodheli, E. Lagunas, N. Maturo et al., "Satellite Communications in the New Space Era: A Survey and Future Challenges," *in IEEE Communications Surveys & Tutorials*, vol. 23, no. 1, pp. 70-109, Firstquarter 2021, *(published)*.

- J2: MM. Azari, S. Solanki, S. Chatzinotas, O. Kodheli et al., "Evolution of Non-Terrestrial Networks From 5G to 6G: A Survey," *in IEEE Communications Surveys & Tutorials*, 2021, *(submitted)*.

Chapter 2

Background and Contributions

In this chapter, an overview of the NB-IoT protocol is given, mainly focused on the PHY and MAC layer characteristics. In addition, the main features of satellite communications that influence the PHY and MAC layer procedures of the NB-IoT are analysed. A literature review on the works related to satellite-based NB-IoT systems is provided, and the contributions of this thesis in covering the literature gaps are highlighted.

2.1 NB-IoT Protocol

Being a cellular technology, the NB-IoT protocol is very similar to the LTE and 5G standard from the PHY and MAC layer perspective, only with simplified procedures to meet the low-complexity and low-power requirement of the IoT devices. As a narrowband technology, the bandwidth assigned for data transmission is only 180 kHz, and depending on what frequency bands are used for operation, three deployment option exist: a) *stand-alone*; b) *in-band* and c) *guard-band*. In the stand-alone operation, a dedicated spectrum is assigned for the NB-IoT using any available bandwidth that is larger or equal to 180 KHz. Since the Global System for Mobile Communications (GSM) frequencies are not being used anymore due to the development of the new generations of mobile communication systems, they are foreseen to be one of the candidates for stand-alone operation [43]. In case both, GSM and NB-IoT are deployed by the same operator, a 100 kHz guard band is recommended for interference avoidance [44]. Regarding the in-band operation, the NB-IoT can utilize one physical resource block (PRB) of the 4G long term evolution (LTE) or 5G new radio (NR) carrier. The bandwidth occupied by one PRB in LTE is exactly 180 kHz, matching perfectly the NB-IoT

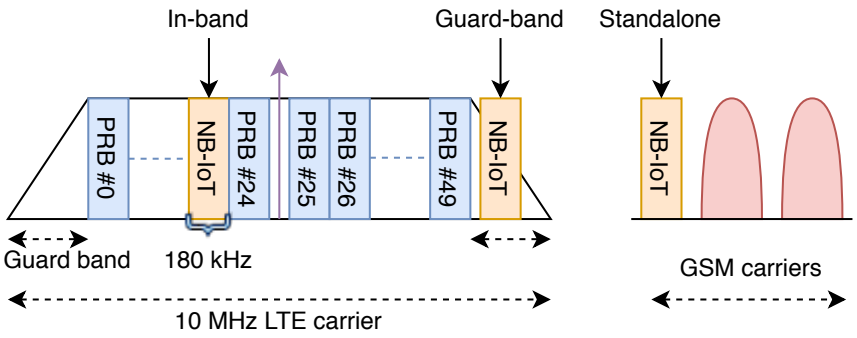

Figure 2.1: NB-IoT deployment options in LTE/GSM

required resources. Another option would be to place the NB-IoT carrier in the guard-band of the LTE/NR carrier. Figure 2.1 illustrates an example of the three deployment options of the NB-IoT.

2.1.1 Physical layer specifications

To analyse in more detail the PHY layer specifications, I would like to first introduce the modulation format and the radio frame structure of the NB-IoT, and then move on into describing the PHY signals and channels. The technical peculiarities that do not contribute towards enhancing the understanding of the subsequent chapters are skipped.

Modulation format and frame structure

Regarding the digital modulation scheme, in the downlink, orthogonal frequency division multiplexing (OFDM) is employed with a subcarrier spacing (SCS) of 15 kHz. In the frequency domain, one OFDM symbol contains 12 subcarriers occupying this way the whole NB-IoT bandwidth of 180 kHz. In the time domain, seven consecutive OFDM symbols form one slot of duration 0.5 ms. In such a way, the subframes and radio frames are created as in LTE. By summing up two slots the 1 ms subframes are obtained, which will then create the 10 ms radio frames. In the uplink, a single-carrier frequency division multiplexing (SC-FDMA) signal is used. In contrast with the OFDM signal, it has a lower peak to average power ratio (PAPR), allowing for more efficient use of the power at the user side. Please note that, according to the LTE terminology, the devices at the user side are also known as user equipments (UEs). To further enhance the coverage, new numerology with a 3.75 SCS was introduced, in addition to the existing one with 15 kHz SCS. Of course, this will result in

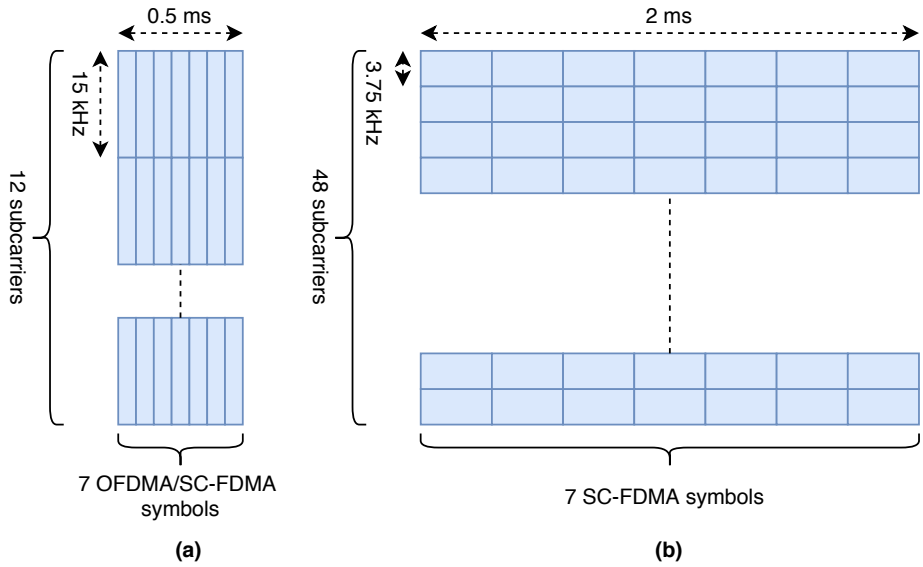

Figure 2.2: NB-IoT resource grid representation of 1 slot: (a) downlink & uplink with 15 kHz SCS; (b) uplink with 3.75 SCS

a longer slot and subframe duration as depicted in Figure 2.2. Both, OFDM and SC-FDM, are multi-carrier modulation techniques. Multiple access is achieved by assigning subsets of subcarriers to individual users, forming this way the orthogonal frequency division multiple access (OFDMA) in the downlink, and single-carrier frequency division multiple access (SC-FDMA) in the uplink. These multi-user access strategies require a strict synchronization in the time-frequency domain, which is assured by the MAC layer. It is well known that such a multi-user multi-carrier technique allows for high data rate transmissions. This justifies the 250 kbps peak data rate of the NB-IoT protocol.

Physical signals and channels

The "channel" terminology in NB-IoT (same as for LTE and NR) is used to identify the type of data that is carried over specific time-frequency resources. Hereafter we will provide a description of the channels and signal involved in three different stages of the NB-IoT operation: a) *synchronization phase*; b) *access phase* and c) *data phase*.

Synchronization phase: The NB-IoT employs a strategy where UEs periodically go into a sleeping mode to extend their battery life. When a UE has data to transmit after a period of inactivity, it needs to firstly synchronize in time and frequency with the serving base station (BS). For this purpose, it utilizes the narrowband physical primary synchronization

signal (NPSS) and narrowband secondary synchronization signal (NSSS). The synchronization phase of the NB-IoT is also the most demanding one from the computational and power perspective. In addition to obtaining the downlink time-frequency synchronization with the serving BS, through NPSS and NSSS the device can extract the cell identity number and frame/subframe number information. NPSS is a base sequence generated at subframe 5 of every radio frame based on a length-11 Zadoff-Chu (ZC) sequence with root index 5 [36211]. Through the cross-correlation properties of this sequence, which is also known at the user side, the UE is able to obtain the carrier frequency and synchronize in a subframe level. On the other hand, NSSS is utilized for obtaining the cell identity and a frame-level synchronization. NSSS is produced by an element-wise multiplication of a scrambled binary sequence with a ZC sequence [45], transmitted at subframe 9 at every even frame. After achieving the downlink synchronization with the BS, the next channel that the UE decodes is the narrowband physical broadcast channel (NPBCH) which carries the master information block (MIB). It is transmitted in subframe 0 of every frame and broadcasted to all the users inside the cell containing useful information for the UEs to operate within a cell, and proceed with the subsequent step, the access phase.

Access phase: Until the synchronization phase, the BS is not aware of the users contained inside its cell. For this purpose, to be introduced in the network and obtain a permanent identification (ID), the users have to initiate the access phase, known as the random access (RA) procedure, by utilizing the narrowband physical random access channel (NPRACH). In addition, the RA procedure is also utilized for obtaining the strict time-synchronization among various UEs sending data in the uplink, which is a crucial precondition in OFDMA/SC-FDMA systems to avoid inter-carrier interference (ICI). The time-frequency resource occupied by the NPRACH channel is also known as a random access opportunity (RAO). Since this is a procedure that involves a 4-message exchange between the BS and the UE and is controlled by the MAC layer, more details will be given later-on when we will describe the MAC layer specifications of the NB-IoT.

Data phase: Once the user has a successful access phase, it can transmit its uplink data using the narrowband physical uplink shared channel (NPUSCH), or receive the downlink data utilizing the narrowband physical downlink shared channel (NPDSCH). It is worth highlighting here that the time-frequency resources, together with other relevant parameters for

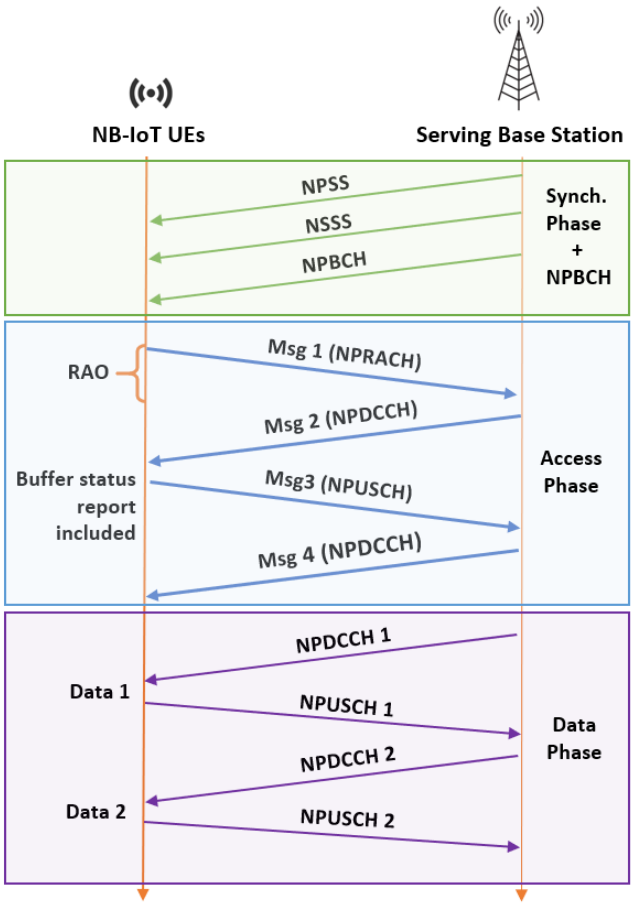

Figure 2.3: An example of UE-BS message exchanges and physical channels involved

demodulation/decoding of the useful data channels, are included in the narrowband physical downlink control channel (NPDCCH). Clearly, for every useful data that the UE has to receive from the BS, or for every uplink data it has to report to the BS, decoding the information contained in the NPDCCH is vital. Similar to the access phase, also the resource allocation for the data phase is controlled by the MAC layer, therefore we will provide further details in the MAC layer specifications section. Figure 2.3 illustrate an example of the message exchanges between the BS and the UE, and the corresponding channel involved.

2.1.2 MAC layer specifications

In the MAC layer, the most important procedures worth analyzing to help the material flow and assist in understanding the subsequent chapters are the RA procedure, the radio resource allocation, and the hybrid automatic repetition request (HARQ) operation.

Random Access procedure

As introduced earlier, the RA procedure is a very critical mechanism controlled by the MAC layer because it enables the NB-IoT UEs to initiate uplink data transmission, achieve uplink synchronization and obtain a permanent identification in the network [46, 47]. It is triggered in various situations during the UE operation within a network, such as initial access after the device is powered on, connection re-establishment in case the synchronization with the BS is lost, or handover when the device is moving from the coverage of one cell to another. There are two types of RA, contention-based and contention-free. While contention-based RA consists of a 4-step message exchange between the UEs and the BS, the contention-free mechanism uses only a 2-step message exchange, as we will treat hereafter.

Message 1: When there is a RAO, the UE will send a random access preamble to the serving BS by using the PRACH. This allows the BS to estimate the round trip time (RTT) for each UE, based on the time of arrival (ToA) of the received preamble. The BS will utilize the ToA estimate for determining a timing advance (TA) to be applied by each UE. By doing so, the uplink transmission from various UEs will be time-synchronized. What is worth emphasizing here is that at this step the UEs will compete for the same PRACH channel (same RAO), hence packet collision may occur. To reduce the probability of collision, there exist a list of possible preamble sequences defined in the standard and the UEs randomly select one. Notably, in case two UEs randomly select the same preamble sequence to initiate the RA procedure, a collision will occur, leading to a failure of the RA procedure. In such a case, the UEs will try again to send the preamble after a back-off time and a power-ramping procedure.

Message 2: The BS will continuously check for preamble reception at a RAO and in case it detects one, it will respond with a random access response (RAR) known as Message 2. The RAR contains the TA parameter that we mentioned earlier, as well as the scheduling information pointing to the radio resources that the UEs has to utilize for subsequent uplink data transmission. This is done to avoid collision with the signal coming from other users inside the same cell. Basically, all the message exchanges among the UE and the BS after this stage will be orchestrated by the BS, as we will analyse in the following section.

Message 3: Until this stage, the UE does not have a unique identity (ID) in the network. The RA preamble sequence number cannot act as an ID because the same one can be selected by multiple UEs. Therefore, the main goal of Message 3 transmission is to initiate a

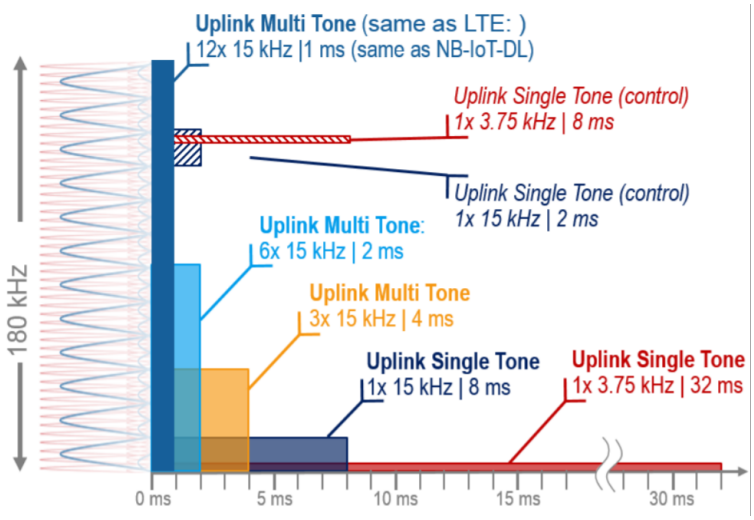

Figure 2.4: NB-IoT RU representations in time & frequency [48].

connection request where the UE is introduced in the network with a unique ID (known as C-RNTI). This phase is also known as the contention resolution phase. Please note that in case of a contention-free RA Message 3 and Message 4 transmission are skipped because in such situations the user is already uniquely identified (e.g. when synchronization is lost). Together with a randomly selected C-RNTI, the UE may also report its data volume status and power headroom to facilitate the scheduling and power allocation algorithms for subsequent transmissions.

Message 4: In this final step, the BS will send back to the UE the confirmation regarding the selected temporary C-RNTI, which will act as a permanent ID for the user for all future message exchanges. This concludes the RA procedure, thus enabling the UE to be connected in the network and synchronized in both, downlink and uplink transmissions.

Radio Resource Allocation

In the downlink, the smallest unit that can be assigned to a user is the physical resource block (PRB), corresponding to 12 subcarriers (12 x 15 kHz = 180 kHz) in the frequency domain and 2 slots in the time domain. Since the PRB occupies the whole NB-IoT available bandwidth, in the downlink the channels are time-multiplexed. On the other hand, in the uplink case, the smallest assignable unit is the resource unit (RU). There are various representations of the RU, occupying different time-frequency resources, as shown in Figure 2.4. In terms of frequency, the RU can occupy 1, 3, 6 or 12 subcarriers corresponding to a time duration of

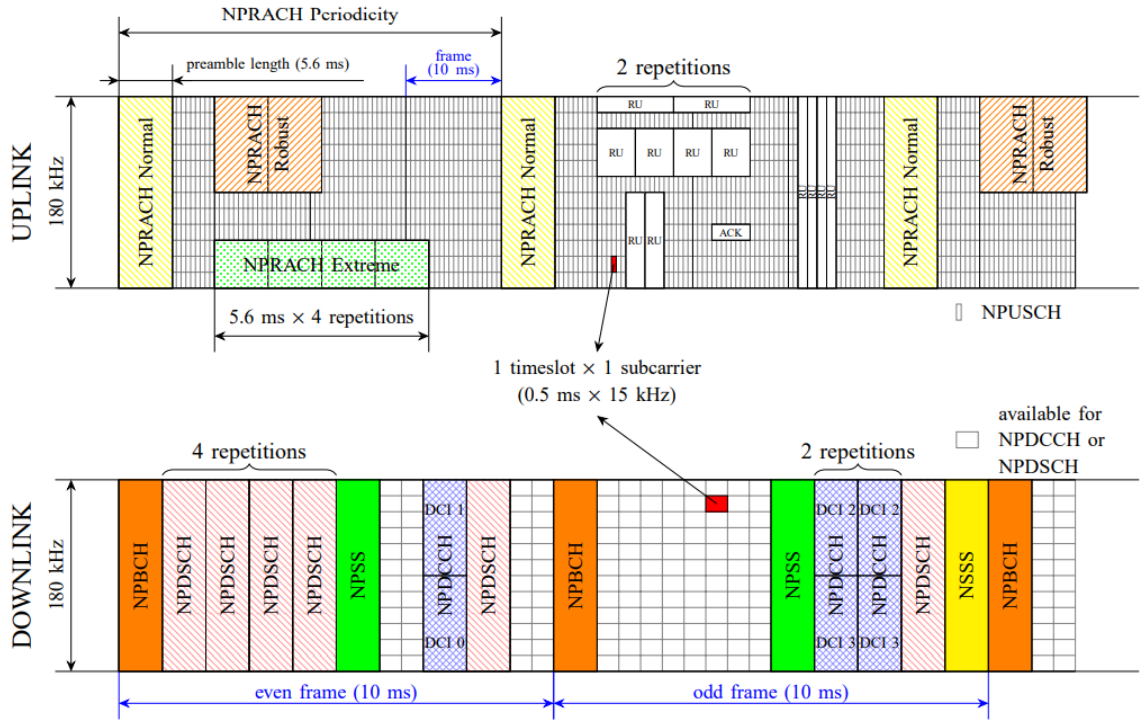

Figure 2.5: An example on how physical channels are placed inside the DL and UL frame [49].

8 ms, 4 ms, 2 ms and 1 ms respectively. When the RU utilizes only 1 subcarrier (15 kHz), it is known as a single-tone transmission, whereas the other configurations as multi-tone. In contrast to downlink, the various RU configurations allow also for frequency multiplexing of channels. Figure 2.5 illustrates an example of how distinct channels can be placed inside the radio frame. Notably, the radio resource allocation is the process that determines the time-frequency allocation of various channels inside the frame. Some of them are determined in the configuration phase, such as the NPRACH placement, while others can be adaptable over time based on the dynamicity of the system (e.g. the number of users, data demand, available resources, etc), such as the NPDSCH and NPUSCH. When the user has to transmit or receive data, there are 5 main parameters that has to be reported in the NPDCCH for the resource allocation, listed below.

1) Time resources for transmission: To assign the resources in time, the BS reports to the user a time-offset k, which represent the number of subframes the UE has to wait for after receiving the NPDCCH, and then decode the downlink data contained in NPDSCH, or transmit the uplink data by utilizing the NPUSCH.

2) Frequency resources for transmission: As it was highlighted earlier, in the down-

Table 2.1: Transport block size (TBS) table for NPUSCH [50].

MCS level	**Number of RUs**							
	1	2	3	4	5	6	8	10
0	16	32	56	88	120	152	208	256
1	24	56	88	144	176	208	256	344
2	32	72	144	176	208	256	328	424
3	40	104	176	208	256	328	440	568
4	56	120	208	256	328	408	552	680
5	72	144	224	328	424	504	680	872
6	88	176	256	392	504	600	808	1000
7	104	224	328	472	584	712	1000	1224
8	120	256	392	536	680	808	1096	1384
9	136	296	456	616	776	936	1256	1544
10	144	328	504	680	872	1000	1384	1736
11	176	376	584	776	1000	1192	1608	2024
12	208	440	680	1000	1128	1352	1800	2280
13	224	488	744	1032	1256	1544	2024	2536

link the channels are time-multiplexed because the whole NB-IoT carrier is occupied only by one channel. Therefore, there is no need for assigning resources in frequency. The same cannot be said for the uplink where various transmission modes exist with a distinct number of subcarriers. To avoid channel collision, the BS assigns to the users different subcarriers for transmitting their uplink data.

3) Modulation and coding scheme (MCS): Regarding the modulation, in NB-IoT there are only two possible options: binary phase-shift keying (BPSK) and quadrature phase-shift keying (QPSK). These simple modulation schemes contribute towards increasing the battery lifetime of the devices since the higher-order modulation are more power-hungry. To vary the coding rate, the NB-IoT employs a strategy where only the amount of useful bits to be encoded in the PRB/RU is reported to the users. This is also known as transport block size (TBS) and there exists a specific table for this in the NB-IoT standard [50] (please see Table 2.1 for the uplink case). Clearly, for the same number of RUs, increasing the TBS size will increase the coding rate since more useful bits will be placed inside the fixed-length RU. Higher TBS values are usually assigned to users in good channel conditions (closer to the serving BS) since their signal propagation path losses are smaller. This is why the users that are closer to the BS can achieve higher throughput, compared to the ones in worse channel conditions.

4) Number of PRB/RUs: The number of PRBs/RUs required for data transmission,

Table 2.2: Parameters reported to the user for NPUSCH data transmission [50].

Time		**Frequency**		**Number of RU**		**Number of Rep**	
I_{Delay}	k_0	I_{sc}	n_{sc}	I_{RU}	N_{RU}	I_{Rep}	N_{Rep}
0	8	0-11	I_{sc}	0	1	0	1
1	16	12-15	$3(I_{sc}\text{-}12) + \{0,1,2\}$	1	2	1	2
2	32	16-17	$6(I_{sc}\text{-}16) + \{0,1,2,3,4,5\}$	2	3	2	4
3	64	18	$\{0,1,2,3,4,5,7,8,9,10,11\}$	3	4	3	8
		19-63	Reserved	4	5	4	16
				5	6	5	34
				6	8	6	64
				7	10	7	128

either downlink or uplink has a direct dependency on the amount of data needed to be transmitted. For example, the more data a certain user has in its buffer, the more RUs are needed for its NPUSCH transmission. Naturally, an alternative option would be to use a higher MCS level, as previously explained, but this depends on the channel conditions. For a particular signal to noise (SNR) level, the only way to transmit more useful information is by increasing the number of PRBs/RUs.

5) Repetition number: The repetition number is a new feature that does not exist in LTE/NR standard. This is done to further extend the coverage of the NB-IoT devices. By utilizing this repetition coding, the users are able to have reliable communication with the BS and satisfy the quality of service (QoS)requirements even at low SNR values (users far away from the BS). Notably, this results in lower data rates because more time is required to send the same amount of useful data (similar to low code rates when more redundant bits are inserted). Table 2.2 provides a summary of all these parameters and their corresponding values taken from the standard. Only the uplink case is shown since it will be useful to understand the assumptions and reasoning in the other chapters of the thesis.

Hybrid Automatic Repetition Quest (HARQ) operation

HARQ is also controlled by the MAC layer and it is an essential procedure to improve the link reliability in NB-IoT. In plain terms, if the transmitted channel, either in downlink or uplink, is corrupted at such a level that the errors introduced by the communication channel were not able to be addressed by the forward error correcting (FEC) code, a non-acknowledgement (NACK) is sent back to indicate the user to re-transmit the same packet. This is not to be confused with the repetition number we discussed earlier. In case the channel is decoded

correctly, an acknowledgement (ACK) is received and the user can proceed with transmitting the next packet in the queue. In order to improve system efficiency and maintain the same data rate as without HARQ operation, multiple parallel HARQ processes are needed (so the next packet can be sent without waiting for the ACK of the previous one). However, increasing the number of parallel processes significantly raises the cost and the complexity of the users. As a consequence, a maximum of two HARQ processes is allowed for the NB-IoT to keep the complexity/cost of the devices under control.

2.2 Satellite communications characteristics

Understanding the main characteristics and impairment in a satellite channel is of paramount importance in designing satellite-based communication systems. In this section, we will only focus on the essential SatCom features that will straightforwardly impact the PHY and MAC layer procedures of the NB-IoT and compare them with a typical terrestrial-based scenario.

Doppler shift

Doppler shift is a classic impairment in non-geostationary (NGSO) satellite communications and is a physical phenomenon caused by the relative movement of the transmitter and the receiver. In particular, while in a terrestrial network the Doppler shift is caused by the movement of the UEs inside the cell, in a satellite communication system an added factor is the high-speed movement of the NGSO satellite. The Doppler shift effects can be sub-categorized in two parts: the common Doppler shift experienced by all the users inside a certain cell ,e.g., the one at the centre of the cell, and the residual or differential one, depending on the relative location of users with respect to the center of the cell. We will treat this in more detail in Chapter 3. A closed-form expression of the Doppler shift at a certain point P on Earth as a function of time is provided in [51]. The formula is as follows:

$$f_d(t) = -\frac{f}{c} \cdot \frac{w_F(t) r_E r \, sin[\psi(t) - \psi(t_0)] \eta(\theta_{max})}{\sqrt{r_E^2 + r^2 - 2 r_E r \, cos[\psi(t) - \psi(t_0)] \eta(\theta_{max})}} \tag{2.1}$$

where

$$\eta(\theta_{max}) = cos[cos^{-1}(\frac{r_E}{r} cos\theta_{max}) - \theta_{max}], \tag{2.2}$$

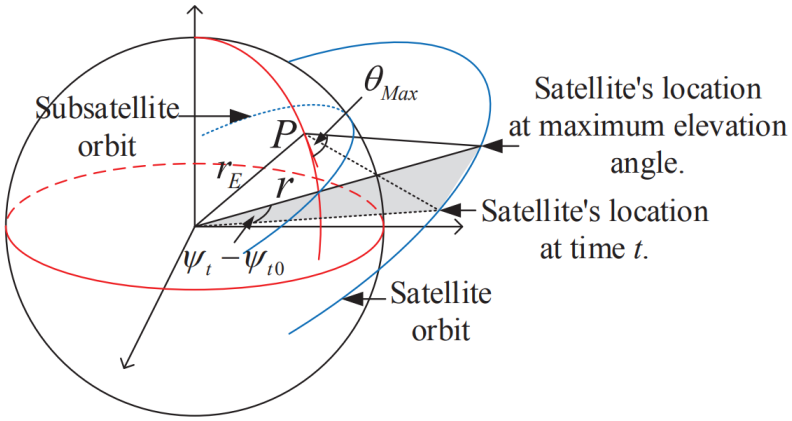

Figure 2.6: Geometric representation of the NGSO satellite.

f is the carrier frequency, r_E is the radius of Earth, r is the orbit radius of the satellite and $\psi(t) - \psi(t_0)$ is the angular difference between satellite location at time t and satellite location at maximum elevation angle θ_{max} (see Fig. 2.6). Furthermore, $w_F(t)$ is the angular velocity of the satellite in the ECF (Earth central fixed) frame which can be approximated as a constant by the following expression:

$$w_f \approx w_s + w_E \, cos(i) \tag{2.3}$$

where w_s is the angular velocity of the satellite in the ECI (Earth central inertial) frame, w_E is the angular velocity of the Earth and i is the satellite orbit inclination. For simplicity let us assume $w_E = 0$ and $t = 0$ the time when the satellite is at the maximum elevation angle. By taking these assumptions equation (2.1) will transform as follows:

$$f_d(t) = -\frac{f}{c} \cdot \frac{w_s r_E r \, sin(w_s t)\eta(\theta_{max})}{\sqrt{r_E^2 + r^2 - 2 r_E r \, cos(w_s t)\eta(\theta_{max})}} \tag{2.4}$$

In Figure 2.7, we plot the results of the Doppler shift with respect to the satellite visibility time t for a particular user. Please note that the negative time means that the satellite is approaching the NB-IoT user on Earth, reaching the maximum elevation angle at time $t = 0$. As it can be noted, the lower altitudes result in higher Doppler shifts due to the increased speed of the satellite movement. In the plotted results, We have considered only two of the main typical LEO orbits (600 & 1200 km) and a carrier frequency fc = 2GHz. Naturally, changing these parameters will affect the results. Nevertheless, what is worth emphasizing

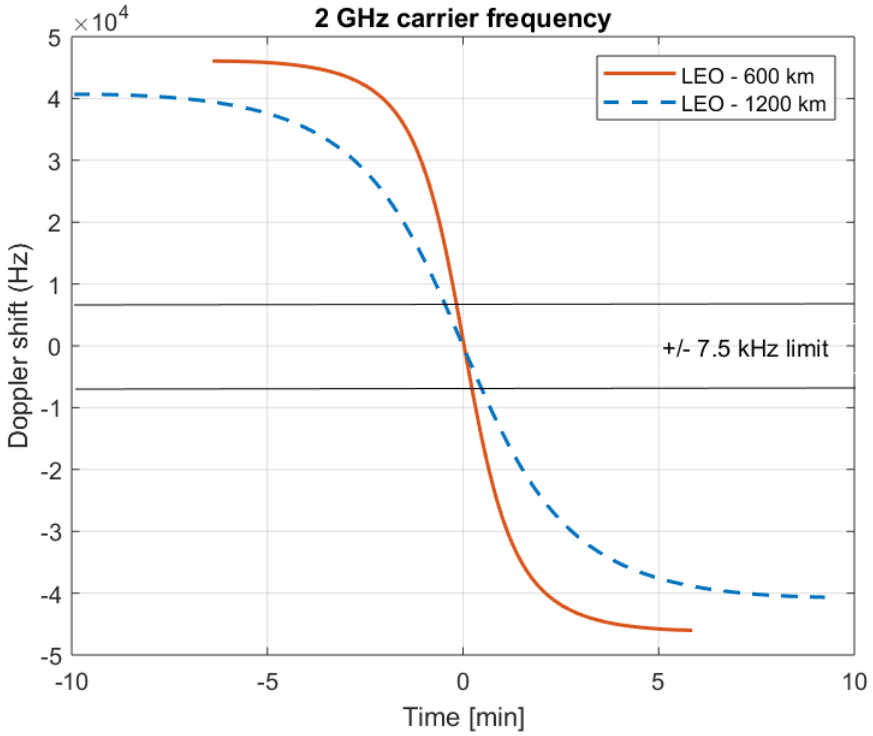

Figure 2.7: Doppler shift as a function of satellite visibility time.

here is that the Doppler shift that the terrestrial NB-IoT can estimate through its NPSS and NSSS signals, as discussed in Section 2.1.1, it is limited to half of the sub-carrier spacing, corresponding to +/- 7.5 kHz [5]. Notably, this can only be achieved for a very small portion of time during the satellite movement over the targeted cell and imposes one of the core challenges to be addressed for NB-IoT systems via NGSO satellites.

Differential Doppler shift

In a multiple access scenario, when many users inside the coverage area of the satellite will need to connect with the serving BS, the signals coming from various users will experience different channels. As a consequence, seeing the satellite at different elevation angles will cause also the Doppler shift to vary among users. As stressed out earlier, in OFDMA/SC-FDMA multiple access schemes it is essential to maintain strict orthogonality to avoid ICI. The differential Doppler shift will violate such condition and should be carefully treated. Obviously, we should first start the reasoning by considering the terrestrial case and derive what is the amount of the differential Doppler shift that the standard can tolerate. By assuming the highest mobility speed of users (500 km/h) allowed inside a cellular cell, it can

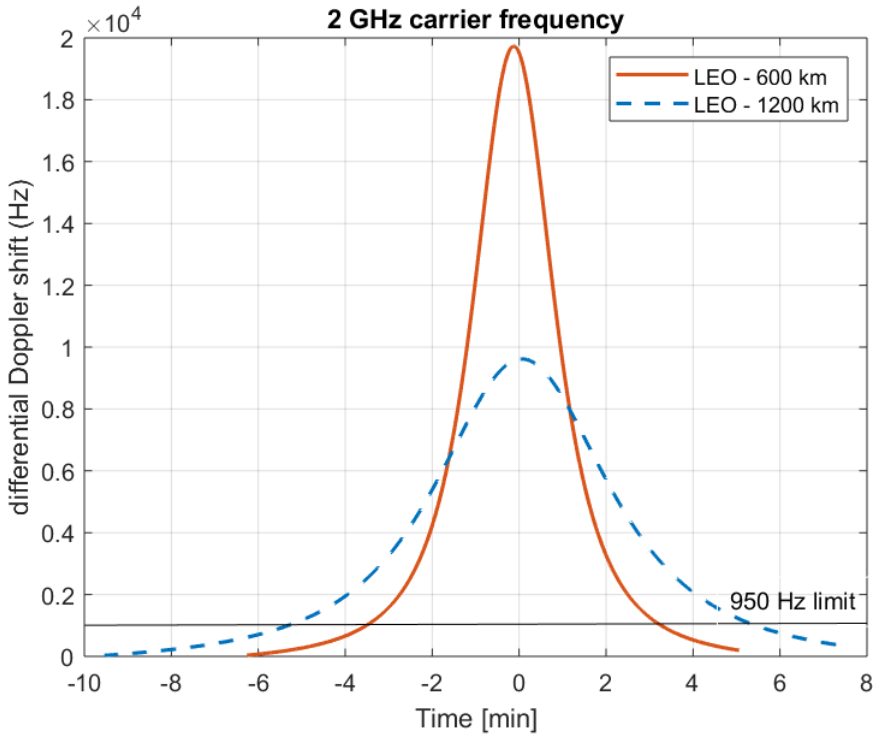

Figure 2.8: Differential Doppler shift as a function of satellite visibility time (120 km cell).

be calculated that the maximum experience differential Doppler shift can reach up to 950 Hz. coming back to our satellite-based scenario, we calculate the differential Doppler shift experienced between two users that are placed at a maximum distance inside the cell since they are the ones to experience the most distinct channels from the Doppler shift perspective. As stated in Section 1.1.1, the maximum cell radius supported by the terrestrial NB-IoT is 120 km, resulting in a maximum distance of 240 km among users. We calculate the Doppler shift for these two users by utilizing Equation (2.4) and plot the difference in Figure 2.8. As it can be observed, the differential Doppler shift overcomes the supported limit for a considerable amount during the satellite passage over the NB-IoT cell.

Round trip time (RTT)

The propagation time from the UE to the BS and vice versa is known as the round trip time (RTT) of the communication. While in a terrestrial scenario the RTT is very small (0.8 ms for 120 km cell), in a satellite-based NB-IoT system it becomes an influential factor to carefully consider. For a transparent satellite, it can be calculated by the following formula:

$$RTD(t) \approx 4 \cdot D(t)/c \tag{2.5}$$

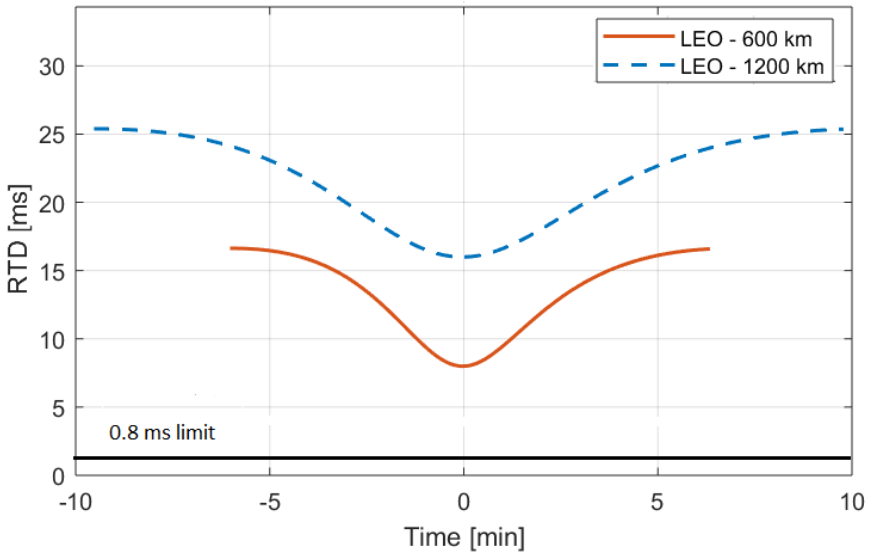

Figure 2.9: Round trip time as a function of satellite visibility time (120 km cell).

where $D(t)$ is the distance from the NB-IoT user to the satellite as a function of the satellite visibillity time t. This is also known as the slant range and is characterized by the following equation:

$$D(t) = \sqrt{R_E^2 \cdot sin(\alpha_u(t))^2 + h_s^2 + 2 \cdot R_E \cdot h_s} - R_E \cdot sin(\alpha_u(t)) \tag{2.6}$$

Please note that in Equation (2.5), an approximation of the distance from the BS to the satellite with the user slant range is done. Clearly, in the case of a regenerative payload with an on-board base station, the RTT will be halved. In fact, for a GEO satellite which has an orbit of 35,786 km, the $RTT_{regen} \approx 240$ ms and $RTD_{transp} \approx 480$ ms. In Figure 2.9, we have shown the simulation results of the RTT for a LEO satellite as a function of the satellite visibility time. This is a drastic increase (especially for the GEO satellite) compared to the terrestrial NB-IoT scenario and will particularly impact the access phase of the NB-IoT, as we will deeply analyse in Chapter 5.

Differential RTT

Similar to the differential Doppler problem, the differential RTT is caused by the distinct slant ranges among users inside a certain cell, thus causing a time-misalignment on their uplink signal. Naturally, this is something that occurs also in a terrestrial scenario where the signals from the users very close to the BS arrive faster compared to the ones that are placed at the edge of the cell. The NB-IoT protocol handles this in the RA procedure, as

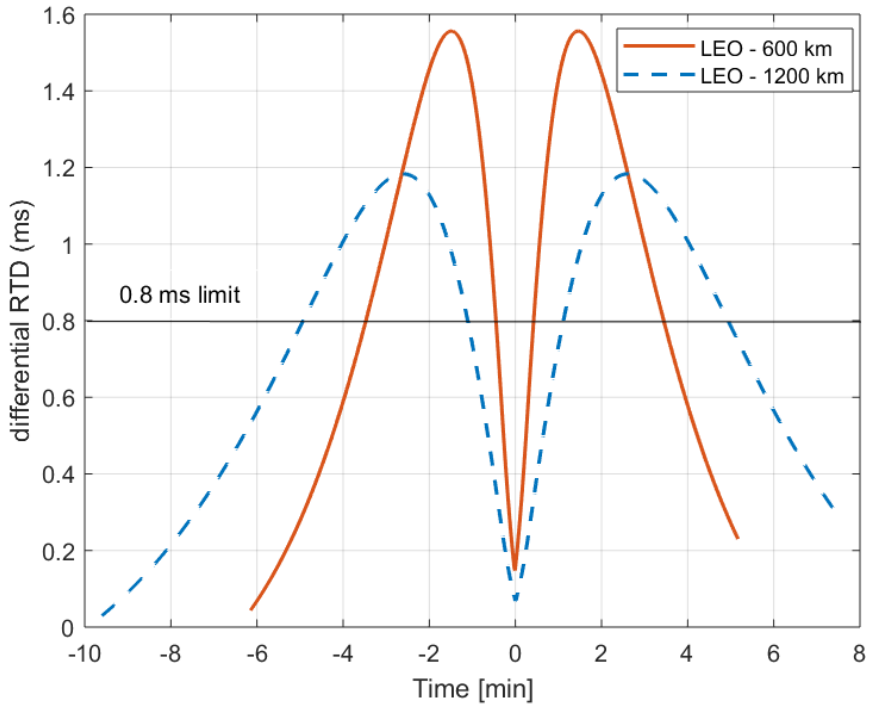

Figure 2.10: Differential round trip time as a function of satellite visibility time (120 km cell).

we described in Section 2.1.2, by informing the UEs with a TA to be applied to their uplink signal with the purpose of achieving strict synchronization. However, for the BS to estimate correctly the ToA of various signals, it is required that the initial time-misalignment should be smaller or equal to the cyclic prefix (CP) length. Please note that the CP in OFDM/SC-FDM signals is inserted to combat the inter-symbol interference caused by the signals arriving at different times at the receiver. In a terrestrial NB-IoT, the maximum CP duration is 0.8 ms, resulting in the maximum cell coverage of 120 km. For a satellite-based NB-IoT system, the differential RTT can be calculated as:

$$\Delta RTT(t) = \frac{D_{max}(\alpha_{min}(t)) - D_{min}(\alpha_{max}(t))}{c} \tag{2.7}$$

where $D_{max}(\alpha_{min}(t))$ represents the maximum slant range experienced by the user with the minimum elevation angle and $D_{min}(\alpha_{max}(t))$ is the minimum slant range at the user with the maximum elevation angle inside the cell. Figure 2.10 yields the results of the differential RTT as a function of the satellite visibility time. Please note that the area where the differential RTT starts to decrease and then increase again corresponds to the region where the satellite is above the targeted NB-IoT cell. In this moment, the closest user to the satellite is always

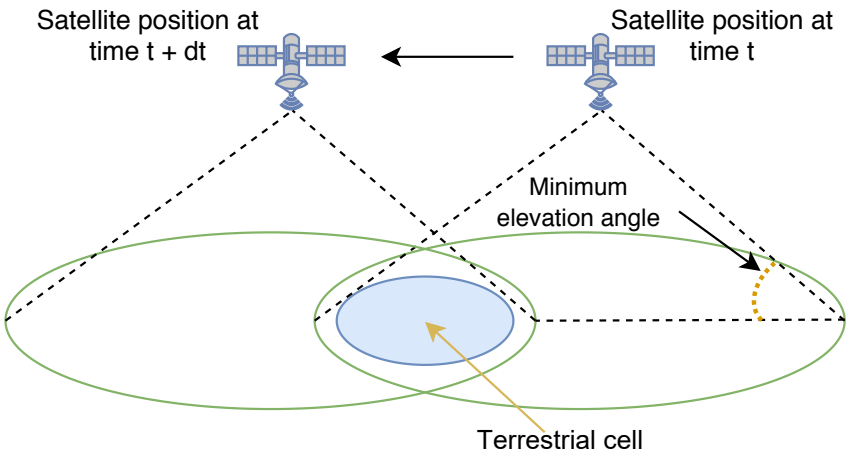

Figure 2.11: NGSO moving beam.

the one at satellite nadir. In contrary, for lower elevation angels the closest and the furthest users are the ones in the edge of the cell. As it can be observed, there are significant periods of time where the differential RTT overcomes the CP length limit. Users trying to initiate the access phase at such periods of time during the satellite passage, will fail to access the network.

Moving beams

The constant movement of the NGSO satellite will lead to a highly dynamic system that is considerably different from the terrestrial one. In a terrestrial NB-IoT scenario the BS is fixed on the ground and placed in the middle of the cell, and the overall system varies very slowly in time due to the movement of the UEs. On the contrary, the high-speed movement of the satellite will result in a limited coverage time for a particular cell (see Figure 2.11). If we refer to the results shown in the previous section (e.g. Figure 2.9), it can be noted that the satellite visibility time for a particular user is only 10 minutes for a LEO satellite at 600 km altitude, and around 20 minutes for a satellite at 1200 km altitude. This becomes even more drastic if we take into account also the minimum elevation angle of the communication which will further shrink the amount of time the user can transmit/receive data. This represents a crucial challenge to be considered. Furthermore, the varying slant range with the movement of the NGSO satellite will be directly reflected in the propagation path loss of the signal, hence causing the NB-IoT users to quickly jump from one coverage class to another. Please

note that in a terrestrial NB-IoT, three coverage classes are defined depending on the UE distance from the BS. Such high dynamicity of the satellite-based system is also an essential feature to be carefully addressed, especially by the resource allocation strategies.

Please note that the content presented in this chapter has been partially published in the following reference:

- [52] O. Kodheli, S. Krishna and S. Chatzinotas, "Narrowband IoT Technologies for Smart City Applications," *in Communication technologies for networked smart cities*, IET 2021, *(published)*.

2.3 Literature Review

The concept of adapting the cellular networks in order to be satellite-compatible has been treated in the literature since the development of the 4G LTE protocol. Hereafter we will review the relevant works performed in this direction, not only in the scientific domain but also in the 3GPP standardization domain. In addition, the literature review will not be limited only to NB-IoT systems via satellites but extended also to 4G and 5G due to the similarities of these protocols from the air interface perspective. We will categorize the related works in four main groups: i) *Architecture definition and challenges*; ii) *Doppler effects*; iii) *Delay impacts*; iv) *Other relevant works.*

2.3.1 Architecture definition and challenges

The first standardization initiatives started to evaluate the OFDM as a satellite radio interface [53], which is the principal signal format of 4G, and continued to be used in 5G as well with extra flexibility in the numerology (various SCS) [54]. With the development of the 5G air interface, a 3GGP study item [27] was initiated with the aim of analyzing the challenges of satellite-based 5G communications. After a successful study phase, a work item was approved with the purpose of enabling a 5G system to support non-terrestrial networks (NTNs) [55]. Clearly, among other NTN platforms, such as high altitude platforms (HAPS) and unmanned aerial vehicles (UAVs), satellites were also included. Two main architecture options were identified depending on the payload type. In the case of a transparent payload type, the serving base station and the user have to be in the footprint of the same satellite. On the other hand, the regenerative payload allows for inter-satellite links (ISLs), and due to this

the base station and the users can be under the coverage of different satellites. Besides, a regenerative payload allows also to incorporate the base station functionalities at the satellite, thus creating the so-called flying base station concept [56]. Regarding the orbital parameters, a LEO satellite with altitude 600 and 1200 km was considered in addition to the GEO satellite. In addition to the 5G NTN progress in the 3GPP standardization, another study item was initiated to explore the feasibility of NB-IoT via NTNs [57]. In contrast to 5G NTN, only the architecture options with a transparent payload type were considered.

In the scientific domain, the first research studies aimed at analyzing the role of satellites in cellular networks and the corresponding challenges. More specifically, in [23, 58, 59], the areas in which the satellites can contribute towards an integrated system within 5G, including the IoT scenarios, were identified. The main challenges of LEO satellite-enabled 4G systems were deeply analysed in [60] and their impact on the PHY and MAC layer were highlighted. In addition, the authors provide two architecture options for an integrated 4G-satellite system: a) a direct-access architecture where the users have to directly send the signal to the satellite; and b) a non-direct architecture option where the traffic generated from the users is firstly aggregated by small BS and then sent to the satellite. Moreover, in [61] two additional architecture options were identified for 5G/NB-IoT NTN with the same principle of having direct user access to the satellite, or through a small base station, but considering a satellite with either a transparent payload or a regenerative payload type. A general discussion and a candidate architecture for hybrid satellite-terrestrial networks operating at low-frequency bands were also provided in [62].

2.3.2 Doppler effects

As highlighted in Section 2.2, Doppler effects are a crucial impairment in NGSO communications. Its impact on the 4G PHY layer design has been thoroughly analysed in [60] and a compensation algorithm has been proposed relying on the position estimate of the user location and the knowledge of the satellite trajectory. Based on this methodology, the common Doppler experienced by all the users under the coverage of the satellite can be compensated at the Gateway. Clearly, the pre/post-compensation at the Gateway can be done by utilizing the centre of the beam as a reference point and the satellite trajectory knowledge. The residual Doppler not handled by the GW has to be computed at the user side. To do so, user terminals has to rely on GNSS positioning capabilities and be periodically updated with

the satellite trajectory data. This idea has been also put forward in the context of 5G and NB-IoT communications via satellites in several scientific contributions [63–66] as well as in 3GPP [27, 57]. Other relevant works relax the need for the knowledge of the satellite trajectory and propose prediction-based algorithms in order to track and compensate the Doppler shift changes over time [67, 68].

Another interesting approach, specifically targeting NB-IoT communication via LEO satellites, has been proposed in [69]. The principal concept is to utilize a frequency advance at the user terminal (similar to the TA concept in the RA procedure) in the uplink transmission based on the Doppler shift estimate in the downlink. An analysis on how to distinguish among the frequency offset introduced by the local oscillator and the Doppler shift introduced by the channel has been provided. Notably, for this technique to work, the amount of time from receiving the downlink signal to transmitting the uplink one should be sufficiently small so that the Doppler shift can be assumed constant. Last but not least, in [70] an extension of the existing OFDM signalling with a new constant envelope coding and modulation scheme called Turbo Frequency Shift Keying (FSK) has been proposed. It has been shown that the proposed waveform has a lower peak to average power ratio (PAPR) and is able to track the Doppler shift variation with the assumption of a perfect compensation of the initial Doppler shift.

2.3.3 Delay impacts

The impact of the increased delay over a satellite link has been initially studied for LTE networks. As a matter of fact, in [71] adaptations to the LTE air interface has been analysed explicitly targeting GEO satellite-based systems. More specifically, new sequences for the RA procedure has been proposed capable of dealing with the extreme delays over satellite links, as well as the use of PAPR reduction techniques to increase the resilience of the OFDM waveform to non-linear distortion. In addition, in [72] an efficient resource allocation has been proposed suitable for LTE multicast communications via GEO satellites. In the 5G and NB-IoT context, one of the well-known and widely accepted solutions to cancel out this increased delay in the satellite channel is the application of a TA from the users when transiting their uplink signal to the base station [63–65]. This methodology utilizes the same principle as the Doppler compensation based on the user location information (fixed for no-mobility users or through GNSS) in combination with satellite ephemeris data. Other works

put forward the idea of a fixed TA employed only by taking into account the delay experienced at the centre of the satellite antenna footprint, while leaving the other part to be handled in the same manner as in a terrestrial scenario [61, 73]. The differential delay part (with reference to the centre of the antenna footprint) would limit the supported beam size by the protocol, as derived in [74]. To extend the supported beam size, new preamble formats for the RA procedure should be specifically designed targeting satellite-based systems, as proposed in [75]. Another widely accepted solution by all previous works is the increase of the relevant timers in the RA procedure considering the signal propagation time over the satellite link. Naturally, the new extended timers would greatly depend on the altitude of the satellite.

In addition to the access phase, the increased delay in a satellite link would also result in a drop of performance for the data phase. This is due to the HARQ protocol implementation in the MAC layer, as explained in Section 2.1.2. Receiving an ACK/NACK for a certain transmitted packet would require a larger waiting time for every user. Indeed, this performance drop for NB-IoT systems via GEO satellites has been deeply analysed in [76] and it has been shown that utilizing a block error rate (BLER) target of 10^{-2} results in a better performance compared to the terrestrial BLER target of 10^{-1}. The reduced utilization of the HARQ protocol leads to such performance gain. Indeed, one of the proposals in the 3GPP standardization [27, 57] is the deactivation of the HARQ protocol, avoiding as much as possible the extra message exchange between the base station and the users.

2.3.4 Other relevant works

Integrating SatComs with the cellular networks would not only bring challenges in the PHY and MAC layer, but also in the upper layers. In fact, one of the main issues to consider in this direction is the mobility management in NGSO systems. Clearly, to enable continuous connectivity of 4G/5G/NB-IoT services to NGSO satellite networks, a satellite constellation is required. The first movers in the space market to establish a global connectivity through LEO constellations were Starlink, OneWeb and Telesat [77]. The handover procedure in such large systems is critical in order guarantee robust service continuity and satisfactory user experience. In this context, a first performance analysis of the conventional 5G NR handover algorithm in a LEO-based NTN deployment has been provided in [78]. Moreover, in [79], the feasibility of NGSO satellites directly accessing 5G on-ground users in mmWaves has been analysed taking into account various aspects of the system level design such as regulatory

aspects, UE characteristics, space segment design and link budget.

2.4 Thesis Contributions

2.4.1 NB-IoT Data Phase

In the first part of the thesis, we focus on the data phase of a satellite-based NB-IoT system by assuming a successful access phase. Notably, without considering the power budget issues and the performance drop, in the case of a GEO satellite scenario, the overall system would be very similar to the terrestrial one from the data phase perspective. Therefore, we particularly analyse a LEO satellite-based NB-IoT system where the Doppler effects have a major impact on the uplink transmission. While the GNSS approaches, as highlighted in Section 2.3.2, may be a good solution to counteract the Doppler effects in 4G/5G communications via satellite, their applicability to NB-IoT systems is questionable and deserves more attention because of the low-complexity requirement. In fact, the increased power consumption from the GNSS utilization has been analyzed in [57], by considering various commercial UEs and scenarios. The simulation results provided in [57] show a reduction in battery life of the NB-IoT devices in the range of 10 - 40 %. Not only this, but even if users with no mobility are assumed (hence no GNSS), extra signalling is required to update the users with the satellite trajectory data, and an algorithm that calculates and compensates the Doppler shift is still needed. Undoubtedly, this will increase the complexity of the algorithms at the user terminals. Also, the other works [67–70] that put forward the idea of correcting the Doppler effects at the UE side require more expensive algorithms, which goes against the IoT vision of low-power and low-complexity devices. In this context, it is highly advantageous to explore alternative solutions which do not touch the complexity at the user side. Therefore, in the first part of the thesis, we propose a user scheduling strategy that is capable of maintaining the differential Doppler under the limit supported by the standard. Please note that the common Doppler shift that will be identical for all users under the coverage of the satellite (e.g. the one at the centre) is assumed to be perfectly pre/post-compensated at the BS side. More specifically, this chapter contribution is described below.

- **Chapter 3: An uplink user scheduling strategy for differential Doppler reduction in NB-IoT via LEO satellite systems.**

In this contribution, we come up with an uplink scheduling technique for a LEO satellite-based NB-IoT system, able to mitigate the level of the differential Doppler down to a value tolerable by the IoT devices, as specified in the standard. The performance of the proposed strategy is validated through numerical simulations of an end-to-end NB-IoT over a satellite communication system, focusing only on the uplink case. In addition, we go one step further and perform a link budget analysis to stress out the requirements at the space segment if no modifications are done at the user segment. The main contributions of this work relative to the recent literature in the field, are summarized as follows: i) The proposed technique does not increase the complexity at the user side, hence no modifications are needed for the NB-IoT devices. This assures seamless connectivity and service to the devices, regardless of the presence of a satellite or a terrestrial network, aligning with the aim of having an integrated satellite-terrestrial network; b) Even though the Doppler effects occur in the PHY layer of communication, we address the differential Doppler through a MAC layer approach; and iii) Although we formulate the problem and validate the techniques using a satellite-based NB-IoT system, the proposed techniques to reduce the differential Doppler shift are applicable to other 5G machine-type applications, such as LTE-M, requiring only small adaptations.

The material presented in this chapter has been already accepted for publication in the following journal and conferences.

- [80] O. Kodheli, S. Andrenacci, N. Maturo, S. Chatzinotas and F. Zimmer, "Resource Allocation Approach for Differential Doppler Reduction in NB-IoT over LEO Satellite," *2018 9th Advanced Satellite Multimedia Systems Conference and the 15th Signal Processing for Space Communications Workshop (ASMS/SPSC)*, 2018, pp. 1-8, *(published)*.
- [81] O. Kodheli, S. Andrenacci, N. Maturo, S. Chatzinotas and F. Zimmer, "An Uplink UE Group-Based Scheduling Technique for 5G mMTC Systems Over LEO Satellite," *in IEEE Access*, vol. 7, pp. 67413-67427, 2019, *(published)*.
- [82] O. Kodheli, N. Maturo, S. Andrenacci, S. Chatzinotas and F. Zimmer, "Link Budget Analysis for Satellite-Based Narrowband IoT Systems," *ADHOC-NOW 2019: Ad-Hoc, Mobile, and Wireless Networks*, pp. 257-271, *(published)*.

After validating the user scheduling strategy through performance evaluation in the PHY

layer, the objective was to go one step ahead and incorporate also the dynamicity of the system coming from the movement of the LEO satellite. As we previously highlighted, the time that the UEs are under the visibility of the satellite is very limited, and it is of paramount importance to take this into account when scheduling users. In addition, with the movement of the satellite, the users will quickly jump from one coverage class to another (in the sense that the SNR will increase or decrease). Delaying the scheduling of a certain user would result in a resource allocation based on outdated parameters, or in the worst-case scenario the user may no longer be in the coverage of the satellite. In this context, this is an untreated problem in the literature, where the main existing resource allocation strategies are designed only for terrestrial systems [83–87]. Therefore, to enhance our proposed scheduling technique and cover this gap in the literature, in this chapter contribution we propose a novel uplink resource allocation strategy, which jointly incorporates the technical peculiarities of the LEO satellite channel with the various channel conditions and different user requirements in terms of data to be transmitted. The novel methodology proposed in this chapter can act as a framework for future works in this area of research. The chapter contributions are described below in more detail.

- **Chapter 4: An efficient resource allocation for uplink data transmission in NB-IoT via LEO satellite systems.**

  The main contributions of this chapter are summarized as follows: a) We mathematically model the user scheduling strategy as a 0-1 Two-dimensional Knapsack Problem. Solving such a problem means selecting the set of users to transmit their uplink data in the available radio resources which maximize the sum profit of the selected users; b) We formulate a profit function that assigns different profits to users depending on their data packet sizes, channel conditions and satellite visibility time. The latter one is a unique and crucial feature, while the data volumes and channel conditions have already been contemplated in terrestrial scheduling; c) By fixing the transmission mode only to single-tone, we convert the problem into a simpler 0-1 Multiple Knapsack Problem (MKP). Exploiting the unique features of our system, we propose an approximate algorithm with a near-optimal performance and low complexity; and d) We study the performance trade-offs of our LEO satellite-based NB-IoT system through numerical simulations by changing the weights of the components which contribute to the profit function of the 0-1 MKP problem. This allows us to find optimal operation points for

three different Key Performance Indicators (KPIs) and rank various algorithms.

The material presented in this chapter has been already published in the following conference and journal.

- [88] O. Kodheli, N. Maturo, S. Chatzinotas, S. Andrenacci, F. Zimmer, "NB-IoT via LEO satellite: An efficient resource allocation strategy for uplink data transmission, *in IEEE Internet of Things Journal*, 2021, *(accepted)*.

2.4.2 NB-IoT Access Phase

In the second part of the thesis, we focus on the access phase of a satellite-based NB-IoT system. In this crucial phase, which is achieved by the RA procedure, the first challenge that impacts its feasibility over a satellite link is the increased RTT in the communication link. Several works in the literature have previously addressed this problem, as we described in Section 2.3.3. While all the existing works in the literature that counteract the impact of the increased delay on the RA procedure hold in theory, some of them fail to be implemented practice, according to the findings of this work. This is because none of the current works have done an experimental validation of their proposals and other crucial challenges that would lead to a failure in the RA procedure over satellites have been ignored. To cover this gap in the literature, we do an in-depth analysis of the RA procedure over satellites and the corresponding challenges imposed by the increased signal propagation delay. We propose novel solutions to counteract the impact of the increased delay on the RA procedure and do a trade-off analysis of different approaches, taking into account also the already existing ones in the literature. Last but not least, we go one step further and validate our proposed solutions on a realistic experimental setup utilizing the Open Air Interface (OAI) implementations of the 3GPP users and base station, and a satellite channel emulator implemented in hardware (HW). The experimental setup has played a crucial role in this work because it allowed us to identify through a trail-and-error approach the new challenges not previously treated in the literature, and to test various solutions from a practical point of view. In order to broaden the scope of applicability, we keep the analysis general targeting 4G, 5G and NB-IoT systems since the RA procedure is quasi-identical among these technologies. The reason why the same could not be done in the first part of the thesis (where we considered the data phase) is because our solutions are applicable only to NB-IoT systems. The chapter contributions

are described below in more detail.

- **Chapter 5: Experimental Analysis and Demonstration of the Random Access Procedure over Non-Terrestrial Networks**

  The main contributions of this chapter are summarized as follows: a) We identify new challenges, not treated so far, regarding the RA procedure over NTN imposed by the considerably increased delay in the communication link; b) We propose novel solutions for the challenges identified in this work, as well as for the ones already treated in other works, and provide a trade-off analysis of various approaches; c) In order to test our solutions, we design a testbed based on OAI implementation for the 3GPP users and base station, and HW implementation for the NTN channel emulating the experienced delay in the communication link between the users and the base station; and d) We measure and show an important KPI of the RA procedure over NTN, such as the single user access time. This will act as a lower bound for future works in this area where more than one user can access the network and collisions may occur during the RA procedure.

  The material presented in this chapter has been already published in the following conference, and accepted for publication in the journal.

  - [89] O. Kodheli, N. Maturo, S. Chatzinotas, S. Andrenacci and F. Zimmer, "On the Random Access Procedure of NB-IoT Non-Terrestrial Networks," *2020 10th Advanced Satellite Multimedia Systems Conference and the 16th Signal Processing for Space Communications Workshop (ASMS/SPSC), (published).*
  - [90] O. Kodheli, A. Abdalla, J. Querol, M. Gholamian, S. Kumar, N. Maturo, S. Chatzinotas, "Random Access Procedure over NTN: From Theory to Practice, *in IEEE Access*, 2021, *(accepted).*

Chapter 3

An uplink user scheduling strategy for differential Doppler reduction in NB-IoT via LEO satellite systems

In this chapter, an NB-IoT over LEO satellite architecture is considered with the purpose of extending the coverage of a terrestrial NB-IoT infrastructure in remote areas and satisfy its goal of ubiquitous global coverage. The problem of the differential Doppler shift is formulated, by assuming a perfect estimation and compensation at the gateway of the residual Doppler part, which is experienced by all the NB-IoT devices in the satellite coverage area. In order to solve the differential Doppler problem, an uplink scheduling technique is proposed, able to mitigate the differential Doppler down to a value tolerable by the standard. The performance of the proposed schemes is assessed through numerical simulations of the NPUSCH channel and compared with the case where the differential Doppler shift is not mitigated. Last but not least, a link budget analysis is performed which derives the requirements of the satellite antenna in order to close the link without changing the antenna characteristics at the user side.

3.1 System Model

3.1.1 System architecture & assumptions

We consider a number of NB-IoT users (UEs), which are directly connected to the Base Station (BS) through the LEO satellite link with altitude $h = 1200$ km, placed in a fixed

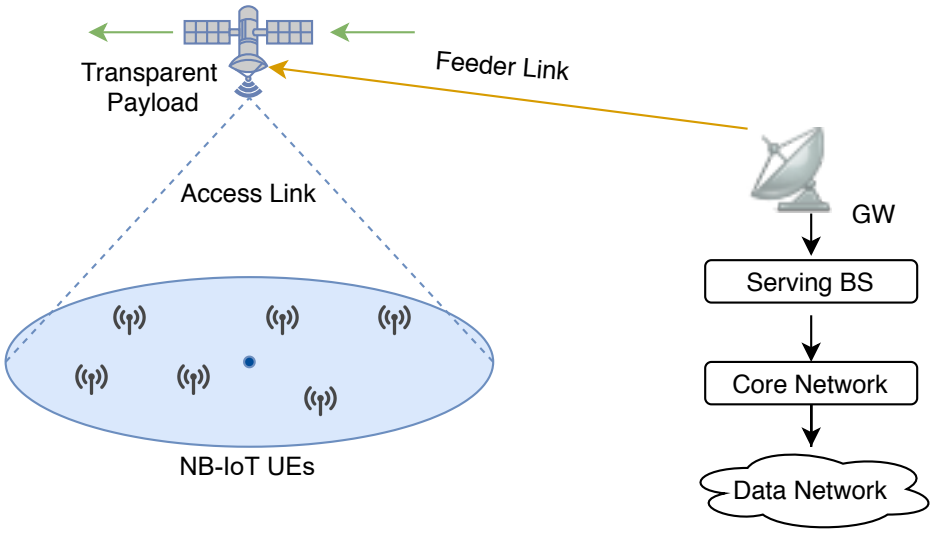

Figure 3.1: NB-IoT via LEO satellite architecture.

area on Earth with diameter $D = 200$ km (see Figure 3.1). This area can be covered by the satellite for a certain amount of time, depending on the altitude of the satellite, the minimum elevation angle of communication and the directivity of the antenna. In addition, the following assumptions are made for the considered NB-IoT over satellite architecture: i) we consider the channel between the eNB and the satellite (feeder link) as ideal. The assumption is justified by the scope of the study, which focuses on the differential Doppler shift; ii) NB-IoT air interface in the user link; iii) a standalone NB-IoT deployment with a carrier frequency $f_c = 2$ GHz; iv) the UEs are fixed on Earth and no mobility is foreseen for them. Please note that the carrier frequency corresponds to the LTE carrier and is normally used for the in-band and guard-band deployment of the NB-IoT [91]. However, we assume that the target area covered by the satellite is isolated from the terrestrial coverage, hence we can use this carrier for our stand-alone NB-IoT deployment, since it is not yet defined by the regulators. Last but not least, the satellite is assumed to be transparent.

3.1.2 Signal Model

The channel model of a satellite-terrestrial communication link can be approximately modeled as additive white Gaussian noise channel by neglecting the multipath fading [92]. This is justified by the assumption of having perfect line of sight (LoS) transmission in a remote area. Therefore, the only component in our satellite link would be the LoS component

impaired by a Doppler shift due to the movement of the satellite.

Downlink transmission

In the downlink, the transmitted baseband analog signal from the BS to the UEs can be written as:

$$s(t) = \frac{1}{\sqrt{N}} \sum_{n=0}^{N-1} a[n] e^{j2\pi f_s n t} \cdot u_T(t) \tag{3.1}$$

where $a[n]$ depicts the symbols (data or pilots) carried by the n-th subcarrier, $u_T(t)$ is a rectangular window function, hence $u_T(t) = 1$ for $0 \leq t \leq T$. Please note that $T = T_s + T_{cp}$ where T_s is the symbol period and T_{cp} is the cyclic prefix length. The parameter $f_s = 1/T_s$ represents the subcarrier spacing. Finally, the received analog signal by the k-th UE after downconversion can be expressed as:

$$\begin{aligned} r_{UE}^{k}(t) &= e^{j2\pi f_{dk}(t)t} \cdot h_k(t) \cdot s(t) + \omega_k(t) \\ &= e^{j2\pi f_{dc}(t)t} \cdot e^{j2\pi \Delta f_{dk}(t)t} \cdot h_k(t) \cdot s(t) + \omega_k(t) \end{aligned} \tag{3.2}$$

where $!_k(t)$ is the additive white Gaussian noise, $f_{dk}(t)$ is the Doppler shift which has a dependency on time based on the position of the LEO satellite, $h_k(t)$ are the channel coefficients and $s(t)$ is the transmitted analog baseband signal from the base station eNB. Please note that the Doppler shift can be written as $f_{dk}(t) = f_{dc}(t) + \Delta f_{dk}(t)$, where $f_{dc}(t)$ is the common part of Doppler shift experienced by all the UEs in the coverage area and is given by the Doppler curve of one of the users taken as reference, for example the one in the middle. $\Delta f_{dk}(t)$ is the differential part of the k-th UE which has a dependency on the relative position of UEs with respect to the reference user. From equation (3.1) and (3.2), and assuming that the frequency offset of the local oscillator is negligible, the received OFDM symbol of the k-th user of a frame transmitted at time $[t', t' + T]$ after sampling at time $t = lT_s/N$, FFT and equalization can be written in the discrete form as:

$$r_{l,k} = e^{j2\pi \epsilon_k l/N} \cdot a_{l,k} + \omega_{l,k} \tag{3.3}$$

where $l = 0, 1, ..., N-1$ is the subcarrier index, N is the number of subcarriers assigned to the k-th UE (12 in the DL) and $a_{l,k}$ is the l-th modulated symbol (QPSK in DL) of

the overall OFDM symbol for the k-th UE . It is worth highlighting that $ffl_k = f_{dk}/f_s$ is the normalized Doppler shift with respect to subcarrier spacing. This parameter also drives the performance degradation in our scenario. Please note that the Doppler shift will also have a small variation during each OFDM symbol time. However this time is so small that we assume a constant f_{dk} along $[t', t' + T]$.

Uplink transmission

In the uplink, the transmitted signal by the k-th UE to the BS will have the following form:

$$s_k(t) = \frac{1}{\sqrt{N_k}} \sum_{n=0}^{N_k-1} b_k[n] e^{j2\pi f_s nt} \cdot u_T(t) \tag{3.4}$$

where $b_k[n]$ are the symbols mapped into subcarriers after applying DFT and N_k is the number of subcarriers assigned for transmission for the k-th UE. As already described in Chapter 2, the number of subcarriers assigned for transmission can be 1 (single-tone), 3, 6 or 12 (multi-tone). Please note that SC-FDMA with single-tone is mathematically identical to OFDM, because the DFT step can be excluded. The received baseband signal at the eNB is given by the superposition of each signal from UEs:

$$\begin{aligned} r_{eNB}(t) &= \sum_{k=1}^{M} e^{j2\pi f_{dk}(t)t} \cdot h_k(t) \cdot s_k(t) + \omega_k(t) \\ &= e^{j2\pi f_{dc}(t)t} \sum_{k=1}^{M} e^{j2\pi \Delta f_{dk}(t)t} h_k(t) s_k(t) + \omega_k(t) \end{aligned} \tag{3.5}$$

where M is the number of UEs transmitting at a certain time. It is worth highlighting here that M will have a dependency on the transmission mode used by the UEs (single-tone or multi-tone). For example, for a single-tone SC-FDMA transmission with $15kHz$ SCS, there can be a maximum 12 UEs simultaneously transmitting. Again, like in the downlink case, assuming that the frequency offset of the local oscillator is negligible, the received SC-FDMA symbol of the uplink frame transmitted at time $[t', t' + T]$ after sampling at time $t = lT_s/N$, FFT and equalization can be written in the discrete form as:

$$r_l = e^{j2\pi\epsilon l/N} \cdot a_l + \sum_{k=0, k\neq l}^{N-1} a_k + \omega_l \tag{3.6}$$

where the total number of subcarriers N in this case can be 12 or 48 depending on the SCS used. Please note that with respect to the downlink transmission, here we will have the presence of a second term $\sum_{k=0,k\neq l}^{N-1} a_k$ which characterizes the inter-carrier interference (ICI) coming from k-th symbols (BPSK or QPSK) modulated in the other subcarriers of the overall SC-FDMA symbol. In the downlink transmission, this term is zero, since the subcarriers are strictly orthogonal between them and the whole NB-IoT band is shifted in frequency. Whereas in the uplink transmission this does not hold, because of the presence of a differential Doppler between subcarriers. Due to the slotted structure of SC-FDMA, the subcarriers assigned to different users will arrive to the satellite with different Doppler shifts, negating the orthogonality in the final SC-FDMA signal.

3.2 Problem Formulation

3.2.1 Maximum Differential Doppler Characterization

We already discussed the Doppler shift and its mathematical expression in Chapter 2. Nevertheless, since the focus of this chapter is on the differential Doppler part, it is of utmost importance to derive a closed-form expression. We start the derivation by the formula of the Doppler shift as a function of time, as shown in Section 2.2.

$$f_d(t) = -\frac{f}{c} \cdot \frac{w_s r_E r \, sin(w_s t)\eta(\theta_{max})}{\sqrt{r_E^2 + r^2 - 2 r_E r \, cos(w_s t)\eta(\theta_{max})}} \tag{3.7}$$

$$\eta(\theta_{max}) = cos[cos^{-1}(\frac{r_E}{r} cos\theta_{max}) - \theta_{max}], \tag{3.8}$$

Having the closed-form expression of the Doppler shift as a function of time (equation (3.7) & (3.8)), we can now characterize the differential Doppler between two points on Earth. In order to simplify the derivation, we separate the analysis into two axes, that we will call as x-axis and y-axis. The x-axis represent the axis along the movement of the satellite and the y-axis is the one perpendicular to it.

Along x-axis

Let us now characterize the differential Doppler along the x-axis (please refer to Fig. 3.2). We are interested in characterizing the upper bound (max value) of the differential Doppler

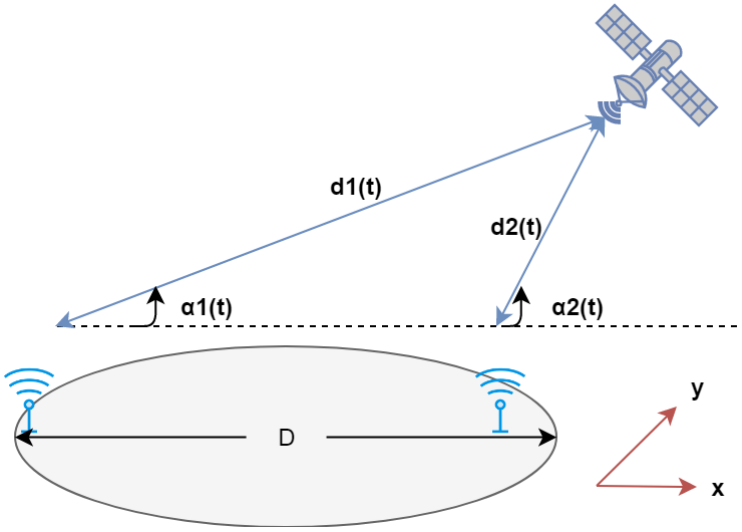

Figure 3.2: Two UE with the maximum differential Doppler shift along x-axis.

along x-axis with respect to time, which happens when 2 UE are placed at the maximum distance D in the coverage area on Earth and in the trajectory where the satellite reaches its maximum elevation angle $\theta_{max} = \pi/2$. Therefore, it can be calculated that:

$$\eta(\pi/2) = cos\left[cos^{-1}\left(\frac{r_E}{r}cos(\pi/2) - \pi/2\right)\right] = 1 \tag{3.9}$$

By geometrical considerations, it can be easily proven that the following formulas hold as in [60]:

$$d_1(t) = \sqrt{r_E^2 + r^2 - 2r_E r\, cos(w_s t)} \tag{3.10}$$

$$cos\alpha_1(t) = \frac{r\, sin(w_s t)}{\sqrt{r_E^2 + r^2 - 2r_E r\, cos(w_s t)}} \tag{3.11}$$

By substituting (3.10) and (3.11) into equation (3.7) we obtain the Doppler shift as a function of the elevation angle.

$$f_{d1}(t) = -\frac{f w_s r_E\, cos\alpha_1(t)}{c} \tag{3.12}$$

Finally, the differential Doppler would have the following form.

$$\Delta f^x_{dmax}(t) = \left|\frac{f w_s r_E}{c} \cdot (cos\alpha_2(t) - cos\alpha_1(t))\right| \tag{3.13}$$

So now the problem of finding the differential Doppler scales down to expressing the elevation angle α_2 as a function of α_1. Taking into account the geometry in Fig. 3.2, it can be written that:

$$d_1(t)\, cos\alpha_1(t) = d_2(t)\, cos\alpha_2(t) + D \tag{3.14}$$

$$d_2(t)^2 = d_1(t)^2 + D^2 - 2Dh_1(t)\, cos\alpha_1(t) \tag{3.15}$$

Solving (3.14) and (3.15):

$$cos\alpha_2(t) = \frac{d_1(t)\, cos\alpha_1(t) - D}{\sqrt{d_1(t)^2 + D^2 - 2Dd_1\, cos\alpha_1(t)}} \tag{3.16}$$

Finally, by plugging this expression into (3.13) and substituting the expressions of $d_1(t)$ and $cos\alpha_1(t)$ we are able to obtain the closed-form equation of the maximum differential Doppler along x-axis with respect to time (see equation (3.17)).

$$\Delta f^x_{dmax}(t) = \left| \frac{f w_s r_E}{c} \left(\frac{r\, sin(w_s t) - D}{\sqrt{r_E^2 + r^2 - 2r_E r\, cos(w_s t) + D^2 - 2Dr\, sin(w_s t)}} - \frac{r\, sin(w_s t)}{\sqrt{r_E^2 + r^2 - 2r_E r\, cos(w_s t)}} \right) \right| \tag{3.17}$$

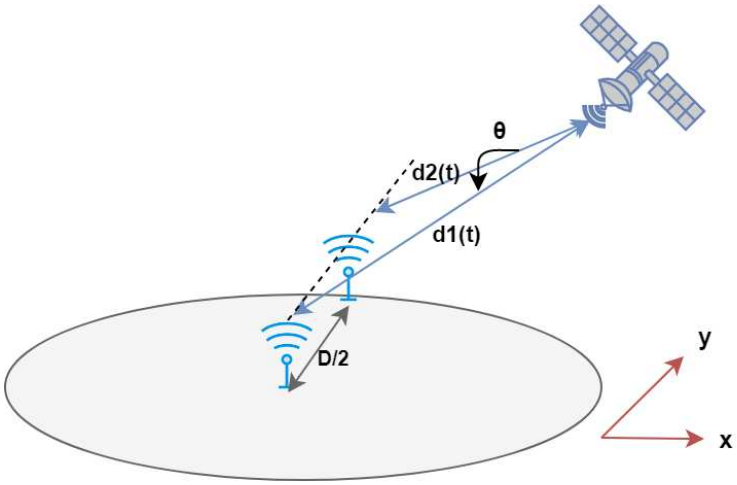

Figure 3.3: Two UE with the maximum differential Doppler shift along y-axis.

Along y-axis

The maximum differential Doppler experienced in a region with diameter D on Earth along the y-axis is between 2 nUEs, one placed at the center of the region and the other at $D/2$ distance in the y-direction. Please refer to Fig. 3.3 for geometry considerations. The only parameter that changes between the 2 UEs is the maximum elevation angle θ_{max} which will be different. For the UE placed at the center of the region, the maximum elevation angle is $\theta_{1max} = \pi/2$. At this point, it can be easily proved that $d1(t) = h$, where $h = r - r_E$ is the altitude of the satellite. This is the moment that the other UEs also experiences the maximum elevation angle, as proved in [51]. From geometrical considerations it can be calculated that:

$$\theta_{2max} = tg^{-1}\left(\frac{h}{D/2}\right) \tag{3.18}$$

Therefore the maximum differential Doppler can be expressed as:

$$\Delta f^{y}_{dmax}(t) = |f_{d1}(t, \theta_{1max}) - f_{d2}(t, \theta_{2max})| \tag{3.19}$$

By plugging the values of θ_{1max} and θ_{2max} into (3.7) and making the difference, the final closed-form expression of the maximum differential Doppler along y-axis as a function of time can be obtained (see equation (3.20)).

$$\Delta f^{y}_{dmax}(t) = \left| \frac{f w_s r_E r\, sin(w_s t)}{c} \left(\frac{\eta[tg^{-1}(\frac{h}{D/2})]}{\sqrt{r_E^2 + r^2 - 2 r_E r\, cos(w_s t)\eta[tg^{-}1(\frac{h}{D/2})]}} - \frac{1}{\sqrt{r_E^2 + r^2 - 2 r_E r\, cos(w_s t)}} \right) \right| \tag{3.20}$$

3.2.2 Problem Statement

As we previously showed in the mathematical representation of the downlink and uplink signals, the factor causing performance degradation is the differential Doppler shift, assuming that the common Doppler shift for all the UEs in the coverage area can be ideally pre(post)-compensated in the gateway. By plugging the system parameters of our scenario in (3.17) and (3.20) and run numerical simulations, we obtain the curves of the differential Doppler as a function of time and elevation angle of the satellite as in Fig. 3.3 and Fig. 3.4. We have

shown the results for elevation angle that goes from 0 to 180 degrees. Finally, the differential Doppler achieves the peak values of approximately 8.5 kHz along x-axis and 0.75 kHz along y-axis.

In the downlink transmission, each UE will receive the 180 kHz NB-IoT carrier with a certain differential Doppler shift depending on user's location. All the UEs acquire time and frequency synchronization with a cell and detect the physical layer ID through cell search procedures. Please note that the differential Doppler with respect to the center of the beam will be half of the values shown in Figure 3.4. Therefore, being inside the 7.5 kHz limit, as we emphasize in Section 2.2, the downlink synchronization is feasible.

In the uplink transmission, each nUE will generate its own signal and transmit it to the BS. As we previously mentioned, to each nUE can be assigned $1, 3, 6$ or 12 subcarriers to transmit in the uplink. Due to the slotted structure of SC-FDMA, all the subcarriers should be synchronized both in time and frequency, in order to avoid overlap among them. However, these subcarriers will arrive to the satellite with different Doppler shifts, negating the orthogonality in the final SC-FDMA signal. It can be calculated that the standard can

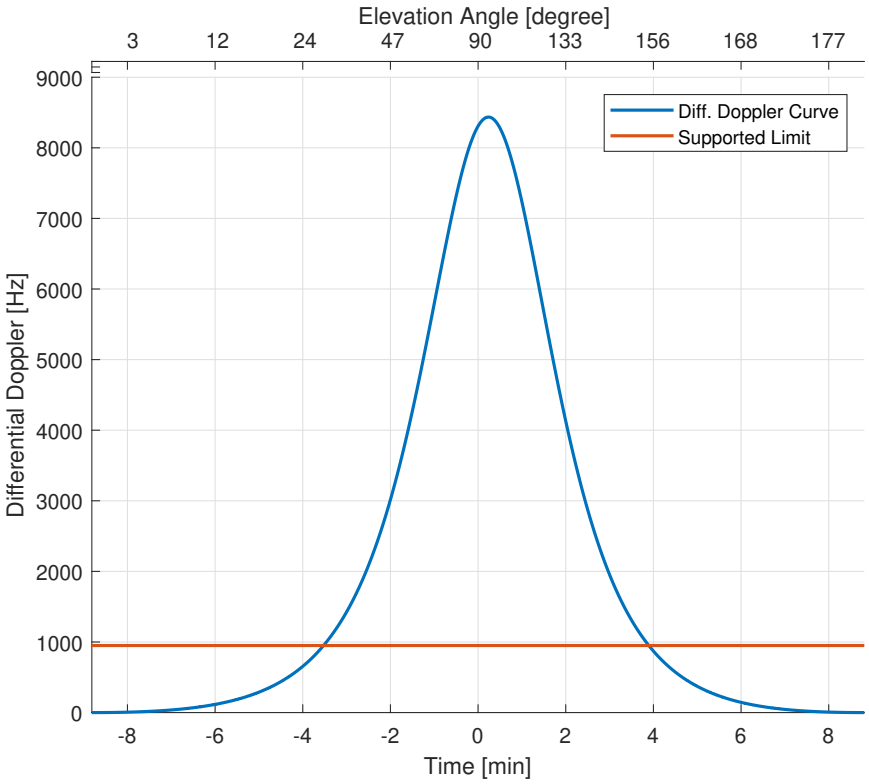

Figure 3.4: Maximum differential Doppler curves along x-axis.

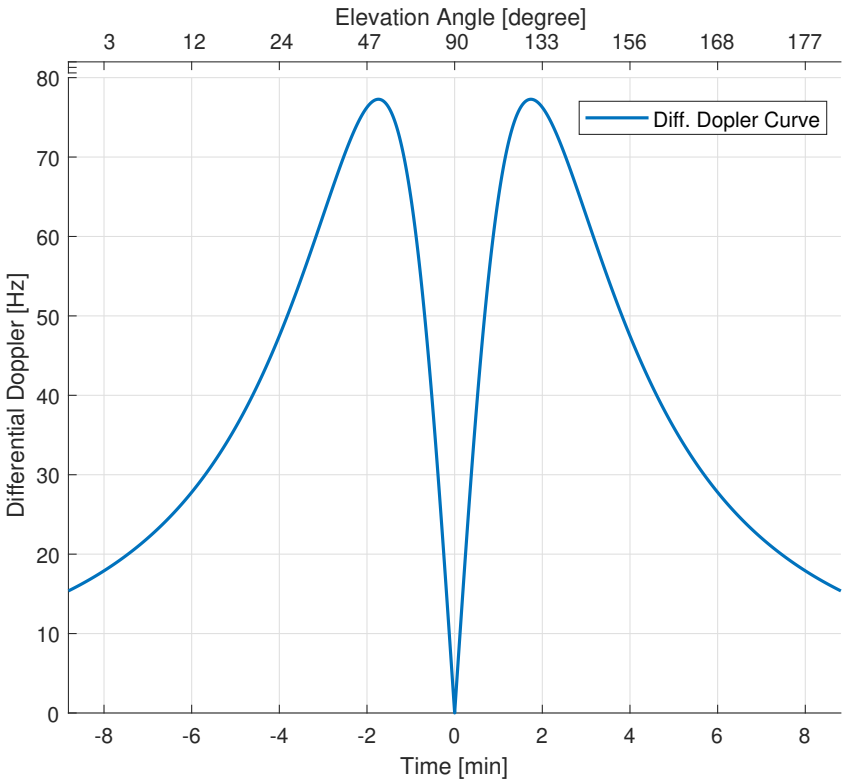

Figure 3.5: Maximum differential Doppler curves along y-axis.

support up to 950 Hz of Doppler shift among subcarriers. This value is derived using 3GPP specification about mobile UEs, carrier at 2 GHz, 15 kHz SCS and maximum speed at 500 km/h [93]. As LTE can support this mobility of users, it means that it can also support and mitigate a loss of orthogonality of up to 950 Hz. Referring now to our numerical results, it can be noted that the differential Doppler is much higher than the supported limit along x-axis. Furthermore, along y-axis the differential Doppler is much lower than the limit, therefore we can consider it as negligible. As a result, the received SC-FDMA signal at the BS will be significantly distorted due to a large amount of overlap between subcarriers (up to 8.5 kHz), when terminals with large distance in the x-axis are scheduled in the same frame.

Of course, if each individual UE can also pre-compensate its differential Doppler before transmitting the signal, the problem can be solved. In order to do so, the users have to know their location on Earth and estimate the position of the satellite at a certain time continuously. However, this would raise significantly the complexity in the user side. Taking into account the IoT vision of very low cost and low complex devices, alternative solutions should be found, in order to maintain the low complexity of the nUEs.

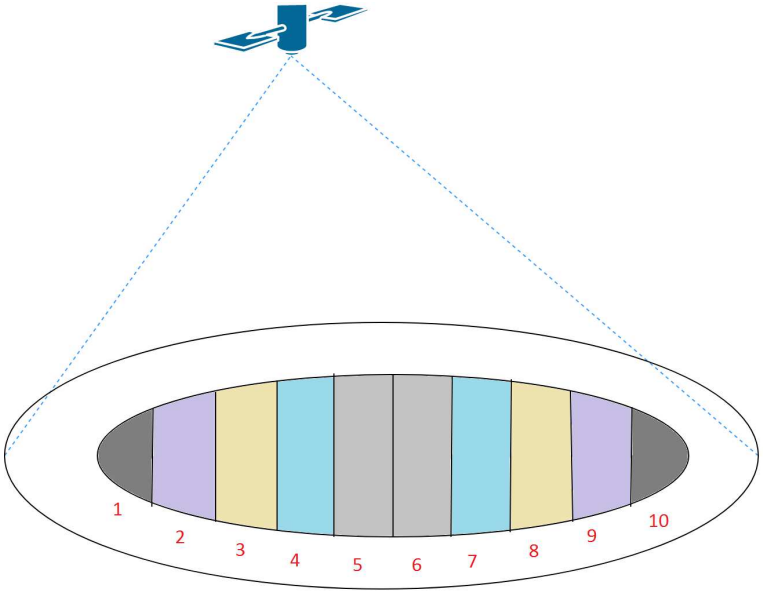

Figure 3.6: Representations of the groups in the coverage region.

3.3 Proposed User Scheduling Strategy for Differential Doppler Reduction

In this chapter, we come up with a technique to reduce the differential Doppler down to a value supported by the standard, which we calculated to be 950 Hz. Therefore, we propose re-grouping the UEs on the coverage area in such a way that the differential Doppler among users inside each group should be below the allowed threshold. Of course, the number of groups that we need will depend on the value of the differential Doppler at a certain time and elevation angle (see Figure 3.4). The smaller the differential Doppler, the larger groups we can create. However, considering the worst case scenario, having the peak of differential Doppler, it can be easily calculated that at $D = 20$ km the maximum differential Doppler along x-axis will be below the threshold of 950 Hz. Therefore, for the worst case, 10 groups of UEs will be needed as in Figure 3.6. It is worth reminding that along the y-axis the differential Doppler is so low that smaller groups are not needed in this direction. By performing numerical simulations, we obtain the maximum differential Doppler curves for all the regions along the x-axis as in Figure 3.7. It can be noted that now the peak values of differential Doppler in each group is approximately 880 Hz along the x-axis. Finally, the problem to be solved is how to schedule the uplink transmission to the created group of users.

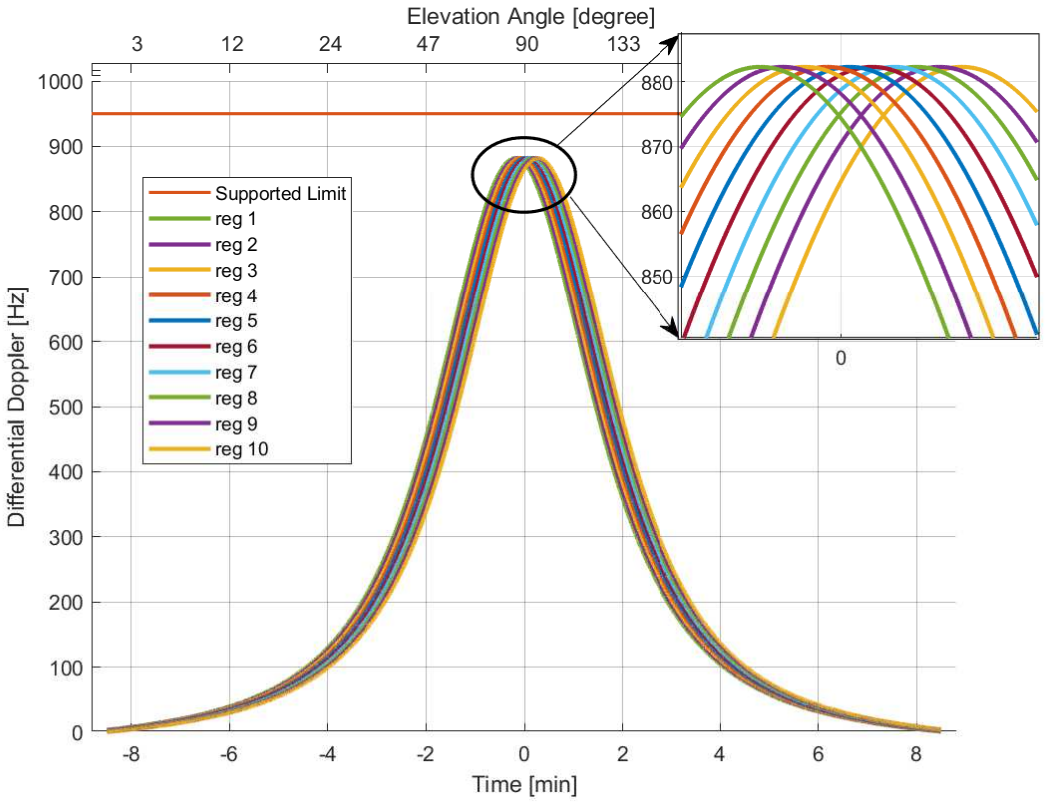

Figure 3.7: Maximum differential Doppler along x-axis in the created groups.

3.3.1 Group Scheduling in Time (GS-T)

One way of scheduling the users and assigning appropriate resources is in the time domain. This implies that NB-IoT carrier is assigned for a certain amount of time to each group by the BS. Thereby, the BS will be capable of decoding correctly the symbols coming from users situated in the same group no matter how the subcarriers are allocated to the users, as the differential Doppler experienced will be under the desirable limit. Please note that SC-FDMA is still used in the uplink by the UEs inside a group. In addition, it is very important to emphasize that the BS must know the position of all the UEs, for the purpose of user-grouping and a proper allocation of the resources. As no mobility is assumed for the UEs, it is possible to calibrate their location in the deployment phase of the devices in the coverage area. In the Attach Request Procedure, as described in [94], the UEs will identify themselves in the network by sending their IMSI (International Mobile Subscriber Identity) or old GUTI (Globally Unique Temporary ID) and a map can be created which connects their ID with the location in the region. In all the other procedures and message exchanges, the UE will be identified in the network through this ID, hence its position in the coverage

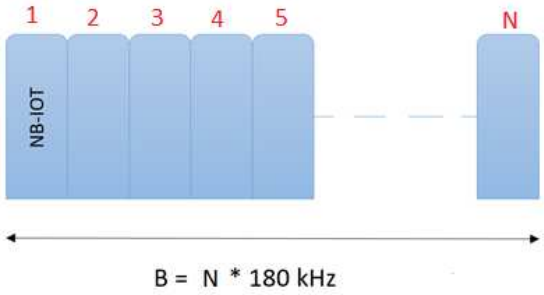

Figure 3.8: Needed resources in the uplink transmission.

area will be known.

3.3.2 Group Scheduling in Frequency (GS-F)

Another possibility of assigning the uplink resources to the users is in the frequency domain. In other words, several NB-IoT carriers are needed, and not just one, for the uplink transmission, as in Figure 3.8. Using secondary carriers in the NB-IoT uplink transmission is totally supported by the standard and specified in the Release 14 [95]. In such a case, we must assign adjacent NB-IoT carriers to adjacent groups, because the differential Doppler between adjacent groups is the smallest possible. It can be calculated that for the worst case scenario (maximum differential Doppler), we will need to create 20 groups. By doing so, we maintain the overlap under the requested limit, not only inside each NB-IoT carrier but also among adjacent carriers. The reason we need to double the number of regions, with respect to the GS-T case, is that now the maximum distance of two UE part of adjacent groups will be 40 km. Finally, we will need an uplink bandwidth of $B = 20 * 180\ kHz = 3,6\ MHz$ for GS-F.

3.4 Numerical Results

The aim of this section is to validate the proposed scheduling techniques for our system architecture under consideration. To this aim, we implement in Matlab the PHY layer of an end-to-end NB-IoT over LEO satellite system, incorporating the technical specifications of NB-IoT standard [45, 50, 96] with the scheduling techniques, and evaluate the NPUSCH channel performance in terms of block error rate (BLER) versus signal to noise ratio (SNR). We use as a starting framework the already available NB-IoT Matlab toolbox [97] to simulate the NPUSCH uplink transmission. Since the toolbox is designed for a terrestrial NB-IoT

network and a point to point communication, needed modifications are implemented in order to adapt it with our scenario. The obtained results are then compared with the case of a perfect synchronous communication link and with the case where the GS approach is not used.

3.4.1 Simulator Design

The block diagram of our simulator is shown in Figure 3.9 and the main parameters are listed in Table 3.1. We consider a certain number of NB-IoT devices uniformly distributed in the coverage area that have data to transmit in the uplink through NPUSCH. The coding and SC-FDMA modulation follow the steps as described in the standard. We fix a single-tone transmission mode for all the users, since it corresponds to the worst case scenario (highest ICI). In addition, we fix the TBS size to be the same for all the users (not realistic) to facilitate the scheduling part of the different NPUSCH channels. This does not impact our simulator because the focus is to show the performance gain of GS-T and GS-F. Overall, the following steps are performed for the BLER calculation:

- The resource grids populated with NPUSCH from different UE is generated. Each NPUSCH will occupy 1 subcarrier in the frequency domain and 16 uplink slots (8

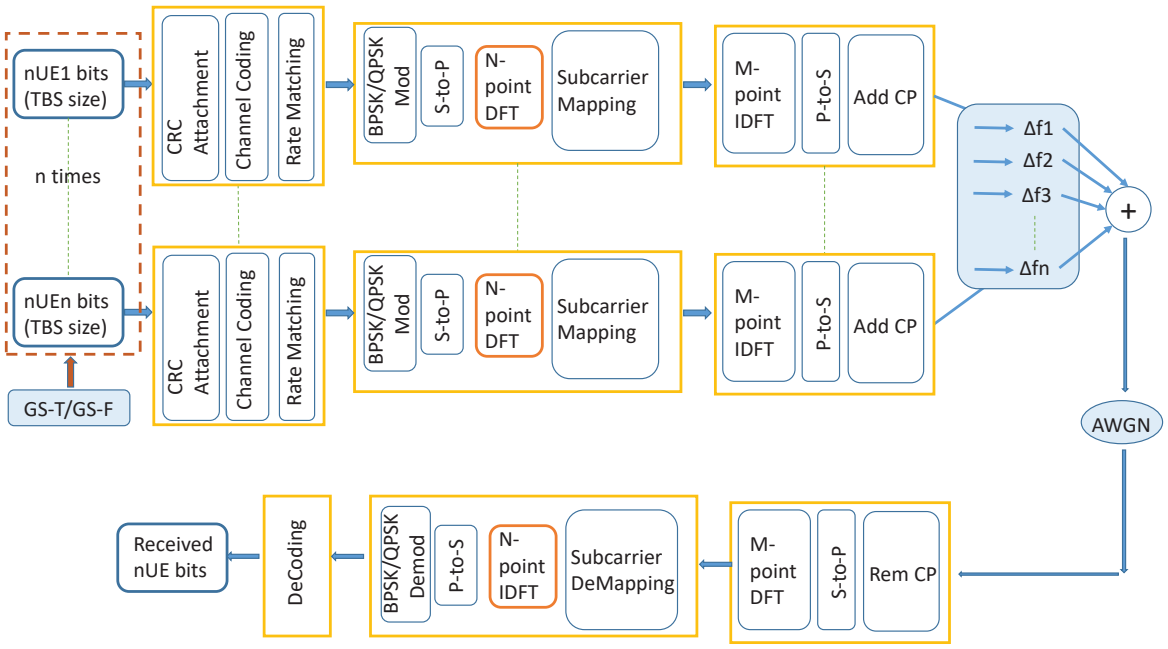

Figure 3.9: Block diagram of the baseband simulator.

Table 3.1: Parameters for NPUSCH Simulation.

Parameter	Value
N FFT	128
Bandwidth GS-T	180 kHz
Bandwidth GS-F	180(n+1) kHz
SCS	15 kHz
Modulation Format	single-tone SC-FDMA
Modulation Order	QPSK
Sub-carrier Mapping	Random with GS-T (GS-F)
Coding Scheme	1/3 Turbo Code
CRC Bits	24
NPUSCH Repetition	1
NRU	1
TBS size	88 bits
Channel	AWGN
HARQ	N/A

ms TTI) in the time domain (refer to Figure 2.4). This is the corresponding RU for single-tone operation. It can be noted that for GS-T, 12 users can be scheduled simultaneously, whereas for GS-F, $12(n+1)$ users can be scheduled, where n is the number of secondary NB-IoT carriers. Each NPUSCH will contain the useful transmitted bits (TBS), generated randomly, and other redundancy bits added by the coder part. Since the time-frequency resources for each NPUSCH are fixed, as mentioned above, changing the TBS will change the coding rate. However, throughout this simulation, we keep the $TBS = 72$ bits fixed. Last but, not least, we make sure that each UE occupies different subcarriers in the frequency domain and the choice of the subcarrier is random.

- The baseband waveform for each UE is then created through SC-FDMA modulation.
- A random Doppler shift is then applied to each waveform taking random values from [-440 +440] Hz for GS-T/GS-F and from [-4250 +4250] for the case of no GS. This allows to create the differential Doppler shift among carriers from [0 880] Hz for GS-T/GS-F and from [0 8500] Hz without GS (refer to Figure 3.4 and 3.7).
- The individual baseband waveforms are then summed up, though forming the final SC-FDMA waveform which now will be distorted due to the overlap among subcarriers and pass it through the AWGN channel.
- The receiver operations are performed and the corresponding NPUSCH coming from

different UEs are decoded.

- The performance of the NPUSCH is finally determined by counting the number of erroneous TBS. We run the simulations in order to assure at least 100 erroneous blocks for each SNR value.

Finally, we compare the obtained results with the case of a perfectly synchronous waveform. In fact, for such case, we just neglect the part where we apply the Doppler shifts among subcarriers which contain the NPUSCH channels, resulting in a perfectly orthogonal SC-FDMA waveform.

3.4.2 Performance Analysis

From the plotted results shown in Figure 3.10 and 3.11, it can be noted that the performance of the NPUSCH when we use GS-T is very close to the one where the waveform is perfectly synchronized. Without GS-T, the results demonstrate that we cannot have a reliable communication under the simulated SNR and the degradation of performance with respect to the perfectly synchronized waveform is huge.

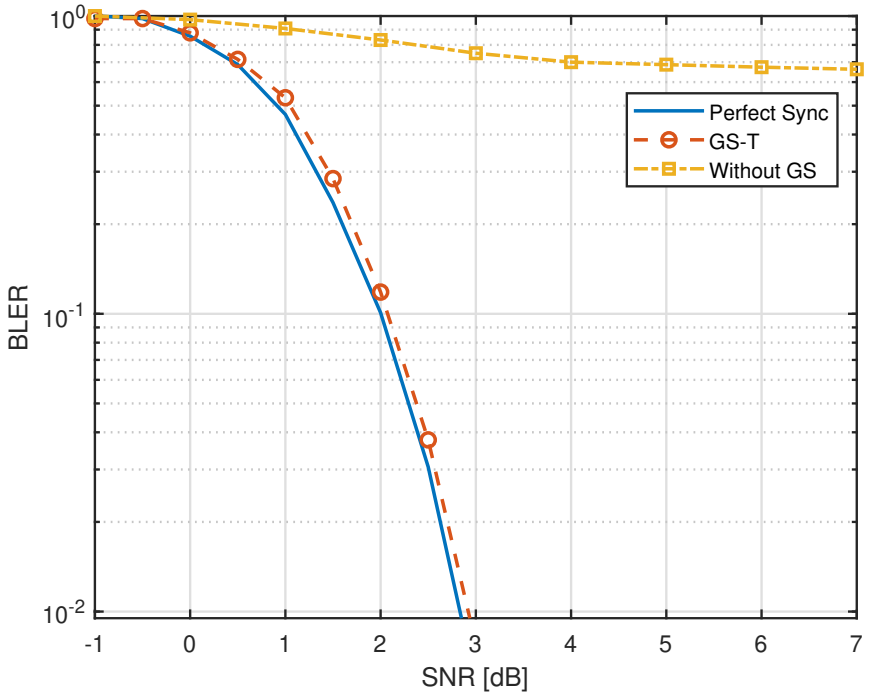

Figure 3.10: Simulation results for GS-T.

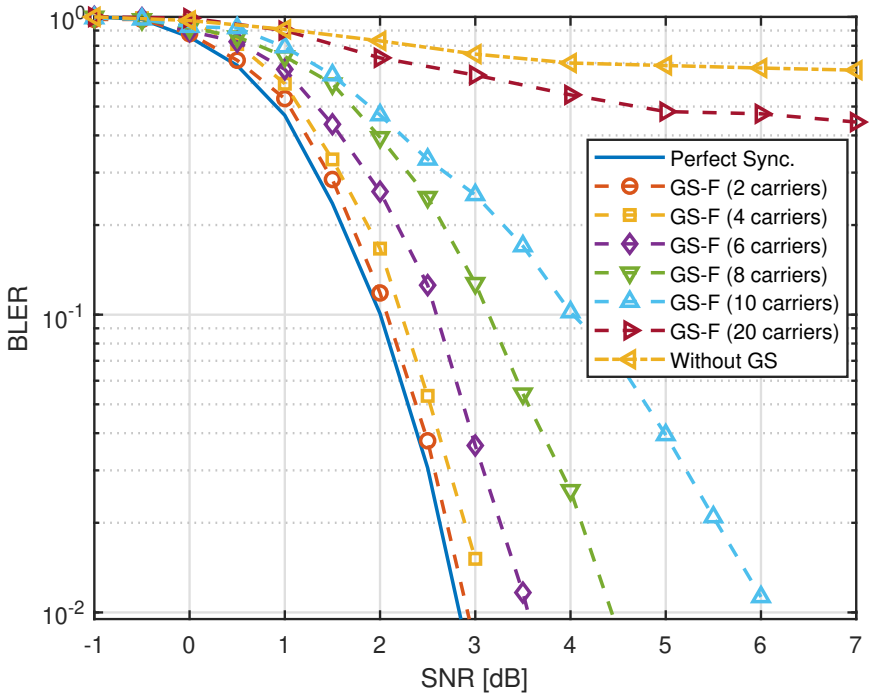

Figure 3.11: Simulation results for GS-F.

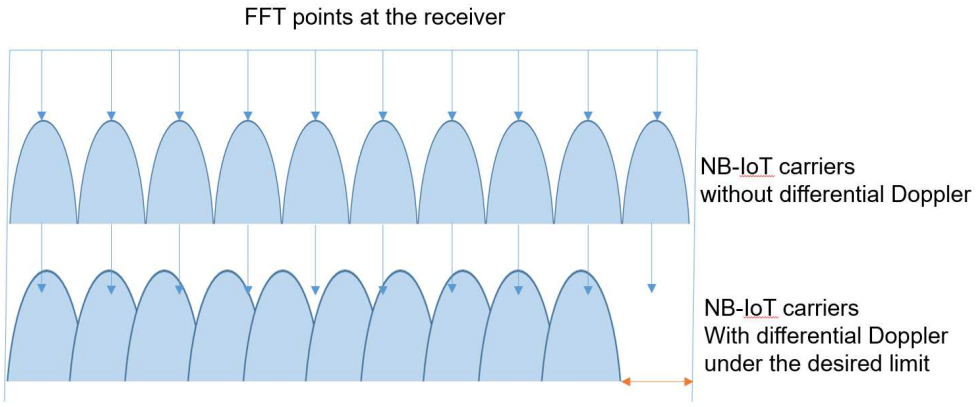

Figure 3.12: Bandwidth compression effect in GS-F.

On the other hand, using GS-F the performance is dependent on the secondary NB-IoT carriers that we use. The more secondary carriers we have, the more performance degradation the uplink transmission will experience. This is due to the band compression effect (due to Doppler spread) that will happen in our scenario (Figure 3.12). Even though by adding secondary carriers, we make sure that the differential Doppler remains under the supported limit, it will sum up and cause a shrink of the bandwidth, which the BS is not aware of and cannot compensate the timing drifts coming from it at the receiver. As a matter of fact,

without modifying the receiver the BS fails to decode and demodulate correctly the data when the number of secondary carriers is high. However, it is worth noting that by keeping the number of secondary carriers low, this effect will be relaxed and we can guarantee a reliable communication having a lower performance degradation with respect to the ideal case.

3.4.3 Link Budget Analysis

Another important aspect worth analysing is deriving the requirements at the space segment (satellite) from the power budget perspective in order to ensure reliable communication and matching the NB-IoT BLER target of 10^{-1}. To satisfy such requirement in the PHY layer, we have to guarantee that the following holds:

$$SNR_{received} \geq SNR_{required} \tag{3.21}$$

where the $SNR_{received}$ is the signal to noise ratio at the receiver, and the $SNR_{required}$ is the signal to noise ratio required to have a specific BLER target (10^{-1} for NB-IoT). Notably, the $SNR_{required}$ will directly depend on the MCS used for data transmission. For example, from the simulation results in Figure 3.10 and 3.10, we can extract the $SNR_{required}$ for ensuring the specific BLER target for both GS-T and GS-F strategies. However, these results are only for MCS level 6 (see Table 2.1) since we have used a TBS size of 88 bits and only 1 RU for data transmission. Extensive simulations are needed to derive the required SNR for all the possible values of MCS. Therefore, we repeat the simulations for different values of MCS for downlink and uplink transmission only for the GS-T strategy case. The simulation parameters and the simulation results are given in Table 3.2 and Table 3.3 respectively

Table 3.2: Simulation Parameters (GS-T).

Parameter	**Uplink MT**	**Uplink ST**	**Downlink**
N FFT	128	128	128
Bandwidth	(45, 90, 180) kHz	15 kHz	180 kHz
SCS (kHz)	15 kHz	15 kHz	15 kHz
Modulation Format	SC-FDM	SC-FDM	OFDM
Modulation Order	QPSK	BPSK, QPSK	QPSK
MCS Selection	Table 16.5.1.2-2 [50]	Table 16.5.1.2-2 [50]	Table 16.4.1.5.1-1 [50]
Coding Scheme	Turbo Code	Turbo Code	Turbo Code
CRC Bits	24	24	24
MCS range	0-13	0-10	0-13
Channel	AWGN	AWGN	AWGN

Table 3.3: Simulation Results (GS-T).

	Uplink MT		**Uplink ST**		**Downlink**	
MCS	$SNR(dB)$	SE (bit/s/Hz)	$SNR(dB)$	SE (bit/s/Hz)	$SNR(dB)$	SE (bit/s/Hz)
0	-5.8	0.1444	-4.2	0.2167	-5.8	0.1444
1	-4.9	0.2	-3.2	0.3	-4.9	0.2
2	-3.9	0.2667	-2.2	0.4	-3.9	0.2667
3	-3	0.324	-1.2	0.4867	-3	0.324
4	-2	0.3867	-0.1	0.58	-2	0.3867
5	-1.1	0.4844	0.9	0.7267	-1.1	0.4844
6	-0.2	0.5611	1.9	0.8417	-0.1	0.5733
7	0.7	0.6944	3.1	1.0417	0.6	0.68
8	1.4	0.7689	4.3	1.1533	1.3	0.7611
9	2.2	0.8722	5.6	1.3083	2.2	0.8722
10	3.1	0.9689	6.9	1.3887	3.1	0.9689
11	4.2	1.1244			4.2	1.1244
12	5.5	1.3889			5.5	1.3889
13	6.9	1.4333			6.9	1.4333

Please note that for each MCS we obtain the required SNR to close the link and derive the spectral efficiency (SE) by utilizing the following formula:

$$SE = \frac{TBS/TTI}{BW}(bit/s/Hz) \tag{3.22}$$

where TTI is the transmission time interval expressed in seconds and depends on the number of RUs (see Table 2.1) and the RU length (see Figure 2.4). It is worth emphasizing here that for each MCS level there exist various values for the TBS size and number of RUs, hence the SE provided in Table 3.3 represent the maximum reachable ones inside each MCS level. Having the $SNR_{required}$ in equation (3.21), we need to calculate the $SNR_{received}$ at the UE (downlink) or the BS (uplink). To do so, we use the following formula of the link budget, accounting for all the gains and looses in the propagation medium from transmitter to receiver and neglecting the interference:

$$SNR_{received}(dB) = EIRP(dBW) + \frac{G_r}{T}(dBi/K) - FSPL(dB) - A_{loss}(dB) - Ad_{loss}(dB) - K(\frac{dBW/K}{Hz}) - 10 \cdot log_{10}(BW) \tag{3.23}$$

Let us now clarify each of the above parameters one by one.

- $EIRP$ is the effective isotopic radiated power of the transmitting antenna and can be

calculated as:

$$EIRP = 10 \cdot log_{10}(G_T P_T) \tag{3.24}$$

where P_T is the transmitting antenna power and G_T is the gain.

- G_r/T is the figure of merit at the receiver having antenna gain G_r and equivalent system temperature T.

$$\frac{G_r}{T} = G_r(dBi) - NF(dB) - 10 \cdot log_{10}(T_o + (T_a - T_o) \cdot 10^{-0.1 \cdot NF}) \tag{3.25}$$

where G_r is the gain of the receiving antenna, NF represents the noise figure, T_o is the ambient temperature and T_a is the antenna temperature.

- $FSPL$ is the free space path loss given by

$$FSPL = 10 \cdot log_{10}(\frac{4\pi D}{c/f})^2 \tag{3.26}$$

with carrier frequency f, speed of light c and slant range D expressed as:

$$D = -R_E \cdot sin(\alpha) + \sqrt{R_E^2 \cdot sin(\alpha)^2 + h_s + 2 \cdot R_E \cdot h_s} \tag{3.27}$$

The slant range is the distance from the user device to the satellite and it can be noted from the formula that it is determined by the radius of Earth R_E, satellite elevation angle α and satellite altitude h_s.

- A_{loss} and Ad_{loss} represent the atmospheric looses due to gases, rain fades etc., and additional looses due to feeder link.

- BW is the communication bandwidth and K is the Boltzman constant.

By utilizing equation 3.23, it is possible to calculate the SNR at the receiver under specific system parameters, both in the downlink and uplink transmission. The user terminal parameters are the ones defined in the NB-IoT standard for 3GPP Class 3 devices [ref-tr36101], whereas the link parameters can be taken from the 3GPP specification for 5G over NTN [ref-R1-1903998], summarized in Table 3.4. Moreover, we leave on purpose undefined the satellite parameters (EIRP in downlink and G/T in uplink) because these are the ones that should be carefully designed before launching new satellites to support NB-IoT services or check

Table 3.4: Link Budget Parameters.

Link Parameters	Downlink	Uplink
Carrier Frequency (GHz)	2	2
Bandwidth (kHz)	180	15, 45, 90, 180
Subcarrier Spacing (kHz)	15	15
Satellite Altitude for LEO (km)	1200	1200
Minimum Elevation Angle (degree)	30	30
Atmospheric Loss (dB)	0.5	0.5
Additional Loss (dB)	1	1
Channel model	AWGN	AWGN
Terminal Parameters		
Terminal Type	3GPP Class 3	3GPP Class 3
Antenna Type	Omnidirectional	Omnidirectional
Receiver Antenna Gain (dBi)	0	-
Terminal Noise Figure (dB)	9	-
Terminal Ambient Temperature (K)	290	-
Terminal Antenna Temperature (K)	290	-
Terminal Transmit Power (dBm)	-	23
Terminal Transmit Antenna gain (dBi)	-	0

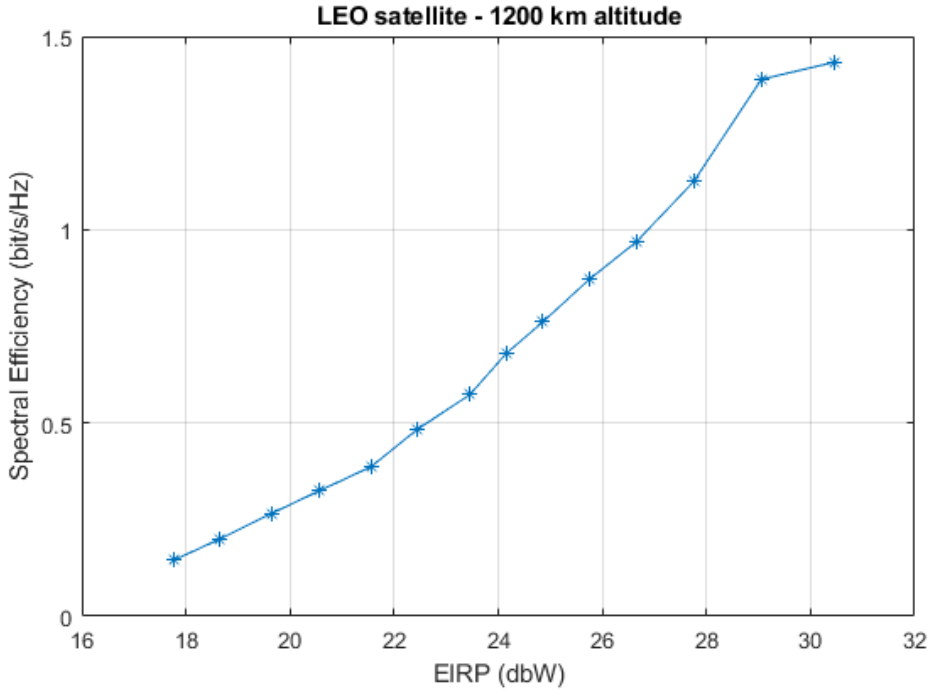

Figure 3.13: Link budget results for downlink transmission

whether the existing ones meet the power budget requirements. Changing these satellite parameters would directly affect the received SNR. By combining the simulation results shown in Tble 3.3 with equations (3.21) and (3.23), tt is possible to obtain the spectral efficiency

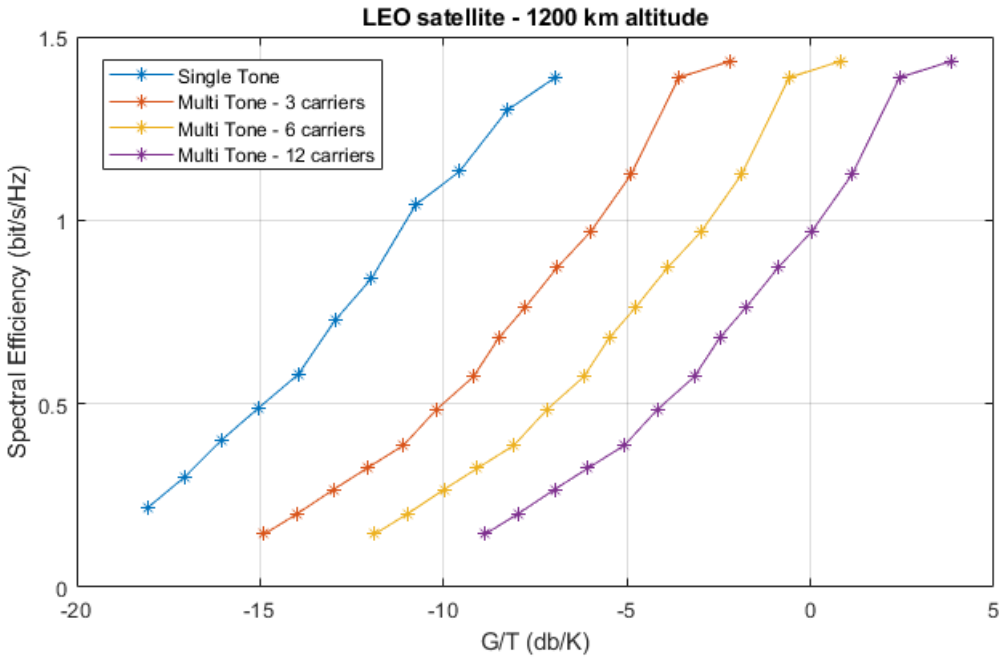

Figure 3.14: Link budget results for uplink transmission

as a function of satellite EIRP for downlink case and G/T for uplink case, as illustrated in Figure 3.13 and 3.14.

3.5 Conclusions

In this chapter, to solve the differential Doppler problem, an uplink scheduling technique has been proposed, able to mitigate the differential Doppler down to a value tolerable by the standard. In particular, by implementing GS-T and GS-F, the differential Doppler has been reduced from 8.5 kHz down to 880 Hz. The performance of the proposed schemes has been assessed through numerical simulations of the NPUSCH channel and has been compared with the case where the differential Doppler shift is not mitigated. The proposed scheduling technique has been validated and it has been demonstrated that the GS-T outperforms GS-F, since the latter has a dependency on the number of secondary NB-IoT carriers used for transmission. Last but not least, a link budget analysis has been performed. The link and device parameters were chosen in accordance with the latest 3GPP specifications, while the satellite parameters were left open for design. The achievable spectral efficiency as a function of satellite antenna EIRP and G/T were shown.

Chapter 4

An efficient resource allocation for uplink data transmission in NB-IoT via LEO satellite systems

In this chapter, we extend the user scheduling strategy treated in Chapter 3 and propose an efficient resource allocation that not only is capable of counteracting the differential Doppler problem, but also takes into account the distinct user channel conditions and data demands coming from various users. This is a crucial problem not previously treated in the literature, and the existing resource allocation algorithms for terrestrial systems are not suitable for the following reasons. First, with the movement of the LEO satellite, the corresponding channel parameters for each user will quickly change over time. Delaying the scheduling of a certain user would result in a resource allocation based on outdated parameters. Second, the differential Doppler shift directly depends on the relative distance among users, as we saw in the previous chapter. Scheduling at the same radio frame users that overcome a certain distance would violate the differential Doppler limit supported by the NB-IoT standard. Third, the propagation delay over a LEO satellite channel is around 4-16 times higher compared to a terrestrial system, imposing the need for message exchange minimization between the users and the base station. To this aim, we design a novel uplink resource allocation strategy, which jointly incorporates the technical peculiarities of the LEO satellite channel with the various channel conditions and different user requirements in terms of data to be transmitted. Extensive numerical results are performed in order to evaluate different performance trade-offs of our LEO satellite-based NB-IoT system.

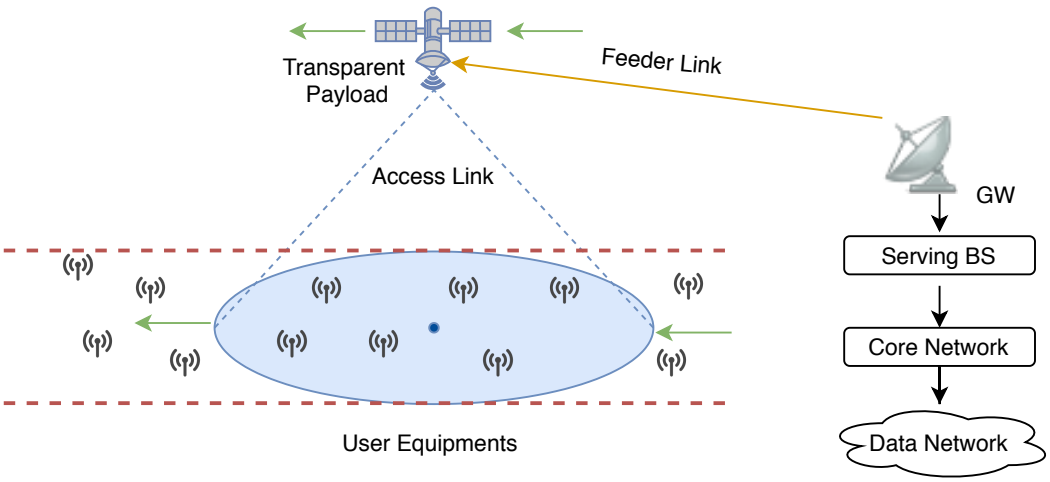

Figure 4.1: NB-IoT via LEO satellite system.

4.1 System Model & Assumptions

Regarding the system model, we consider a LEO satellite with a transparent payload, providing NB-IoT coverage to a certain number of on-ground UEs. The satellite acts as a relay providing the link between the UEs and the on-ground serving BS through the Gateway (GW). The air interface in the access and the feeder link is the same as the terrestrial one, based on the 4G Uu air interface or 5G New Radio (NR) one. This is because the NB-IoT protocol was initially standardized to be compatible with the 4G network, and later it was agreed to address the IoT traffic of the 5G as well. In either case, the technical specifications for the NB-IoT would be the same, only with different terminology for the network components. The BS is then connected to the 4G/5G Core and Data Network. Last but not least, we consider an Earth-moving cell, hence creating a dynamic system with users continuously entering/leaving the coverage area. The advantage of this cell type is that it does not require a steering mechanism for the satellite beam, resulting in lower satellite cost. Please note that this architecture option is already defined for the 5G non-terrestrial networks (NTN) in 3GPP [55], and an illustration is shown in Fig. 4.1. For our scenario, we make the following assumptions.

Fixed user location on Earth

We assume a scenario where the UEs have a deterministic location and no mobility is foreseen for them. This allows the BS to obtain the geographical coordinates of the users in the

deployment phase, and use this information to help in the radio resource allocation strategy.

Perfect pre/post compensation of the common Doppler shift at the GW

As we analyzed in Chapter 3, the Doppler shift in a LEO satellite channel can be subdivided into a common Doppler part, experienced by all the users under the same satellite footprint, and a differential Doppler part depending on the relative position of users in the footprint. While the common Doppler shift can be pre/post compensated at the GW since there is enough computational power to continuously estimate and track the position of the satellite, as also proposed in [60, 61], the same cannot be done at the user side. The low-complexity of the on-ground NB-IoT UEs is of utmost importance. Therefore, assuming an ideal compensation of the common Doppler shift (e.g. the one at the center of the beam) at the GW, leaves out only the differential Doppler shift impacting the transmissions among the BS and the UEs. It is worth reminding here that in the uplink transmission (UE $->$ BS), there exist the possibility of frequency multiplexing of channels (see Figure 2.5). Consequently, the differential Doppler shift among users will cause an overlap among sub-carriers inside the whole NB-IoT carrier, thus introducing the so-called inter-carrier interference (ICI). In contrast, in the downlink transmission, the whole NB-IoT carrier is dedicated to one channel, hence such an overlap does not occur.

Separation of access and data phases

As we discussed in Chapter 2, there may be different configurations of the NPRACH channel, which is the one responsible for the access phase. It is possible that the NPRACH occupies all the available frequency resources, or part of them (see Figure 2.5). In addition, the

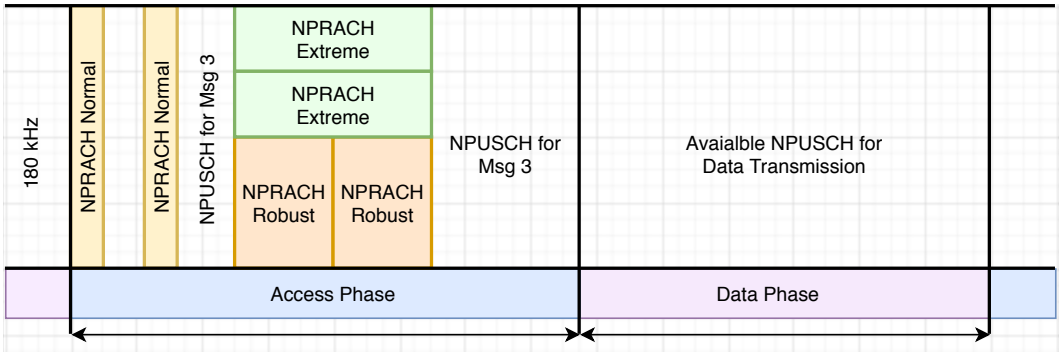

Figure 4.2: Example of access and data phase configuration in uplink.

time-duration of the NPRACH channel may be different depending on the targeted coverage class. Of course, the NB-IoT standard does not impose a fixed configuration, rather then give a possible set of parameters under which a certain operator should take into account when designing a system. In our NB-IoT over LEO satellite scenario, it is advantageous to avoid a frequency multiplexing of access and data channels due to the following reasons. First, it enables us to control the differential Doppler shift in the uplink transmission for the data phase, and the corresponding ICI imposed by it, through a resource allocation strategy. The same cannot be done in the access phase because the BS specifies only the NPRACH resources to be utilized, and then users randomly initiate the RA procedure based on their need to transmit data. Of course, overcoming the differential Doppler limit is also an issue to be addressed in the access channel, but it is out of the scope of this work. Second, having distinct operational phases helps in taking proactive "short-term" resource allocation decisions by considering only the latest users with a successful access phase (with the most accurate estimated parameters) to be scheduled in the following data phase. This is crucial for our highly dynamic system where the channel parameters would change quickly over time. In Fig. 4.2 we show an example of a possible access and data phase configuration. Obviously, the time-duration of the access phase and its periodicity would be open for design. Please note that the NPUSCH also plays a role in the access phase since it enables msg 3 transmission where the buffer status is reported.

4.2 Radio Resource Allocation Strategy

Resource Allocation Objectives

After the access phase over a certain random access opportunity (RAO), the BS will have to assign resources to users for the data phase. The parameters to be considered are: i) the buffer status reported in msg3 of the RA procedure, ii) the satellite coverage time derived by the UE location on Earth, and iii) the signal to noise ratio (SNR) estimate obtained during the message exchange in the RA procedure. Taking into account the peculiarities of our system, an efficient resource allocation strategy should have the following objectives:

Maximize the radio resource utilization The available resources for the data phase are limited, thus there is a need to maximize its utilization. A failure to do so would result

in wasted resources and decrease the efficiency of the overall system. Of course, this will also depend on how the access phase is designed in terms of length and periodicity. Since the scope of our work is to focus on the data phase, we consider a fully-loaded system in which there will be sufficient users after the access phase competing for the limited radio resources in the data phase.

Select the users to be scheduled Apart from assigning the time-frequency resources to the users, the BS has to efficiently select the users to transmit in the available radio frames. Certain users will have a shorter satellite coverage time depending on their location in the satellite footprint, hence there is a need that the BS should account for this when assigning resources because these users have a higher probability to be out of the coverage area in the subsequent data phase. Also, giving some priority to the users with better channel conditions would help in increasing the throughput, and consequently more data can be aggregated by the BS. In addition, the users with a higher buffer status may have a more urgent need to offload their data because the buffer size is limited and can lead to missed information due to overflows. A balance among the above-mentioned considerations is needed in order to satisfy the predefined key performance indicators (KPIs) of a certain system. Last but not least, to keep the differential Doppler limit under the allowed threshold, only particular users can be scheduled together in the same frame.

Minimize the message exchange between UEs and the BS As we already mentioned, in a terrestrial NB-IoT scenario, the BS can decide to empty the buffer of a certain user through subsequent NPUSCH transmissions. This may be advantageous in situations where the available resources are limited in a "short-term", and the data that the user has to transmit can be distributed over a longer time through a set of smaller NPUSCH transmissions. Nevertheless, the same approach cannot be followed for a LEO satellite-based NB-IoT scenario due to the highly dynamic nature of the overall system and the increased RTD in the satellite channel. Notably, every NPUSCH transmission requires the corresponding information regarding the resources to be utilized, which is reported in the NPDCCH. Consequently, the increased message exchanges between the user and the BS would further delay the system because of the considerably higher RTD compared to the terrestrial case. In addition, the estimated parameters under which the resource allocation would be performed may be outdated. For example, assigning the wrong MCS for a certain NPUSCH transmission, for

which the channel conditions are worsening over time due to the satellite movement, may result in an erroneous transmission. Therefore, it is highly crucial that the resource allocation strategy should maximize the amount of data encoded in a specific NPUSCH transmission aiming to empty the buffer status of the users in as few attempts as possible. Obviously, there are some boundaries imposed by the NB-IoT protocol which cannot be exceeded, such as the finite number of the MCS or the RUs available.

4.2.1 Problem Formulation

Let N denote the set of un-collided devices which perform a successful RA procedure after a specific access phase.After this step the BS will have the SNR estimate of each user UE_i, for $i = 1, 2, ..., N$, and has to guarantee that the following holds:

$$SNR_i^{rec} \geq SNR(MCS_i, N_i^{sc}) \tag{4.1}$$

where SNR_i^{rec} is the estimated SNR of the received signal and $SNR(MCS_i, N_i^{sc})$ is the SNR needed to close the link under a specific modulation and coding scheme MCS_i and number of subcarriers N_i^{sc} assigned for uplink data transmission. Please note that according to the NB-IoT standard, MCS_i can take discrete values from 0 to 13 (see Table 2.1), and the number of subcarriers N_i^{sc} can be 1, 3, 6 or 12. A table that relates these parameters can be found in [82], where the required SNR levels under different MCS_i and N_i^{sc} are obtained. Through a look up table, the serving BS can derive the possible options under which Eq. (4.1) would be satisfied.

Furthermore, after the access phase, each user will have an uplink request with data size $D_i > 0$, which it reports in Msg3 of the RA procedure. Since our goal is to minimize the message exchange between the UE and the BS, it is crucial to empty the buffer size in as few transmissions as possible. Therefore, we need to select the highest reachable MCS for each user. To derive the number of RUs needed for emptying the buffer size D_i of the i-th user, the following must hold:

$$N_i^{RU} = \begin{cases} \frac{D_i}{16 \cdot R[max(MCS_i)]}, & \text{if } N_i^{sc} = 1 \\ \frac{D_i}{24 \cdot R[max(MCS_i)]}, & \text{otherwise} \end{cases} \tag{4.2}$$

where $R[max(MCS_i)]$ is the average data rate of the maximum reachable MCS_i for the i-th

user expressed in bits/(subcarrier x slot). It should be noted that according to the standard, the maximum number of RUs $maxN_i^{RU} = 10$, so in case a larger number of RUs is needed to empty all the buffer, we chose the maximum one and the user will try to transmit the remaining data on the buffer in another access attempt. The only remaining parameter to be calculated is the duration of the NPUSCH channel w_i as follows:

$$w_i = N_i^{RU} \cdot \frac{N_i^{slot}}{2}(subframes) \tag{4.3}$$

where N_i^{slot} is the number of slots for each RU according to the standard.

$$N_i^{slot} = \begin{cases} 16, & \text{if } N_i^{sc} = 1 \\ 8, & \text{if } N_i^{sc} = 3 \\ 4, & \text{if } N_i^{sc} = 6 \\ 2, & \text{if } N_i^{sc} = 12 \end{cases} \tag{4.4}$$

Please note that two consecutive slots form one subframe. So basically, after solving equation (4.1), (4.2), (4.3), (4.4) the base station will have the NPUSCH representations for all the users with a successful access phase in terms of number of subcarriers in the frequency domain and number of subframes in the time domain. An example is illustrated in Fig. 4.3. As it can be noted, there may be more than one option in the time-frequency domain for the NPUSCH representation. Obviously, this will depend on the channel conditions. Some users with a successful access phase may close the link only for single-tone transmission, whereas others may have a reliable communication with the BS even for multi-tone. The more subcarriers are utilized for data transmission by the UE, the more difficult it is to close the link because the same power of the UE will be distributed over a larger bandwidth (as treated in Chapter 3). Notably, this results in shorter channels in time due to Eq. (4.4). So far, we have addressed only one of the resource allocation objectives, which was to minimize the message exchange among UE and BS, through selecting the highest reachable MCS and number of RUs depending on the user channel conditions and buffer status report.

The problem to be solved now is how to efficiently select the scheduled user set which optimize the available resource utilization in the data phase. This can be modeled as a packing problem, since we have to select a set of rectangles (users), which best fit in another rectangle (available resources for NPUSCH transmission), and maximizes a certain profit function (to

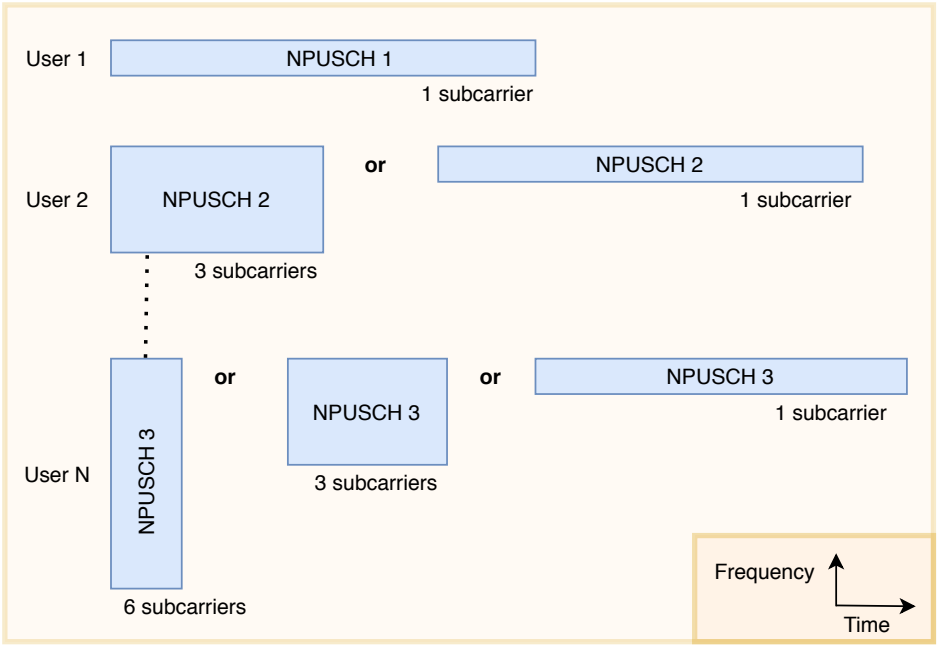

Figure 4.3: Time-frequency representations of users.

be designed). Our specific problem falls into the 0-1 Two-dimensional Knapsack Problem (KP). It is a 0-1 KP because we have to select or reject a user from scheduling in the current data phase, and 2D-KP because we have to assign the exact time-frequency resources for each scheduled user. Since we have discrete values for the frequency (subcarriers) and time domain (subframes), we can formulate the problem as an integer linear programing (ILP) model as follows.

Let P_i be the profit of selecting the i-th user for scheduling in the data phase, $X = \{p \in Z | 1 \leq p \leq W\}$ represent the time domain and $Y = \{q \in Z | 1 \leq q \leq B\}$ the frequency domain. By defining z_{ipq} and g_{ij} as follows:

$$z_{ipq} = \begin{cases} 1, & \text{if } UE_i \text{ is selected for scheduling with} \\ & \text{its left bottom corner (p,q)} \\ 0, & \text{if } UE_i \text{ is not selected for scheduling} \end{cases} \tag{4.5}$$

$$g_{ij} = \begin{cases} 0, & \text{if } UE_i \text{ belongs to group } G_j \\ 1, & \text{otherwise} \end{cases} \tag{4.6}$$

we are able to mathematically formulate our problem through equation (4.7) - (4.13).

$$\max_{Z} \sum_{i=1}^{N} \sum_{p \in X} \sum_{q \in Y} P_i \cdot z_{ipq} \tag{4.7}$$

subject to

$$\sum_{i=1}^{N} \sum_{\{p \in X | r - w_i + 1 \leq p \leq r\}} \sum_{q \in Y} b_i \cdot z_{ipq} \leq B \qquad \forall r \in X \tag{4.8}$$

$$\sum_{i=1}^{N} \sum_{p \in X} \sum_{\{q \in Y | s - b_i + 1 \leq q \leq s\}} w_i \cdot z_{ipq} \leq W \qquad \forall s \in Y \tag{4.9}$$

$$\sum_{i=1}^{N} \sum_{\{p \in X | r - w_i + 1 \leq p \leq r\}} \sum_{\{q \in Y | s - b_i + 1 \leq q \leq s\}} z_{ipq} \leq 1 \qquad \forall r \in X, \forall s \in Y \tag{4.10}$$

$$\sum_{p \in X} \sum_{q \in Y} z_{ipq} \leq 1 \qquad \text{for i = 1,2, ... N} \tag{4.11}$$

$$z_{ipq} \in \{0, 1\} \qquad \text{for i = 1,2, ... N, } p \in X, q \in Y \tag{4.12}$$

$$\sum_{j=1}^{M} \sum_{i=1}^{N} \sum_{\{p \in X | r - w_i + 1 \leq p \leq r\}} \sum_{q \in Y} g_{ij} \cdot z_{ipq} = 0 \qquad \forall r \in X \tag{4.13}$$

Please note that B is the available bandwidth expressed in subcarriers (12 in our NB-IoT scenario) and W the available subframes for the data phase. Fig. 4.4 may be helpful to understand the other parameters of equation (4.7) - (4.13). The objective function (4.7) represents a scheduling pattern of maximum profit. Constraints (4.8) ensures that for any subframe, the sum of the assigned bandwidths b_i of the scheduled users (utilizing the particular subframe) does not exceed the maximum bandwidth available B. In analogy, constraint (4.9) ensures the same, but in the other dimension. The non-overlapping constraints are given in (4.10), imposing any point (r, s) of the time-frequency grid is utilized by one and only one user. Constraint (4.11) is related to the fact that each user can be scheduled no more than once. The variables domain is given by (4.12). Last but not least, constraint (4.13) ensures that at any subframe only users belonging to the same group can be scheduled together. The groups are created in such a way that users inside the same group G_j do not violate the differential Doppler limit. The higher the distance among users along the x-axis (corresponding to the satellite movement direction), the higher the differential Doppler would be, whereas the contribution of the y-axes is negligible (as we saw in Chapter 3). Depending on the configurations of a particular system (carrier frequency, satellite altitude etc.), the

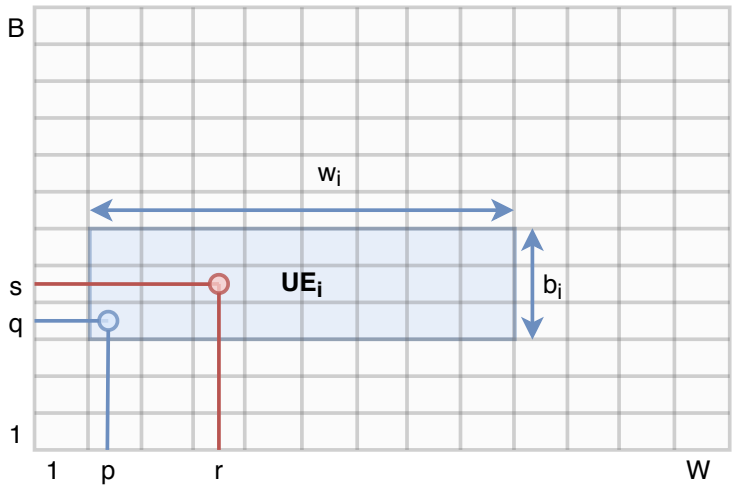

Figure 4.4: Scheduling a user in the available resources.

maximum tolerated distance along x-axes can be calculated. This allows us to create fixed groups of users in the satellite footprint as demonstrated in Fig. 4.5. The problem to be solved (4.7) - (4.13) is strongly NP hard and thus any dynamic programming approach would result in strictly exponential time bounds. It is crucial to further simplify the problem.

The problem can be relaxed by removing the last constraint (4.13) and solving (4.7) - (4.12) for each of the user groups G_j separately. Of course, this would require an optimal time resource share W_j among different groups, obtained by solving the following problem. Let

$$S_j = \sum_{i \in G_j} P_i \tag{4.14}$$

be the profit for the j-th group created in the satellite footprint given by the sum of the profits of every user inside that particular group. Then find:

$$\max_{w_j} \min_{j} \frac{W_j}{S_j} \tag{4.15}$$

subject to

$$\sum_{j=1}^{M} W_j \leq W \tag{4.16}$$

$$W_j \in \mathbb{N} \qquad \forall j \in 1, 2, ..., M \tag{4.17}$$

where M is the number of created user groups. This can be quickly solved through linear programing. The remaining problem (4.7) - (4.12) would be a typical 2D-KP where the

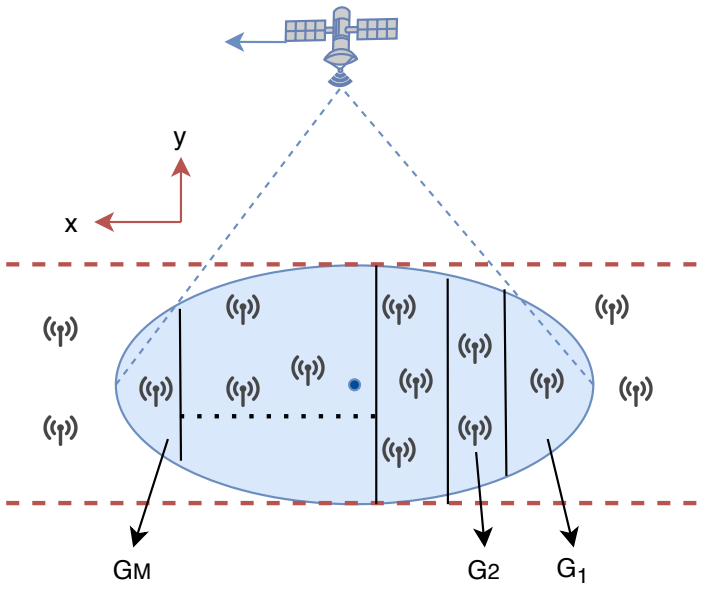

Figure 4.5: Satellite footprint divided in smaller regions.

items are not allowed to rotate. The main algorithms in the literature that find the exact solutions for this type of problems can be found in [98–100]. However, the proposed solutions can quickly converge only for small number of items. The largest problem they solve is for $N = 50$. It is worth highlighting here that in our scheduling problem the number of users to be scheduled competing for the available resources can be higher than 50, even in the case or smaller groups. In addition, for every user there may be more than one representation, significantly increasing the search space, and consequently the complexity of the problem. Therefore, it is essential to reduce the complexity of the problem as much as possible intending to accommodate the high dynamicity of the system.

To further relax the problem, it is possible to fix the transmission mode only to single-tone. In other words, this would mean that the UEs can transmit only utilizing 1 subcarrier in the frequency domain. This approach is also advantageous from the link-budget perspective since the available power at the user is distributed over a narrower bandwidth, as we calculated in Chapter 3. Fixing the allowed transmission mode only to single-tone would transform our 0-1 2D-KP into a 0-1 Multiple Knapsack Problem (MKP). This is a 1D problem because the only parameter deciding the item representation is the time-length while the frequency is fixed, and it is a multiple knapsack because there will be B subcarriers (or knapsacks) where users can be scheduled. The problem to be solved would be how to optimally select B

disjoint subset of users to be scheduled in the B available subcarriers without exceeding the knapsack capacities (available time for data phase). Mathematically it can be written:

$$\max_{z} \sum_{i=1}^{B} \sum_{k=1}^{N_j} P_k \cdot z_{ik} \tag{4.18}$$

subject to

$$\sum_{k=1}^{N} w_k \cdot z_{ik} \leq W_j \qquad \text{for } i = 1, 2, ..., B \tag{4.19}$$

$$\sum_{i=1}^{B} z_{ik} \leq 1 \qquad \text{for } k = 1, 2, ..., N_j \tag{4.20}$$

$$z_{ik} \in \{0, 1\} \qquad \text{for } i = 1, 2, ...B, \quad k = 1, 2, ..., N_j \tag{4.21}$$

where

$$z_{ik} = \begin{cases} 1, & \text{if } k\text{-th UE is selected to be scheduled} \\ & \text{in the } i\text{-th subcarrier} \\ 0, & \text{otherwise} \end{cases} \tag{4.22}$$

N_j and W_j are the number of users and the available time for data phase of the j-th user group. Evidently, the problem has to be solved for each of the user groups (see Fig. **??**). The re-formulated problem (4.18) - (4.21) is less complex because we have fixed one of the dimensions and reduced the search space. Every user to be scheduled will have only one representation (instead of many as depicted in Fig. 4.3) given only by its NPUSCH time-length.

4.3 Solutions to the Resource Allocation Problem

4.3.1 Exact Solution

For the exact solution of the 0-1 MKP, we refer to the method proposed in [101] where an exact algorithm is presented, particularly designed for solving large problem instances. In general terms, this algorithms utilizes three main steps shown below:

- **Derive an upper bound:** The algorithm utilizes the surrogate relaxation to derive an upper bound, through relaxing constraint (4.20). Doing so, the 0-1 MKP prob-

lem will be converted in an ordinary 0-1 KP, easily solvable through dynamic linear programming:

$$\max_{z'} \sum_{j=1}^{N_j} P_k \cdot z'_k \tag{4.23}$$

subject to

$$\sum_{k=1}^{N_j} w_k \cdot z'_k \leq B \cdot W_j \tag{4.24}$$

$$z'_k \in \{0,1\} \qquad \text{for } k = 1, 2, ..., N_j \tag{4.25}$$

where the introduced decision variable $z'_k = \sum_{i=1}^{B} z_{ik}$ indicates whether the k-th user is chosen for scheduling in any of the subcarriers (knapsacks) and the new knapsack capacity (data phase time-length) $W' = B \cdot W_j$ is given by the capacity of the united knapsacks.

- **Derive a lower bound:** The lower bound is obtained by splitting the chosen users after equation (4.23) - (4.25) for the united knapsack into the B individual knapsacks. This is done by solving a series of Subset-sum Problems as follows:

$$\max_{z} \sum_{k=1}^{N'_k} w_k \cdot z_k \tag{4.26}$$

subject to

$$\sum_{k=1}^{N} w_k \cdot z_k \leq W_j \tag{4.27}$$

$$z_j \in \{0,1\} \qquad \text{for} j = 1, 2, ..., N'_j \tag{4.28}$$

where N'_j is the number of users in the subset (not to be confused with N_j) from the optimal solution z' of problem (4.23) - (4.25). It can be noted that this problem tries to fit as many items (from the ones selected by the upper bound solution) as possible in every individual knapsack.

- **Bound and bound (B&B) algorithm:** This algorithm is a particular tree-search technique which utilizes the lower bound calculation to determine the branches to follow in the decision tree. If at any tree node, through the lower bound calculation procedure,

we are able to fit all the selected items (after solving upper bound) into the B knapsacks, the lower bound equals the upper bound, and we may immediately backtrack. There is no need to explore other tree nodes because the optimal solution is found. Otherwise a feasible solution is obtained which contains some (but not all) of the items, and the algorithm continues by exploring other tree nodes considering other items.

Notably, how fast this algorithm converges to the optimal solution will depend on the particular problem instance, and the quality of the obtained upper bound. Taking into account equation (4.3) and (4.4), and the fact that we fix the transmission mode only to single-tone, we can observe that the possible time-length of the users w_k to be scheduled will be:

$$w_k = 8 \cdot N_k^{RU}(subframes) \tag{4.29}$$

Regardless of the users we select to schedule, their merged time-duration will be a multiple of 8. Having knapsack capacities W_j that are not a multiple of 8, will lead to radio resource wastage and a week upper bound calculation (slowing down the convergence of the B&B algorithm). As a result, it is crucial for our scenario to take advantage of this feature and impose it in equation (4.15) - (4.17), where we obtain the available time shares (W_j) among different groups. Changing constraint (4.17) to:

$$W_j \in 8\mathbb{N} \qquad \forall j \in 1, 2, ..., M \tag{4.30}$$

will not only avoid resource wastage, but also significantly improve the upper bound calculation in (4.23) - (4.25), resulting in a faster convergence of the B&B algorithm.

4.3.2 Greedy Algorithm

This is a quick procedure to find a feasible solution as proposed in [102]. The first step is to order the items according to their profit per unit weight:

$$\frac{P_1}{w_1} \geq \frac{P_2}{w_2} \geq ... \geq \frac{P_{N_j}}{w_{N_j}} \tag{4.31}$$

Then the items are consecutively inserted into the knapsack until the first item, s, is found which does not fit. This is called the critical item.

$$s = min\Big\{l : \sum_{k=1}^{l} w_k > W_j\Big\} \tag{4.32}$$

The greedy algorithm is firstly applied to the first knapsack, then to the second one by using only the remaining items, and so on. Through this procedure, the overall profit G of the selected users to schedule would be:

$$G = \sum_{i=1}^{B} \sum_{k=s_{i-1}}^{s_i-1} P_k \tag{4.33}$$

Obviously, the greedy algorithm will most probably waste resources. When a critical item is found, the remaining capacity of the i-th knapsack $\overline{W_j}$ (remaining available time for users to schedule in the i-th subcarrier) will be empty.

$$\overline{W_j} = W_j - \sum_{k=s_{i-1}}^{s_i-1} w_k \tag{4.34}$$

However, this is a good algorithm for maintaining very low complexity since it moves only forward (index i and k in equation (4.33) always increasing).

4.3.3 Approximate Solution

Exploiting also the unique features of our scenario, it is possible to further improve the solution of the greedy algorithm. The one that we propose here consist in four main steps:

- **Step 1:** Order the items according to their profit per unit weight as in equation (4.31).
- **Step 2:** Merge the B knapsacks into 1 with single capacity $W' = B \cdot W_j$ and solve it through the Greedy algorithm. The advantage of this approach is that it reduces the resource wastage compared to the case where you have to apply the Greedy algorithm for each individual knapsack.
- **Step 3:** Re-sort the selected items according to their weight w, in a decreasing order. This is important since we want to place in each knapsack the "bad" items first with the highest weights w, in order to leave the "good" items (with low weight) at the end.

Please note that the more items we place in the knapsack, the smaller the remaining capacity would be. Therefore, getting rid of the items with high weight first while the capacity is still large will increase the probability of fitting the remaining items with lower weights into each individual knapsack.

- **Step 4:** Place the items into the knapsacks according to the order in Step 3, and at every iteration select the knapsack with the maximum remained capacity $\overline{W_j}$.

Notably, this algorithm tries to imitate the steps of the exact solution, but with reduced complexity, since we derive an upper bound (4.23) - (4.25) through the Greedy algorithm, and then attempt to separate the selected items of the upper bound solution into B individual knapsacks through heuristics. Specifically, the complexity of the approximate solution is $O(n \log n)$ for sorting plus $O(n)$ for placing the items into the knapsacks. Although this represents the same complexity as the Greedy algorithm, the running time would be higher because the sorting procedure and the item placement is repeated more than once.

4.4 Numerical Results

4.4.1 Comparison Among Algorithms

To compare among the algorithms, we solve our 0-1 MKP problem (4.18) - (4.21) in a hypothetical scenario where many users compete for scheduling in the available data phase. For the numerical simulations, we use the parameters summarized in Table 4.1. Please note

Table 4.1: Simulation Parameters for algorithm comparison.

Parameter	Value
User Profit P_k	Integer values randomly selected inside the range [1 1000]
User Weights w_k **expressed in SF**	{8, 16, 24, 32, 40, 48, 64, 80} SF According to Table 2.1 and Eq. (4.3) and (4.4)
Number of Knapsacks B **fixed for NB-IoT**	12 (subcarriers)
Knapsack Capacity W_j **expressed in SF**	160 SF
Number of Users N **to be scheduled**	[150 500]
Number of Iterations (problem instances)	1000

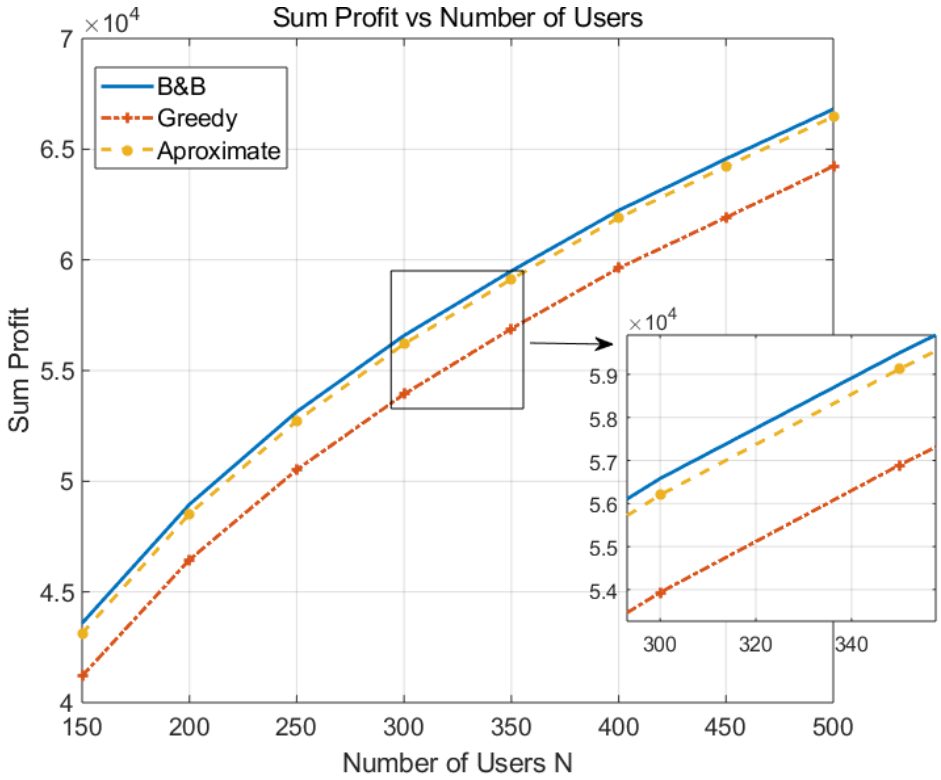

Figure 4.6: Average sum profit under different number of users.

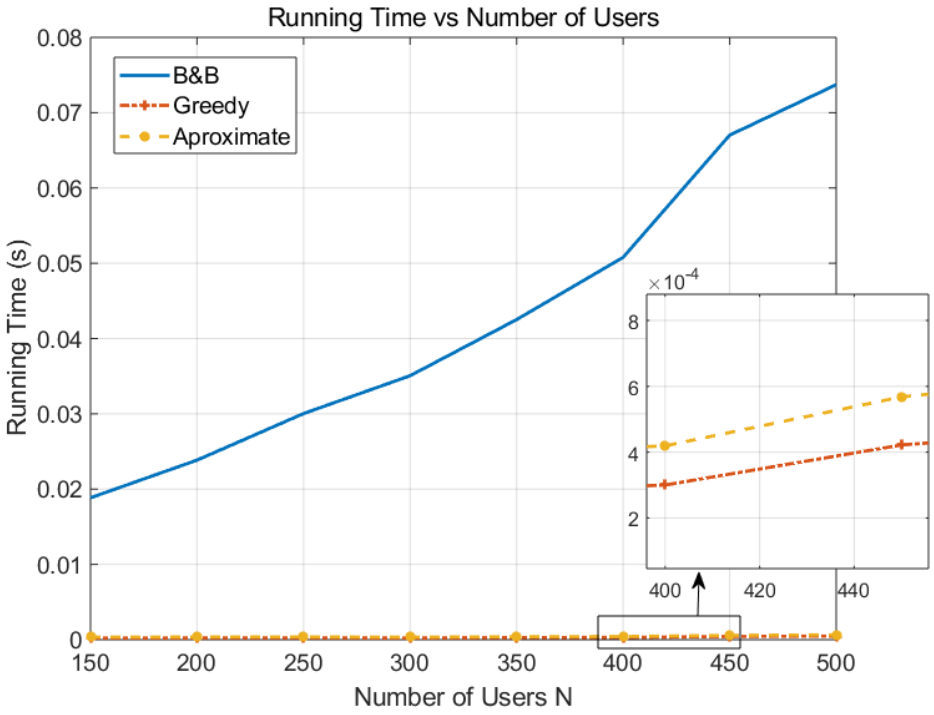

Figure 4.7: Average running time under different number of users.

that we run the algorithm for different problem instances and average over the whole number of iterations with the aim of obtaining the average sum profit and the average running time required by the three different algorithms, as demonstrated in Fig. 4.6 and 4.7. Also, we make sure to select a knapsack capacity W_j large enough to avoid user exclusion, and the number of users N large enough to avoid trivial solutions where all the users can be scheduled together. Last but not least, we assume the candidate users with a successful access phase belong to the j-th group, thus the differential Doppler limit inside the radio SF is not violated.

As it can be noted, the optimal solution is given by the B&B algorithm, through which the maximum sum profit is obtained. Nevertheless, its higher complexity requires more time to converge to the optimal solution compared to the other investigated algorithms in this paper. The Greedy algorithms gives the worst results in terms of sum profit, but the best ones in terms of running time. Our proposed Approximate solution performs very close to the exact one in terms of sum profit, and very close to the Greedy one in terms of running time. This is due to the fact that the knapsack capacities $\overline{W_j}$ and the user weights w_k are correlated (both multiple of 8). For other problem instances, with very random capacities and weights, the performance of this algorithm would be comparable to the Greedy one.

Using the best possible algorithm for the resource allocation problem, as shown in the previous section, does not guarantee the efficiency of the overall NB-IoT system, which will greatly depend on the way we assign priorities (profits) to various users. In addition, it is crucial to define specific key performance indicators (KPIs) for our NB-IoT via LEO satellite system, as a means to find optimal operational points in the profit function design and compare among different algorithms.

4.4.2 Simulation Setup

To perform simulations, we consider a dynamic scenario where a LEO satellite with altitude h is moving over a specific geographical area of interest with length L and width D. The latter corresponds also to the diameter of the satellite footprint (cell) ob ground (please refer to Fig. 4.8). The users are uniformly distributed over the geographical area of interest with coordinates (x;y). Based on their specific locations, every user will have a certain overall coverage time by the satellite t_{sat}. In addition, the satellite altitude h will also determine its periodicity over the geographical area of interest. Regarding the traffic model, we use the one defined in the 3GPP for the IoT applications [44]. Users will generate packets following

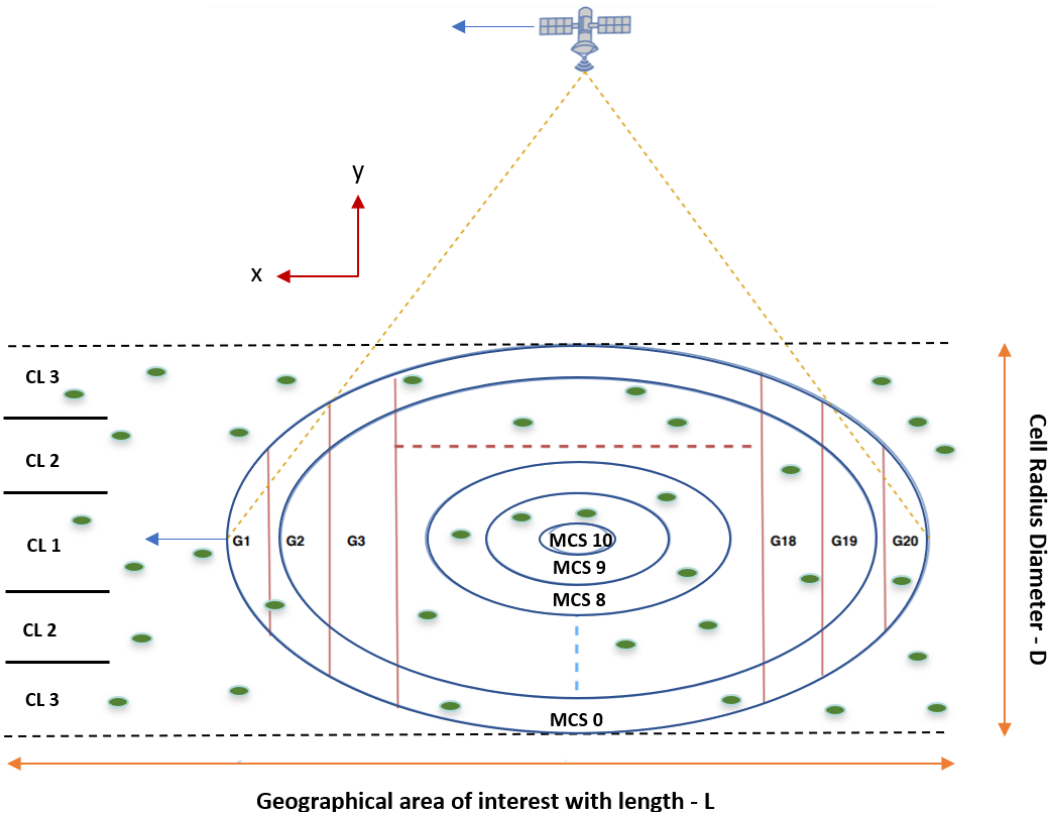

Figure 4.8: Reference Scenario for Numerical Simulations.

a Pareto distribution with shaping parameter $\alpha = 2.5$ range between 20 and 200 Bytes. The periodic inter-arrival time of new generated packets is: 1 day (40 %), 2 hours (40 %) , 1 hour (15 %), and 30 minutes (5 %).

4.4.3 Profit Function Definition

To assign profits to different users, the BS has to be based on the estimated/known parameters. As we stressed out in Section 4.2, these parameters include a) the buffer status reported msg3 of the RA procedure, b) the satellite coverage time derived by the user location of the users on-ground and c) the SNR estimate obtained during the message exchange in the access phase. The SNR estimate of the signals transmitted by various users will greatly depend by the satellite antenna parameters and the antenna beam pattern, whereas the ones of the NB-IoT devices will be the same as in the terrestrial case. To simplify our simulator, we assume that the antenna at the satellite is designed in such a way that allows transmission at MCS 0 for the users in the edge of the satellite footprint, and at MCS 10 (which is the maximum reachable MCS for single-tone transmission) for the users in the center of the footprint. Two

contributors towards this SNR change among users at the satellite beam edge and center are the difference in the propagation path loss and satellite antenna gain. While we can calculate the former one, the latter would depend on how the satellite antenna is designed. However, this assumption does not impact our analysis, since our goal is to find a simple way in representing a fair (reasonable) SNR change among users on ground for our simulator. Through this assumption, it is possible to obtain the maximum reachable MCS for every user just by utilizing their specific coordinates in the geographical area of interest. In a realistic scenario, the BS would have to rely on the SNR estimate in the access phase. Overall, the profit function would have the following form:

$$P_k = \alpha \frac{D_k}{max(D)} + \beta \frac{1 + MCS_k}{1 + max(MCS)} + \gamma(1 - \frac{t_k^{sat}}{max(t_k^{sat})}) \tag{4.35}$$

where the first term driven by the parameter α assigns priority to the users with higher buffer status D_k, the second driven by β to the ones with higher SNR values (and consequently MCS_k), and the third one driven by γ to the users with lower satellite coverage time t_k^{sat}. Obviously, the closer are the users to the edges of the geographical area of interest, the smaller would be the satellite coverage time, thus is crucial to take this into account. Furthermore, users with better channel conditions guarantee a higher throughput. Whereas, the advantage of scheduling users with higher buffer status is to avoid data expiration. Varying α, β and γ will result in different KPIs, which we will define in the following section.

4.4.4 KPI Definition

The first important KPI to evaluate our system is the achievable throughput for the data phase given by:

$$R = \frac{T_{bits}}{n \cdot W \cdot m} \tag{4.36}$$

where W is the available time (converted in ms, 1 SF = 1 ms) between two access phases for data transmission, n is the number of data phases during one satellite passage over the geographical area of interest and m is the number of satellite passages. The total transmitted bits during this time is given by T_{bits}. In addition to the throughput, it is important to guarantee a fair distribution of service among users in the geographical area of interest. To do so, we define the second KPI as follows. Let $u_k = s_k/d_k$ be the satisfaction ratio per user k, where s_k represents the sent bits by the k-th user in the overall data phase opportunity

and d_k is the demand in bits (sum of packets generated with time). Then, to compute the user fairness, we utilize the Jain's index give by:

$$J = \frac{(\sum_{k=1}^{N} u_k)^2}{N \cdot \sum_{k=1}^{N} u_k^2} \tag{4.37}$$

where N is the number of users in the geographical area of interest. In addition to the user fairness given by equation (4.37), there is a need for a third KPI, which gives an indication on the fairness among different coverage levels. Obviously, in our area of interest, there will be users with always bad coverage conditions, which are the most difficult ones to serve. A high user fairness J does not guarantee that the service is fairly distributed among various coverage levels. We define three coverage levels (CL), in analogy to the terrestrial NB-IoT case. Users with good coverage condition (CL 1) will be the ones reaching MCS 7 - 10, medium coverage (CL 2) reaching MCS 3-6, and bad coverage (CL 3) reaching MCS 0-2 (refer to Figure 4.8). We utilize again the Jen's formula for measuring the fairness in different CL expressed as:

$$J_{CL} = \frac{(\sum_{i=1}^{N_{CL}} U_i)^2}{N_{CL} \cdot \sum_{i=1}^{N_{CL}} U_i^2} \tag{4.38}$$

where N_{CL} represents the number of the CL, $U_i = (\sum_{k=1}^{N_i} s_k)/(\sum_{k=1}^{N_i} d_k)$ is the group satisfaction given by the ratio of the total transmitted bits with the total generated bits from the users in a certain CL. Please note that N_i is the number of users inside the i-th CL.

4.4.5 Performance trade-offs evaluation

To evaluate the performance of our system, we perform numerical simulations in MATLAB using the simulation parameters summarized in Table 4.2. Please note that for the selected carrier frequency of 2 GHz, the maximum distance along x-axis that does not violate the

Table 4.2: Simulation Parameters for system level analysis.

Parameter	**Value**
Geographical area length L	4000 km
Satellite beam diameter D	400 km
Satellite altitude h	1200 km
NB-IoT Carrier Frequency	2 GHz
Data phase time W	3600 SF (ms)
Number of satellite passages m	480
Number UEs in the geographical area N	600 000

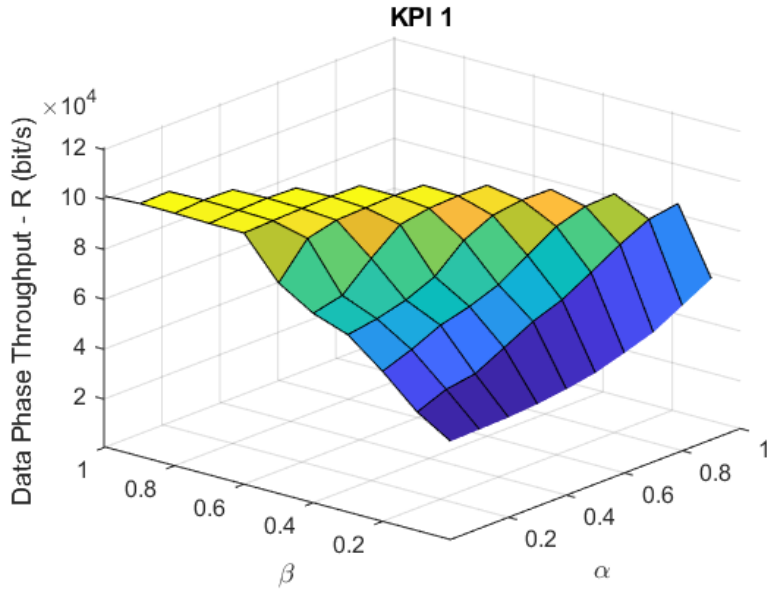

Figure 4.9: Data phase throughput - maximum at $\alpha = 0.2$, $\beta = 0.7$, $\gamma = 0.1$. (Note: $\alpha + \beta + \gamma = 1$).

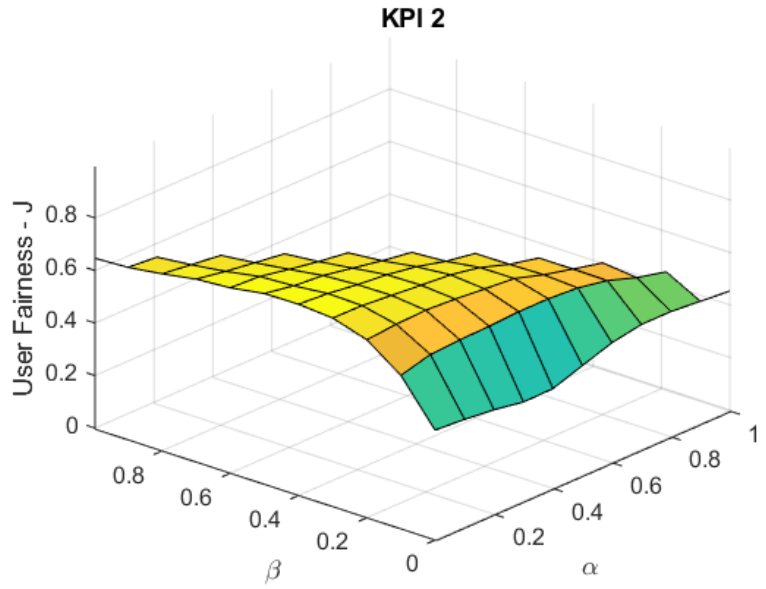

Figure 4.10: Jen's index for user satisfaction - maximum at $\alpha = 0$, $\beta = 0.4$, $\gamma = 0.6$. (Note: $\alpha + \beta + \gamma = 1$).

differential Doppler limit is 20 km [80]. This means that there will be 20 user groups needed for our scenario. Selecting a higher frequency would result in a bigger number of user groups and vice versa. The simulation results are shown in Fig. 4.9, 4.10 and 4.11. As it can be noted, maximizing the data phase throughput is mainly driven by the parameter β. This is

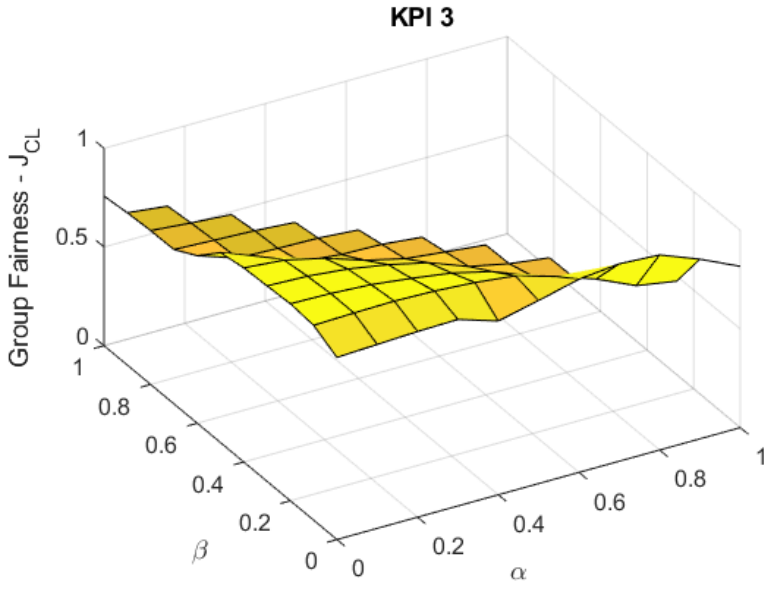

Figure 4.11: Jen's index for coverage level satisfaction - maximum at $\alpha = 0.8$, $\beta = 0$, $\gamma = 0.2$. (Note: $\alpha + \beta + \gamma = 1$).

because scheduling users with better channel conditions for the data phase directly increases the throughput. Whereas, for the user fairness, assigning a higher importance to γ allows for a better distribution of services towards users with lower satellite coverage time. Finally, for the third KPI, the maximum fairness among different coverage levels is reached when we assign most of the profit to the users with a high buffer status. To better understand these results, in Fig. 4.12 we show through a color mapping the remaining data in the users' buffer after the 480 satellite passages at maximum KPIs. Please note that the higher remaining data in the buffer the darker the color. Selecting which KPI to optimize will greatly depend on the parameters of a realistic system, which in our case are unknown, such as, the number of LEO satellites in a constellation, the number of NB-IoT carriers to offer service over an area, the user distribution, and the satellite antenna characteristics. Nevertheless, our hypothetical scenario allows us to make the following analysis.

Maximizing KPI 1 Maximizing the overall throughput of the system, which is our case it reaches 103 kbit/s, would result in a narrower beam mainly serving user that are closer to the satellite (higher antenna gains and lower propagation path losses). More specifically, in our simulated scenario, we notice from Fig. 4.12 that to satisfy all the user demand we need to double the amount of satellites so as to cover with service the rest of the unsatisfied users

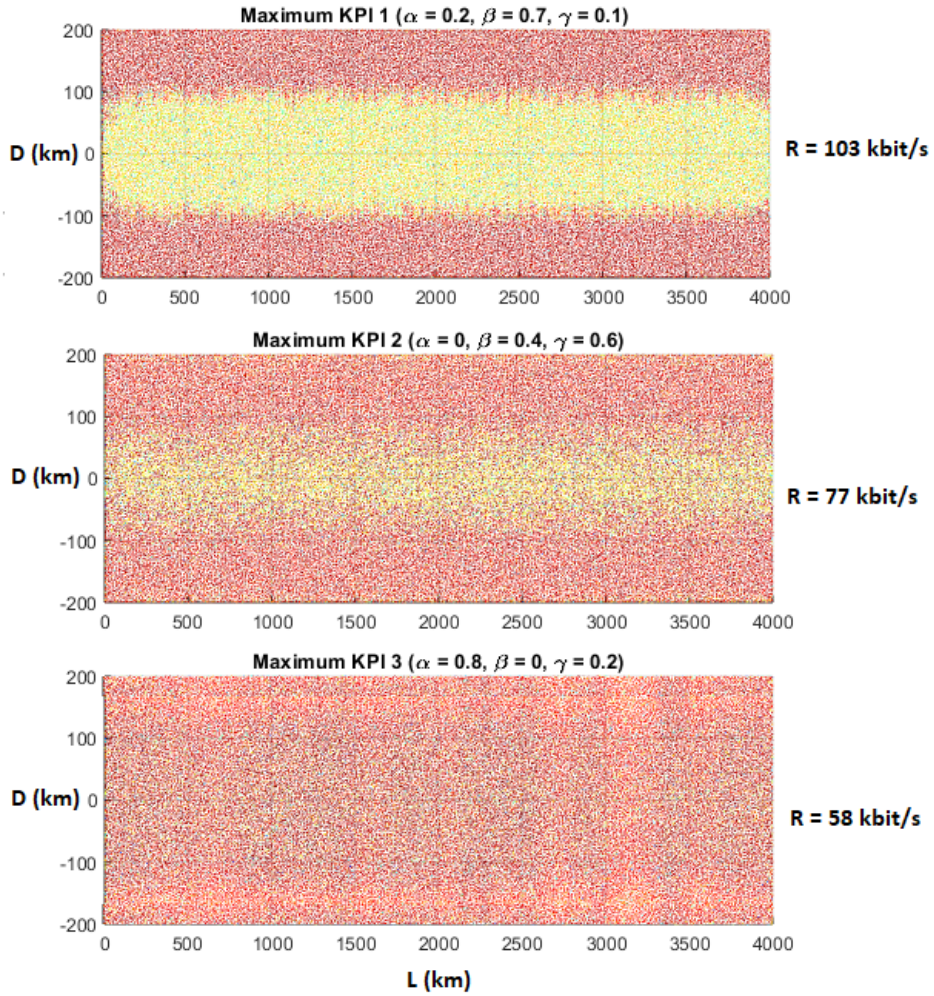

Figure 4.12: Color mapping of remaining bits in the users' buffer.

placed at the edge of the geographical area. Obviously, this is only an observation and the specific number of satellites required would depend on a realistic user demand and satellite antenna characteristics. Nevertheless, we can conclude that maximizing KPI 1 would be favourable for a system with a large number of LEO satellites in a constellation with highly directive antennas.

Maximizing KPI 3 Maximizing KPI 3 gives us the best distribution of services among users in different coverage levels, but the lowest throughput (58 kbit/s). Depending on the data demand over a particular area, this scenario would be beneficial for operators targeting to aggregate the IoT traffic through a lower number of LEO satellites with a wide antenna beam on Earth. Nevertheless, to satisfy the data demand and fully serve a particular area, more than one NB-IoT carrier may be required. Explicitly, for our simulated scenario, we would

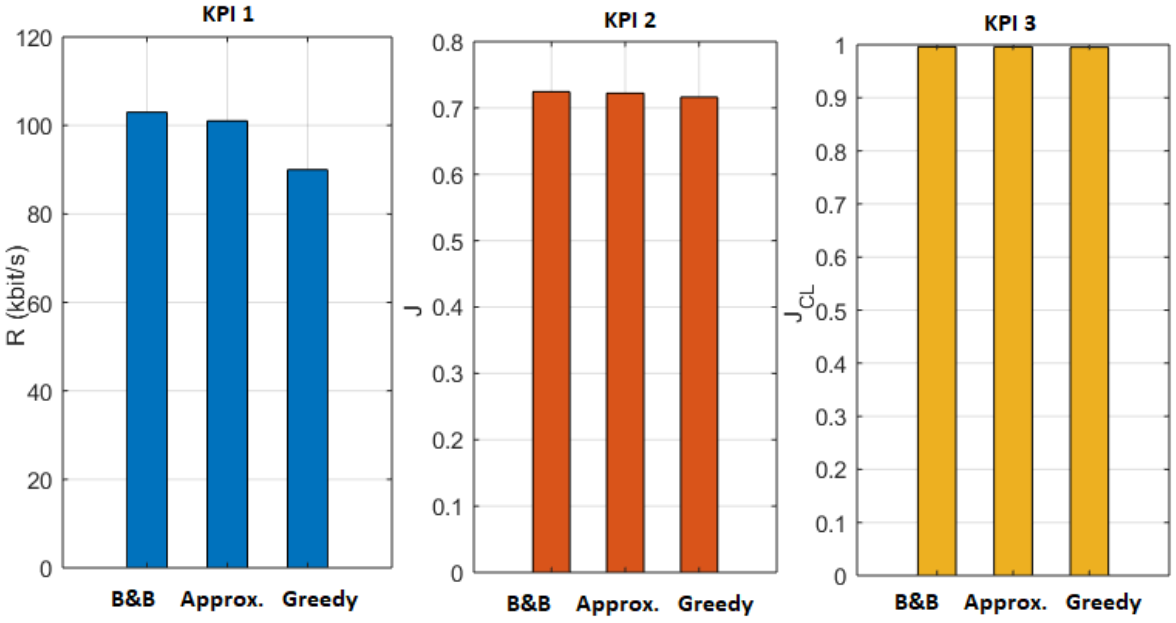

Figure 4.13: Comparison among algorithms for maximum values of KPI 1, KPI 2 and KPI 3.

need to double the number of NB-IoT carriers since the resulting throughput is approximately halved.

Maximizing KPI 2 The maximum user fairness provides a better distribution of services compared to the case with maximum KPI 1, but it fails to guarantee a fair distribution over users in different coverage levels. It still gives a certain priority to users with good channel conditions because it allows more data to be aggregated by the satellite, thus quickly increasing the number of users satisfied with service (and consequently the user fairness). Maximizing KPI 2 would be advantageous in a system where you want to save spectrum (NB-IoT carriers) and at the same time keep the number of satellites in a constellation low, as in the case of maximum KPI 3.

Another interesting fact worth mentioning here is that a certain system may be in favour of different performance targets at different times. Obviously, in our hypothetical scenario we consider an overloaded system where users are uniformly distributed in order to stress test our algorithm. However, in a realistic scenario, the user distribution will change over time, depending weather the satellite is passing over a city (high number of congested users) or an ocean (e.g. users in ships distributed over a larger geographical area).

The simulation results shown so far where obtained by utilizing the optimal solution of

the 0-1 MKP problem. We repeat the simulation also for the Greedy and the Approximate algorithm proposed in this paper, and the comparison results are shown in Fig. 4.13. As it can be noted, the proposed Approximate algorithm achieves a maximum throughput of 101 kbit/s, being very close to the one achieved by the optimal solution (103 kbit/s) and better than the Greedy algorithm (90 kbit/s). In terms of user and group fairness, the three algorithms perform the same.

4.5 Conclusions

In this chapter, a LEO satellite-based NB-IoT system has been considered. To minimize the message exchange between the BS and the UEs, counteracting the increased RTD in the satellite channel, the amount of data transmitted by every user has been maximized determined by their specific channel conditions, data demands and NB-IoT standard limitations. Also, for the purpose of accommodating the high dynamicity of the system, a separation of access and data phases has been assumed, allowing for "short-term" resource allocation decisions with the latest and most accurate estimated parameters by the BS. A profit function has been designed which assigns different priorities to users depending only on the known parameters by the BS. The problem has been modelled as a 0-1 MKP which selects the set of users to be scheduled together in the data phase, maximizing the sum profit of the scheduled users, and minimizing the radio resource wastage. In order to tackle the differential Doppler problem, groups of users have been created and the available resources for data transmission have been optimally divided. Exploiting the unique features of our system, an Approximate algorithm for solving the 0-1 MKP has been proposed with a near-optimal performance and very low complexity. Finally, three KPIs have been designed with different performance targets and their optimal operational points have been found through numerical simulations.

Chapter 5

Experimental Analysis and Demonstration of the Random Access Procedure over Non-Terrestrial Networks

In Chapter 3 and 4 we focused only on the NB-IoT data phase with the assumption of having a successful access phase. In this crucial phase, which is achieved by the RA procedure, the first impairment that impacts its feasibility over a satellite link is the increased delay in the communication link. Therefore, in this chapter, we analyse the challenges imposed by the considerably increased delay in the communication link on the RA procedure and propose new solutions to overcome those challenges. A trade-off analysis of various solutions is provided taking into account also the already existing ones in the literature. In order to broaden the scope of applicability, we keep the analysis general targeting 4G, 5G and NB-IoT systems since the RA procedure is quasi-identical among these technologies. Last but not least, we go one step further and validate our techniques in an experimental setup, consisting of a user and a base station implemented in open air interface (OAI), and an NTN channel implemented in hardware that emulates the signal propagation delay. The laboratory test-bed built in this work, not only enables us to validate various solutions, but also plays a crucial role in identifying novel challenges not previously treated in the literature. Finally, an important key performance indicator (KPI) of the RA procedure over NTN is shown, which is the time

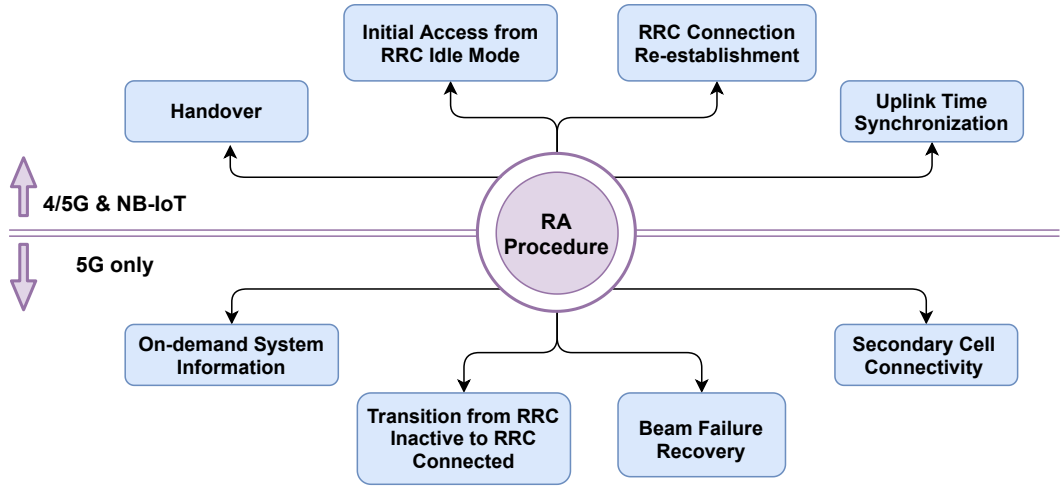

Figure 5.1: Situations when RA procedure is triggered.

that a single user requires to establish a connection with the base station.

5.1 Challenges of RA Procedure over NTN

The aim of this section is to analyse the obstacles that would make the RA procedure fail when larger delays (compared to terrestrial scenario) are introduced in the communication link. The RA procedure is triggered in different situations as illustrated in Figure 5.1. Please note that compared to LTE and NB-IoT, there is a stronger necessity of the RA procedure in NR, and this is also an indicator of why this mechanism is highly important, and worth analysing its feasibility over NTN. A description of the RA procedure is give in Chapter 2. However, more details will be provided here when necessary. To facilitate and assist the explanation of the challenges in the following section, we provide in Figure 5.2 and Figure 5.3 the state machine representation of the UE and BS in an example scenario where the UE is attempting the initial access, transitioning from radio resource control (RRC) Idle mode to RRC Connected mode. Before going on with the investigation, we would firstly like to emphasize another crucial aspect that is common among LTE, NR and NB-IoT. The radio frames of all these three important technologies are 10 ms long, consisting of 10 subframes (SF), each of 1 ms duration (as stated in Chapter 2). This shared feature enables us to keep the analysis general since the following challenges would hold for all these three technologies. To improve the material flow, the technical divergences among them are highlighted when needed.

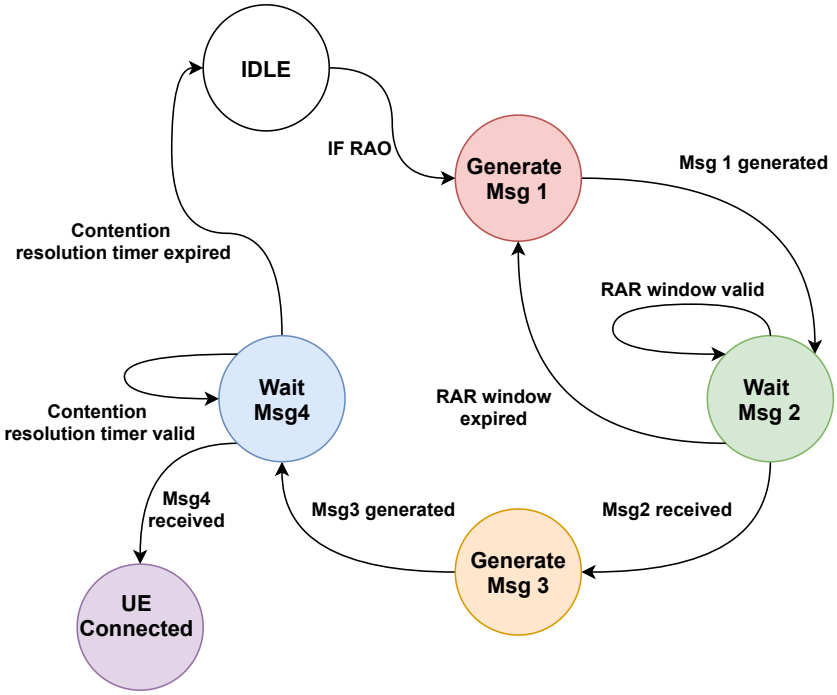

Figure 5.2: State machine representation during the RA procedure at UE side.

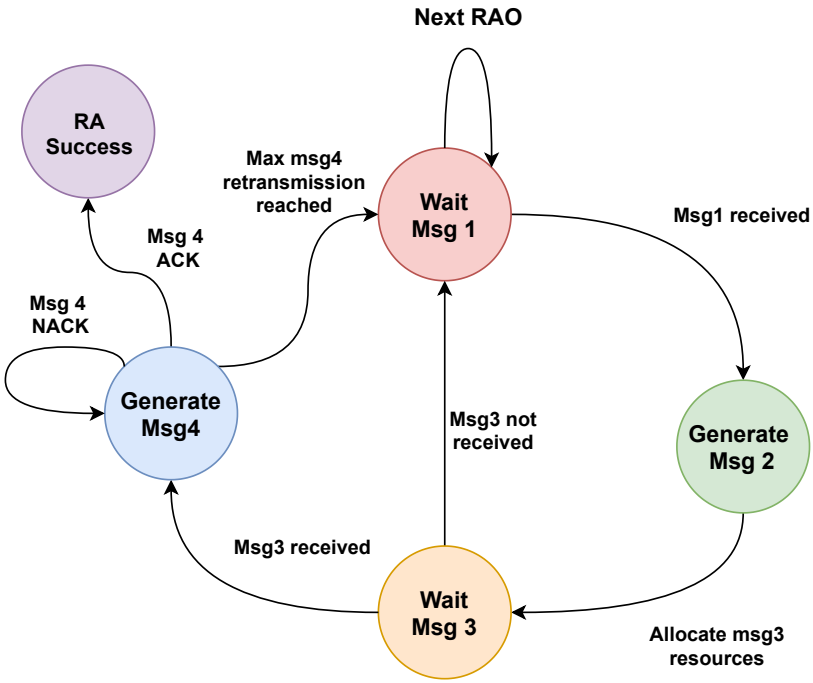

Figure 5.3: State machine representation during the RA procedure at BS side.

5.1.1 RAO mismatch between the UE & BS

The PSS/SSS signals that are responsible for downlink synchronization, are sent over fixed SF, known by the UEs. This allows the UEs under the coverage area of the BS to be synchronized at a frame and SF level, as well as assign the SF numbering with reference to the PSS/SSS placement inside the frame. On the other hand, the system frame number is included in the master information block (MIB), which is directly decoded by the UEs after PSS/SSS synchronization process. As previously stated, the RAO time and periodicity is determined by the PRACH configuration index, which is encapsulated and broadcasted to all the UEs through the system information block (SIB). Table 5.1 gives only a set of possible RAO time/periodicity for LTE and NR. Obviously, a much larger number of configurations exist, especially for NR, which can be specifically found in the standard (Table 5.7.1-2 for LTE [45] and Table 6.3.3.2-2 for NR [103]). In NB-IoT there is no PRACH configuration index reported, thus the PRACH time and periodicity are communicated separately in SIB (Section 10.1.6 [45]). However, the principle would be the same. Assuming an LTE BS, operating over a PRACH configuration index 3, the UEs will initiate the RA procedure at SF number 1 at any frame. Also the BS will check at SF 1 for preamble detection and measure the ToA of the preambles, so as to estimate the TA and correct the time-misalignment (see Figure 5.4).

Let us now assume the same BS operating over an NTN platform (e.g. LEO satellite at 600 km altitude). The minimum RTT in such a scenario would be 4 ms. Due to this drastic change of the delay, the PSS/SSS signals will arrive at the UE at least 2 ms after they are produced. Nevertheless, despite the increased delay, the SF-level synchronization and numbering at the downlink is not impacted, only shifted in time (2 SF in our example

Table 5.1: PRACH configuration index mapped into RAO time & periodicity [45, 103].

Configuration Index	**LTE**		**NR**	
	SF Number	Frame	SF Number	Frame
0	1	Even	1	1, 17, 33,..
1	4	Even	4	1, 17, 33,..
2	7	Even	7	1, 17, 33,..
3	1	Any	9	1, 17, 33,..
4	4	Any	1	1, 9, 17,...
-	-	-	-	-
-	-	-	-	-

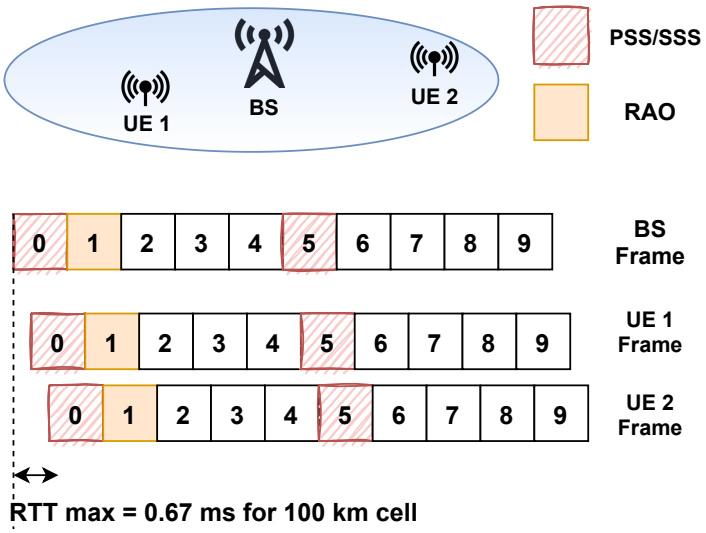

Figure 5.4: Terrestrial cellular network example.

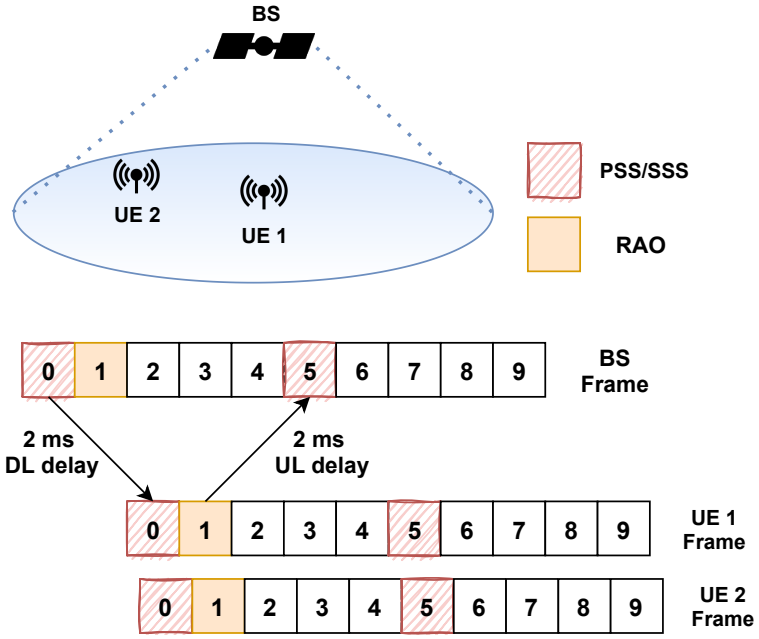

Figure 5.5: NTN at altitude 600 km.

as shown in Figure 5.5). This time-shift in downlink, together with the time that the signal required to propagate in the uplink, would cause a mismatch between the RAO at the UE and BS. Referring to the state machines in Figure 5.3, the BS will be stuck forever on state "Wait Msg1" if no modifications are done in the current standard, because it will process only SF 1 for preamble reception according to this PRACH configuration index, while in fact the preambles will arrive at SF 5.

5.1.2 Message 2 withdrawal by the UE

Assuming that we are able to solve the above-mentioned challenge, the next obstacle that would occur in the RA procedure is the Message 2 withdrawal by the UEs. When the UE initiate the RA procedure, it assigns to the preamble a specific random access ID, known as RA-RNTI, which is explicitly derived by the time-frequency resources utilized for preamble transmission. The following equations are utilized for RA-RNTI derivation, as specified in the standard (NB-IoT/LTE [104], NR [105]).

$$\textbf{LTE:} \quad RA-RNTI = 1 + t_{id} + 10 \cdot f_{id} \tag{5.1}$$

$$\textbf{NB-IoT:} \quad RA-RNTI = 1 + \lfloor \frac{t_{id}}{4} \rfloor + 256 \cdot c_{id} \tag{5.2}$$

$$\textbf{NR:} \quad RA-RNTI = 1 + s_{id} + 14 \cdot t_{id} + 14 \cdot 80 \cdot f_{id} + 14 \cdot 80 \cdot 8 \cdot c_{id} \tag{5.3}$$

Please note that t_{id} is the index of the SF related to the RAO when the preamble is sent, f_{id} is the index that relates to the frequency used for preamble transmission, c_{id} is the carrier index and s_{id} is the symbol index. The exact same equations are utilized also by the BS to calculate the RA-RNTI that will be encoded in the RAR message, which will then be sent to the UE. However, similar to the previous problem, because there is a mismatch in the SF numbering of the RAO between the UE and the BS, the RA-RNTI associated with Message 1 transmission would be different from the one received together with Message 2. The UE will withdraw the RAR message received because it will assume that it belongs to another user. In fact, also the parameters related to the frequency domain may be impacted due to the frequency shift caused by the high-speed movement of the NTN platform. However, this analysis is out of the scope of this work, and we study only the impact of the timing difference. In such a case, the UE will be stuck on the loop "Wait Msg2 - Generate Msg1" according to the state machines shown in Figure 5.2, because the RAR window size will always expire.

5.1.3 Expiry of the RAR window size and contention resolution timer

Even if we are able to solve the Message 2 withdrawal problem, for certain values of NTN altitudes the RAR window size will expire. When this happens, the UEs assume that their preamble is lost and will repeat sending Message 1 after a back-off time and a power ramping procedure, as specified by the standard. The same holds for the contention resolution (CR)

phase. When the UE Transmit Message 3 to the BS, it will monitor the downlink channels for Message 4 reception until the expiration of the CR timer. The set of values for the RAR_{window} and CR_{timer} for NB-IoT/LTE [106] and NR [107] are given below:

$$\begin{aligned} \textbf{LTE: } RAR_{window} &= \{1, 2, 4, 6, 8, 10\}\ SF \\ CR_{timer} &= \{8, 16, 24, 32, 40, 48, 56, 64\}\ SF \end{aligned} \tag{5.4}$$

$$\begin{aligned} \textbf{NB-IoT: } RAR_{window} &= \{2, 3, 4, 5, 6, 7, 8, 10\}\ PP \\ CR_{timer} &= \{1, 2, 3, 4, 8, 16, 32, 64\}\ PP \end{aligned} \tag{5.5}$$

$$\begin{aligned} \textbf{NR: } RAR_{window} &= \{1, 2, 4, 8, 10, 20, 40, 80\}\ SL \\ CR_{timer} &= \{8, 16, 24, 32, 40, 48, 56, 64\}\ SF \end{aligned} \tag{5.6}$$

Please note that SF stands for subframe duration, SL for slot duration and PP for physical downlink control channel (PDCCH) periodicity. As it can be seen, the maximum RAR window and CR timer supported in LTE are 10 ms and 64 ms, respectively. For NB-IoT, the calculations are done based on PDCCH periodicity, which varies from 1 ms to 10.24 seconds. Notably, these range of timers are enough to cover even NTN delays, which in the worst case scenario would be as high as 480 ms (GEO satellite with transparent payload). Hence, this challenge does not apply to NB-IoT. Last but not least, the calculations for the NR are a bit more complex because of its flexibility in the PHY layer. While it is true that the frame structure is the same as NB-IoT/LTE, the number of slots contained in 1 SF and the slot duration have a direct dependency on the subcarrier spacing (SCS). The NR standard [103] defines several SCS for the OFDM signal, thus in Table 5.2 we show the maximum RAR window supported for every numerology. Finally, regarding the CR timer for NR, it is identical to LTE.

Table 5.2: Slot duration and maximum RAR window sizes for various NR numerology.

μ	$SCS = 2^{\mu} \cdot 15$	SL duration	Max RAR_{window}
0	15 kHz	1 ms	80 ms
1	30 kHz	0.5 ms	40 ms
2	60 kHz	0.25 ms	20 ms
3	120 kHz	0.125 ms	10 ms
4	240 kHz	0.0625 ms	5 ms

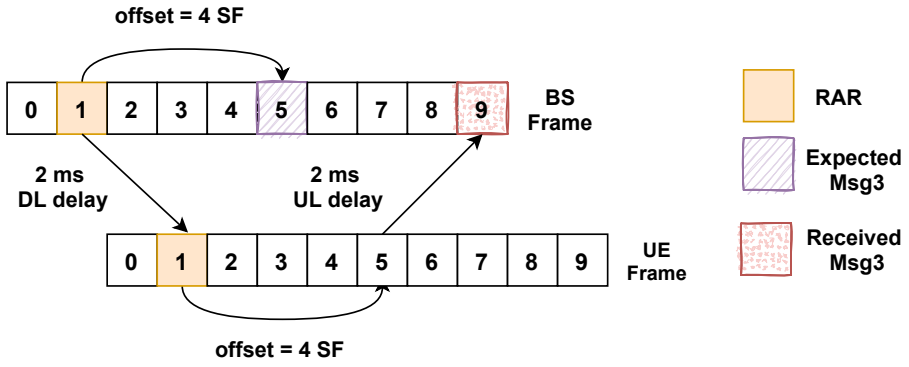

Figure 5.6: Scheduling problem illustration (e.g. satellite at 600 km altitude)

5.1.4 Message 3 & HARQ scheduling mismatch between the UE & BS

The contention resolution (CR) phase of the RA procedure is orchestrated by the BS, and the time-frequency resources that the UE has to utilize for Message 3 are reported in the random access response (RAR or msg2). Apparently, this is done to avoid collision among different UEs. In the time-domain, the resource allocation for Message 3 is done through informing the UEs about the amount of time they have to wait (time-offset) after RAR reception, before transmitting their uplink signals. The minimum value for this time-offset is 4 SF (ms) in NB-IoT/LTE [50] because this corresponds also to the amount of processing time at the user side before initiating an uplink transmission. Regarding NR, the minimum value of such time-offset is dependent on the numerology [108]. Based on the offset that the UE has to apply, also the BS has to prepare for Message 3 reception. However, due the the increased delay in the communication link (which overcomes the SF length and the BS is not aware of in the current protocol), Message 3 will arrive at the BS not according to the resource allocation (see Figure 5.6). This will cause a failure in Message 3 reception and the BS will never enter in the "Generate Msg4" state (Figure 5.3). The same reasoning can be done also for the HARQ scheduling. The BS will monitor certain SF for receiving the ACK/NACK during the CR phase, which in fact will be further delayed.

5.1.5 Message 3 demodulation & decoding problems

Solving the scheduling problem investigated earlier, does not still guarantee a correct reception of Message 3 at the BS side. This is because of the following reasons.

Demodulation reference signals (DMRS) mismatch

For the purpose of coherent demodulation and channel estimation, both at UE and BS side, reference symbols (pilots) are inserted in the downlink and uplink channels. Message 3 is sent over the physical uplink shared channel (PUSCH), therefore hereafter we will provide more details regarding the DMRS signals for the PUSCH channel to better explain this challenge. For NB-IoT/LTE standard, DMRS occupies the center symbol of every slot (contained by 7 symbols overall). Although understanding the positioning of DMRS sequence is quite straightforward, its generation is a bit more complex and involves many parameters. Referring to the NB-IoT/LTE standard [45], the generation of DMRS sequence directly depends on three main parameters as shown below:

$$r_{DMRS}(n) \sim e^{j\alpha n} \cdot r_{u,v}(n) \tag{5.7}$$

where α is the cyclic shift which defines the rotation of the sequence, $r_{u,v}$ is the base sequence determined by two other parameters (UE-specific) u and v that define the group hopping and sequence hopping, respectively. The cyclic shift α is given by:

$$\alpha = 2\pi \cdot \frac{\{n^{(1)}_{DMRS} + n^{(2)}_{DMRS} + n_{PRS}(SF)\} mod 12}{12} \tag{5.8}$$

where $n^{(1)}_{DMRS}$ and $n^{(2)}_{DMRS}$ take integer values from 0 to 10 defined in the standard [45]. What is worth noticing here is the last parameter that has a direct dependency on the SF number. This results in applying different cyclic shifts to the base sequence, leading to distinct DMRS symbols inserted at every SF. To correctly demodulate Message 3, the BS will have to utilize the same symbols (pilots), allowing to extract relevant parameters for the demodulation. However, due to the the SF-mismatch caused by the increased delay that overcomes the SF length (as shown in Figure 5.6), the estimated parameters for the demodulation process will be erroneous, greatly distorting Message 3 reception. Please note that we provided further details for NB-IoT/LTE to assist the explanation of this challenge, but the same will occur also in NR because of the SF-dependency of the DMRS sequence [103].

Gold sequence mismatch

The Gold sequences are used in various wireless technologies as a scrambling code because of their high auto-correlation and low cross-correlation properties. Through the scrambling code that is applied to the bits after encoding and before proceeding with the modulation, the BS can separate signals coming simultaneously from various UEs, as well as the UEs can distinguish the signals coming from many different BS. In NB-IoT/LTE [45] and NR [103], the Gold sequence c is generated by combining two m-sequences x_1 and x_2 through an XOR gate, as follows:

$$c(n) = \{x_1(n + N_c) + x_2(n + N_c)\} mod 2 \tag{5.9}$$

where $N_c = 1600$ is fixed. The final obtained Gold sequence will depend on the initialization value:

$$c_{init} = x_{1init} + x_{2init}(SF) \tag{5.10}$$

As it can be noted, the initialization of one of the m-sequences has a SF-dependency, resulting in distinct scrambling codes for different SF. This will cause Message 3 decoding issues because the de-scrambling sequence applied at the BS side will be different from the scrambling one at the UE (similar to the demodulation problem previously explained).

Please note that the demodulation and decoding problems will occur only in the uplink transmission (UE $->$ BS). In the downlink (BS $->$ UE), the SF numbering matches, being assigned with reference to PSS/SSS location in the frame, as previously emphasized.

5.2 Proposed Solutions to overcome the challenges and trade-off analysis

The aim of this section is to describe the proposed solutions which counteract the challenges treated in Section 5.1. Furthermore, a trade-off analysis will be provided for the various approaches.

5.2.1 Timing advance (TA) at the UE side

To compensate for the RAO mismatch between the UE and BS, a TA can be applied, so that the preambles transmitted by the on-ground UEs arrive at the right RAO at the BS, as specified by the PRACH configuration parameters. To do so, the UEs has to estimate the

RTT in the NTN channel, which can be realized through the GNSS positioning capability together with the knowledge of the NTN orbital parameters. Although this solution is already proposed in the literature [63–65], it lacks a detailed description implementation-wise. The existing TA concept, either in NB-IoT, LTE or NR, can be only applied in a sample-level, and due to this, there are practical limitation to be considered. To illustrate this, let us take as an example the TA application in LTE. The minimum TA that can be applied in LTE is $TA = 16 \cdot T_s \cdot TAC$, where T_s is the sample duration given by:

$$T_s = \frac{1}{FFT_{size} \cdot SCS} = \frac{1}{2048 \cdot 15000} \tag{5.11}$$

and the TAC is the timing advance command reported in RAR. There are 11 bits reserved for reporting TAC, ranging from 0 to 1282, corresponding to TA values of up to 0.67 ms. Although being able to estimate higher values of the TA before transmitting Message 1, it is practically impossible to apply a TAC greater than 2048 samples which is also the FFT size in LTE. The TAC needed to counteract NTN delays has to be much larger than the SF length, thus overcoming the FFT size. Alternative ways should be proposed.

In this work, we put forward the idea of applying a SF-level TA at the UE side, in addition to the sample-level one already defined by the standard. This can be done through applying a time correction in the mapping of the PRACH configuration index into RAO time and periodicity at the UE side, as shown in Table 5.1, while leaving it unchanged at the BS. Table 5.3 gives an example of how the configuration index would be mapped in RAO time and periodicity for NR. Obviously, the specific SF advance (SFA) and/or frame advance (FA) will have a direct dependency on the old value of the RAO Frame and SF, and the estimated

Table 5.3: PRACH configuration index mapped into RAO time & periodicity at UE side for NR over NTN scenario.

Configuration Index	**NR over NTN**	
	SF Number	Frame
0	1 - SFA	1-FA, 17-FA, 33-FA,..
1	4 - SFA	1-FA, 17-FA, 33-FA,..
2	7 - SFA	1-FA, 17-FA, 33-FA,..
3	9 - SFA	1-FA, 17-FA, 33-FA,..
4	1 - SFA	1-FA, 17-FA, 33-FA,..
-	-	-
-	-	-

RTT. For example, if the BS is operating over an PRACH configuration index 3 and the estimated RTT by a specific UE is 4.3 ms, SFA will be 4 and FA will be 0. The remaining part of 0.3 ms can be handled by the sample-level TA.

In a similar way, relying on GNSS estimates at the UE side, such SF-timing correction can be also included in Equation (5.1) - (5.3) to solve the Message 2 withdrawal by the UE, and in Equation (5.7) - (5.10) to solve the demodulation and decoding issues. Doing so would make the RA-RNTI associated with the sent preamble to match the one received in RAR, and enable correct demodulation/decoding at the BS.

5.2.2 SF-level timing delay (TD) at the BS side

The TA concept, even at a SF-level, fails to solve the scheduling mismatch between the UE and the BS treated in Section 5.1.4. As we explained, the resource allocation in time-domain for Message 3 is performed by assigning a time-offset to the UEs, which has to be applied after the reception of the RAR message (where the time-offset information is included). If we take the NB-IoT standard as an example, such time-offset ranges from 4 to 64 [50]. However, the RTT over an NTN channel overcomes this range of values, making the application of the TA totally unfeasible when the time-offset is set to 4 (required for processing), and partially unfeasible for the other set of values (depending on the NTN altitude). Therefore, this raises the need of a SF-level TD to be applied at the BS, as illustrated in Figure 5.7. Please note that in order to delay the reception of Message 3, the BS has to be aware of the NTN altitude and the RTT experienced at the center of its beam. Such information can be provided/included in the deployment phase of the network since it will be fixed over time.

In a similar way, the SF-level TD can be executed at the BS side for the RAO mismatch.

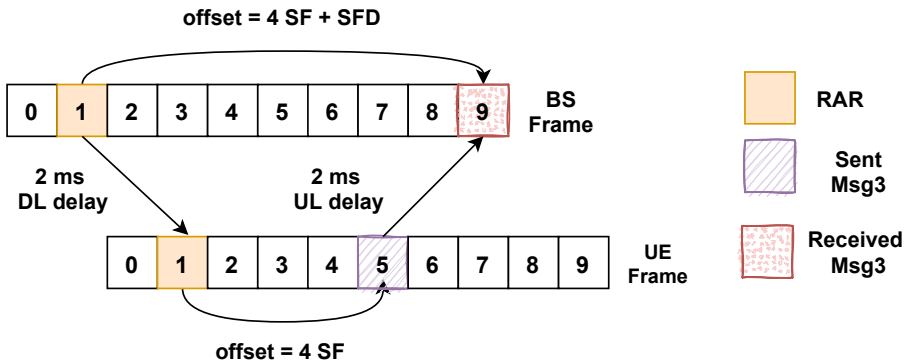

Figure 5.7: Solving the scheduling problem by adding the SF Delay (SFD)

Clearly, this will require a new mapping of the PRACH configuration index into the RAO time and periodicity at the BS, resembling Table 5.3, but with the difference of applying a SF delay (SFD) and frame delay (FD) instead of SFA and FA. Furthermore, the same concept can be utilized for SF-timing corrections in Equation (5.1) - (5.3) and (5.7) - (5.10). This solution will not require any modification at the UE side.

5.2.3 Adaptation of timers

To avoid the expiry of the RAR window size and contention resolution timer, the adaptation can be done either at the UE or the BS. If done at the UE side, again the GNSS estimates will play a role. The estimation of the RTT has to be added on top of the values reported by the BS, as shown in Equation (5.4) - (5.6). If done at the BS side, the new values should be reported in the SIB, where all the relevant parameters for the RA procedure are included. In the current NB-IoT/LTE and NR standard, only 3-bits are reserved for reporting the RAR window size, and other 3-bits for the contention resolution timer. This is because there are only up to 8 possible values reported. Including more values in the current standards with the purpose of covering also the NTN delays would require extra bits in the SIB field.

5.2.4 Trade-off analysis

As it has been pointed out, some of the above-mentioned solutions can be implemented at the UE or the BS. This raises the need for a trade-off analysis to compare among these two different approaches.

Power consumption

The TA approach covered in Section 5.2.1 relies on the utilization of the GNSS signals to estimate the UE position, before starting the RA procedure (see Figure 5.8). To have a rough estimation of the RTT in the NTN channel, the UE has to be provided also with the two-line element set (TLE) of the NTN platform in order to predict its location over time. This added procedure compared to a terrestrial network (TN) will directly impact the power consumption of the UE, which is a very sensitive matter, especially for the NB-IoT standard. In fact, the increased power consumption due to GNSS has been deeply analyzed in [57], by considering various commercial UEs and scenarios. The simulation results provided in [57] show a reduction in battery life in the range of 10 - 40 % for UEs placed in a medium

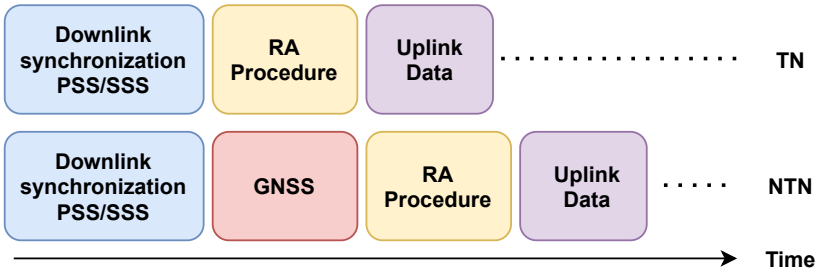

Figure 5.8: Chronology of UE procedures for TN and NTN

coverage level with maximum coupling loss (MCL) of 154 dB. Clearly, the diversity of the battery life-time reduction comes from the various applications the UEs are being used for (different packet sizes for the uplink data reports), and the various GNSS modules utilized for positioning. In contrast to the TA, implementing the TD approach at the BS side, as described in Section 5.2.2, will eliminate the need for the extra GNSS processing at the UE (without an impact in the battery life-time), leading to coverage limitations, as we will see below.

NTN Coverage

In a terrestrial network, the cell radius R_{cell} is dependant on the cyclic prefix (CP) length T_{cp} of the preamble generated during Message 1 transmission of the RA procedure. To correctly receive the preambles from various UEs in a RAO, the differential RTT of signal propagation among the UEs should not overcome the CP length of the preamble. This can be expressed by the following equation:

$$D_{max} - D_{min} = R_{cell} \leq c \cdot T_{cp}/2 \tag{5.12}$$

where D_{max} and D_{min} represent the maximum and the minimum UE distance from the BS. There exist different preamble formats defined in the NB-IoT/LTE [45] and NR [103] standard, where some are captured in Table 5.4. As it can be seen, the CP length alters with the preamble format, resulting in distinct cell sizes.

While in a terrestrial network $D_{min} = 0$ and $D_{max} = R_{cell}$, the same does not hold in NTN (please refer to Figure 5.5). To derive the cell sizes in NTN we exploit the system geometry in Figure 5.9 and write the following equations, in a similar way to [74]. The distance D from

Table 5.4: CP length for some preamble formats.

Preamble Format	**CP length in ms**		
	NB-IoT	LTE	NR
0	0.027	0.1	0.1
1	0.067	0.68	0.68
2	0.8	0.2	0.15

a UE to the BS in NTN can be calculated by:

$$D(\alpha) = \left(\sqrt{R_E^2 sin(\alpha)^2 + h_s^2 + 2R_E h_s} - R_E \cdot sin(\alpha)\right) \tag{5.13}$$

where α is the elevation angle, h_s is the altitude of the NTN platform and R_E is the radius of Earth. Given the minimum elevation angle α_{min} of a certain cell, we can easily derive $D_{max}(\alpha_{min})$ by Equation (13), and $D_{min}(\alpha_{max})$ by the following:

$$D_{min}(\alpha_{max}) = \min_{\alpha} D(\alpha) \tag{5.14}$$

such that:

$$D_{max}(\alpha_{min}) - D(\alpha) \leq c \cdot T_{cp}/2$$

$$\alpha \in [\alpha_{min} \quad 90°]$$

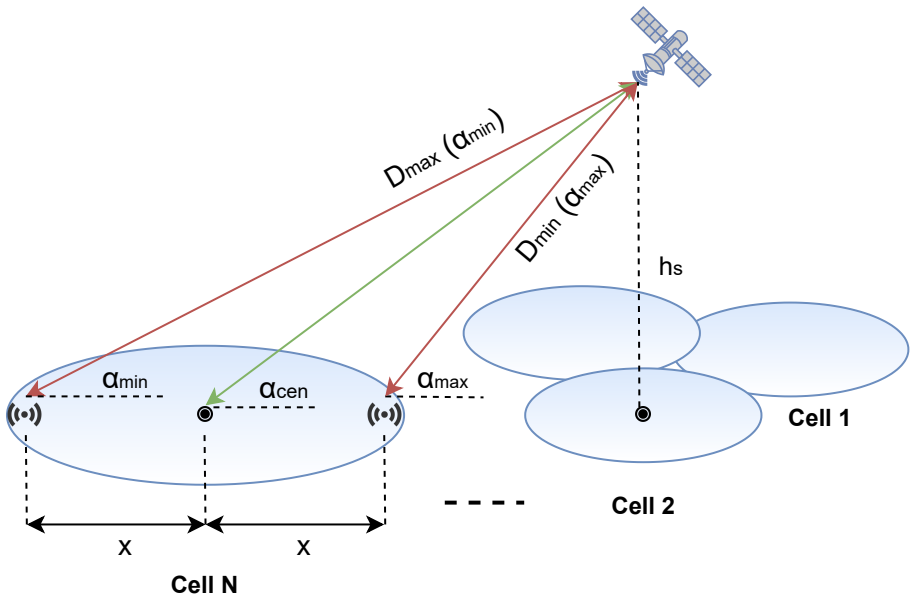

Figure 5.9: NTN system geometry

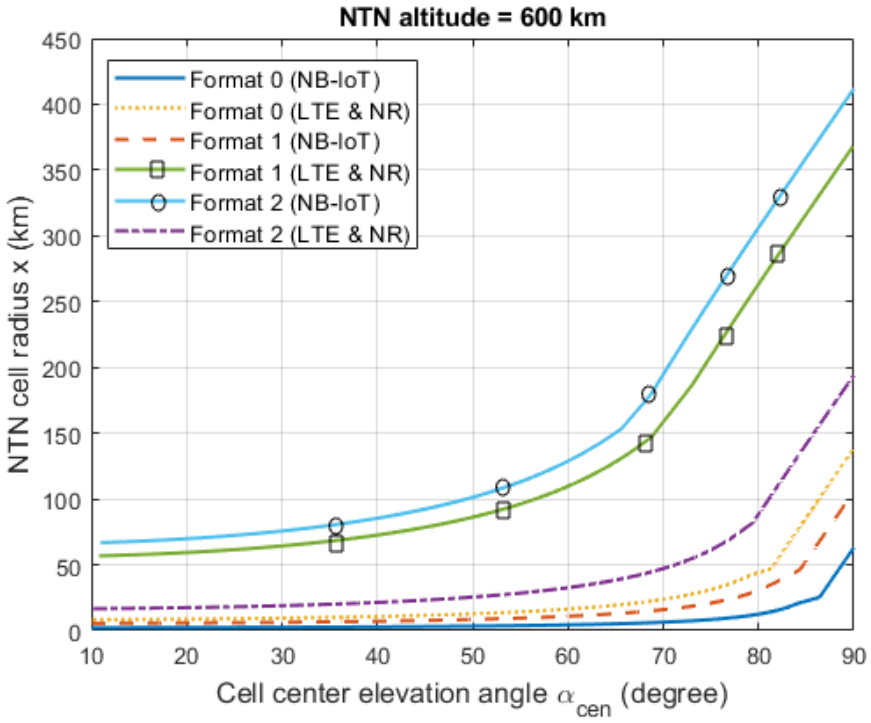

Figure 5.10: NTN cell radius as a function of the cell center elevation angle.

After obtaining D_{min} and D_{max} for a particular cell, the radius x can be calculated as follows:

$$x = \frac{\sqrt{D_{max}^2 + D_{min}^2 + 2D_{max}D_{min}cos(\alpha_{max} + \alpha_{min})}}{2} \tag{5.15}$$

Through numerical simulations, we obtain the NTN cell sizes for different preamble formats in NB-IoT, LTE and NR, for a LEO satellite at 600 km altitude (see Figure 5.10). For simplicity, we show the results with respect to the cell center elevation angle α_{cen}, derived after fixing α_{min} and obtaining x.

As it can be observed, there is a limitation in the size of the NTN cells supported, driven by the preamble format and α_{cen}. This does not occur in the case of TA approach, because the TA is applied individually at Message 1 by the UEs, making sure that they arrive at the BS at the correct RAO. Whereas, in the TD approach, the BS can delay the RAO to accumulate the preambles from all the UEs inside a cell, but cannot have several RAO. Alternative NB-IoT/LTE or NR carriers are needed for the other cells, having different PRACH configurations and applying different TD at the BS, depending on the characteristics of the cell. Please note that the TD does not need to be continuously estimated, but rather fixed at the deployment

phase of the network. For example, if the range of the RTT in a cell is 4.1 - 4.6 ms, the BS has always to apply a fixed SFD = 4 for that cell, while leaving the residual 0.1 - 0.6 ms to be handled by the protocol itself (clearly the preamble format selected should have $T_{cp} \geq 0.6$). Another interesting observation here is that certain cells cannot provide services at all. For example, let us assume an LTE over NTN scenario, and a cell where the range of RTT is between 5.6 and 5.9 ms. While the BS can apply SFD = 5, the residual part of 0.6 to 0.9 ms cannot be estimated/corrected with the current existing preamble formats. This will obviously cause further limitations in the coverage. Again, such restriction does occur in the case of the TA technique, because in addition to the SF-level TA, a sample-level TA can be employed at the UE side.

5.3 Experimental Validation

5.3.1 Experimental Setup

The infrastructure illustrated in Figure 5.11 has been developed using OpenAirInterface (OAI) [109]. OAI is open-source software that is being used for the experimentation, evaluation, development of current 3GPP wireless communication standards such as LTE and 5G [110], and several 3GPP proposals towards 5G and beyond. The experimental validation of our proposed techniques has been done by employing the LTE protocol stack since it is the most mature one currently developed by OAI. Figure 5.12 and 5.13 show the block diagram of OAI implementation of the 3GPP LTE stack coupled with our incorporated NTN

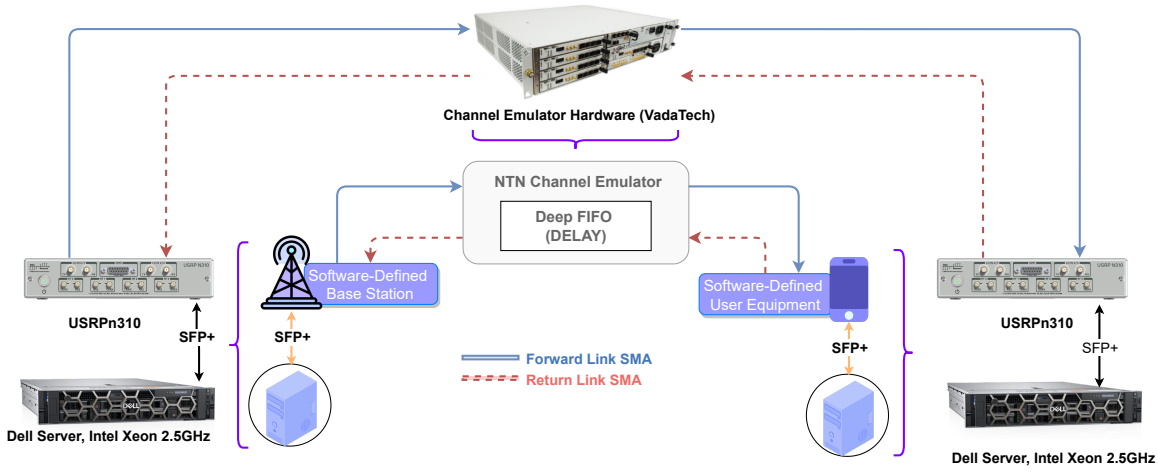

Figure 5.11: Infrastructure setup for the realization of Non-Terrestrial Network

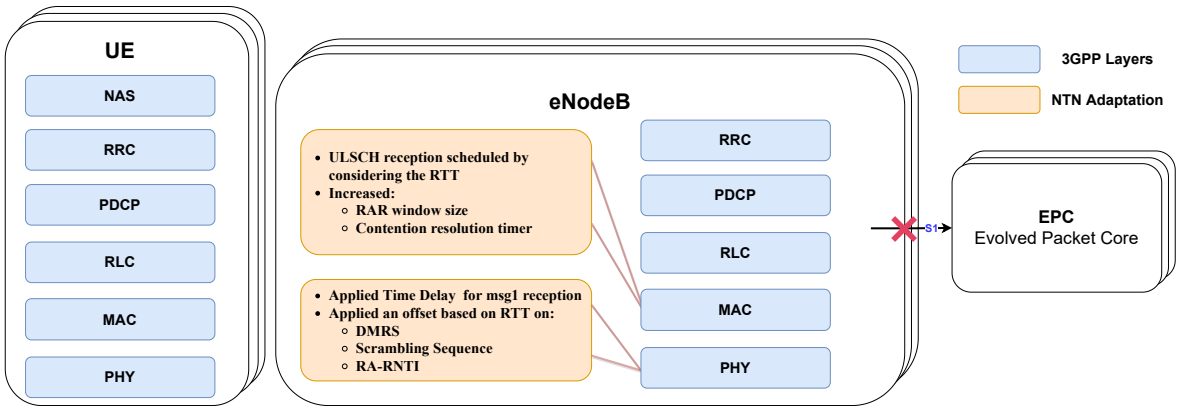

Figure 5.12: OpenAirInterface LTE Stack with NTN adaptations - TD Approach

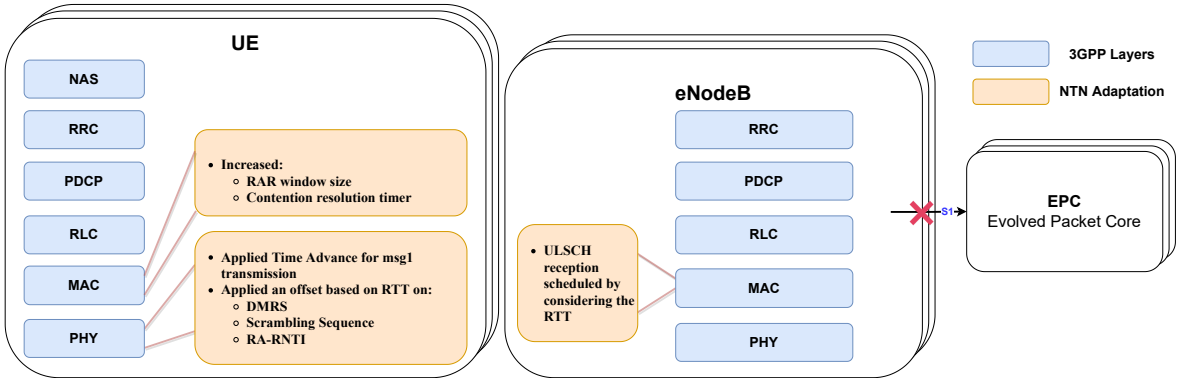

Figure 5.13: OpenAirInterface LTE Stack with NTN adaptations - TA Approach

adaptations, spanning Physical (PHY) and Medium Access Control (MAC) layers. As it can be noted, both the TA and TD approach have been tested, as described in Section 5.2. More specifically, we deployed the OAI LTE stack on general-purpose processors coupled with software-defined radio for signal generation and acquisition. This experimental setup focuses more on the radio access network (RAN) side with abstracted connection to the EPC so-called *noS*1 mode. Hence, it allows testing of OAI base-station and UEs without the support of the core network, which is a great advantage of OAI for accelerating the development time.

The physical interconnections between the system components is also illustrated in Figure 5.11. The connection between the processing units and the software-defined radio (SDR) units is established via small form-factor pluggable (SFP+) transceivers, which support 10 Gigabit Ethernet (GigE) connection. Accordingly, it gives a better realization for high-speed communication networks between the processing units (host computers) and SDRs. Thus, the host-based OAI software can seamlessly control the SDR hardware to receive and transmit

data over the $10GigE$ link.

The NTN channel emulator, a core component for verifying and validating the NTN development, has been implemented on top of a field-programmable gate array (FPGA) using custom-designed hardware from VadaTech. It provides an IP-Core implementing the RTT delay using a deep first in first out (FIFO) buffer, which utilizes an external Double Data Rate (DDR) Synchronous Dynamic Random-Access Memory (SDRAM) chipset. The implemented delay length is based on the frequency rate at which the data writes and reads to/from the Deep FIFO, and the depth of the FIFO buffer. By fixing the depth of the FIFO buffer and manipulating the frequency of the sample generation, which then are passed through the Deep FIFO, we are able to emulate various delays, reaching RTT values of up to 600 ms.

Table 5.5: Experimental configuration

Knobs	**Meters**
Band	7
Duplex	FDD
Downlink frequency	2.68 GHz
Uplink frequency	2.56 GHz
Bandwidth	5 MHz
TM mode	1
Satellite Attitude	600 - 35793 km
Satellite payload	regenerative/transparent
RTT Range	4 - 480 ms

*The table indicate the baseline for the Base Station, UE and NTN channel configuration which have been used in this experiment

We specifically used in that setup USRPn310 from National Instruments as a software-defined base station and software-defined UE. Further, the NTN channel emulator receive and transmit the signals from/to SDRs using SMA (SubMiniature version A) RF connectors. Accordingly, we assume that the software-defined base station can either be placed at the NTN platform, e.g. in case of a regenerative payload type, or be placed on-ground in case of a transparent payload type. Clearly, the payload type will impact also the RTT in the communication link. In this experiment we assume an NTN altitude ranging between 600 to 35793 km, which results in RTT values between 4 to 480 ms. Table 5.5 shows some of the most relevant configuration parameters. The system uses the LTE band 7, which is a

frequency division duplex band (FDD) operating on a downlink frequency 2.68 GHz with an uplink offset of 120 MHz. In LTE the available bandwidths (BW) are 1.4, 5, 10, and 20 MHz. For this experiment we use the 5 MHz BW configuration.

5.3.2 Experimental Results

Through the experimental setup we validate that our proposed solutions are able to counteract the induced challenges by the extreme delays in the communication link, thus leading to a successful RA procedure. Figure 5.14 illustrates the specific adaptations implemented in order to have a successful signal reception, either at UE or BS, for every single step involved in the RA procedure. Such trial-and-error approach enabled us to identify the new challenges not previously treated in the literature, such as the Message 2 withdrawal (Section 5.1.2) and the Message 3 demodulation and decoding problems (Section 5.1.5). Furthermore, we tested that the TA concept, as previously proposed in the literature (although lacking an implementation-wise description), has practical limitations if applied only at a sample-level, leading us to propose a SF-level TA. While this was able to solve the RAO mismatch between the UE and the BS (Section 5.1.1), it failed to deal with the Message 3 and HARQ scheduling mismatch (Section 5.1.4). This is the reason why for the TD approach all the NTN adaptations can be applied at the BS side (see Figure 5.12), whereas for the TA approach we still need the Message 3 and HARQ scheduling mismatch to be resolved at the BS, and not at the UE (see Figure 5.13).

In addition to achieving a successful RA procedure, we measure the time required by a

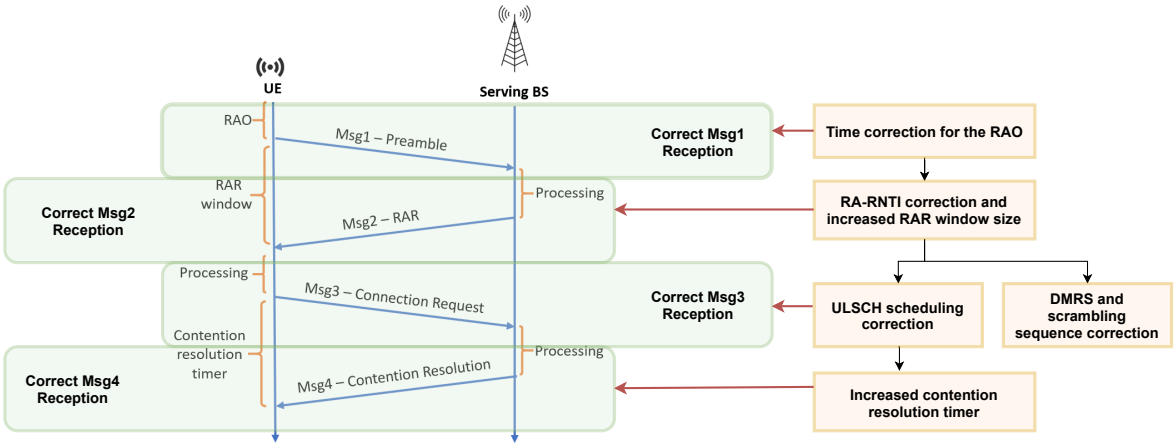

Figure 5.14: NTN adaptations in the experiment that led to a step-by-step success of the RA procedure.

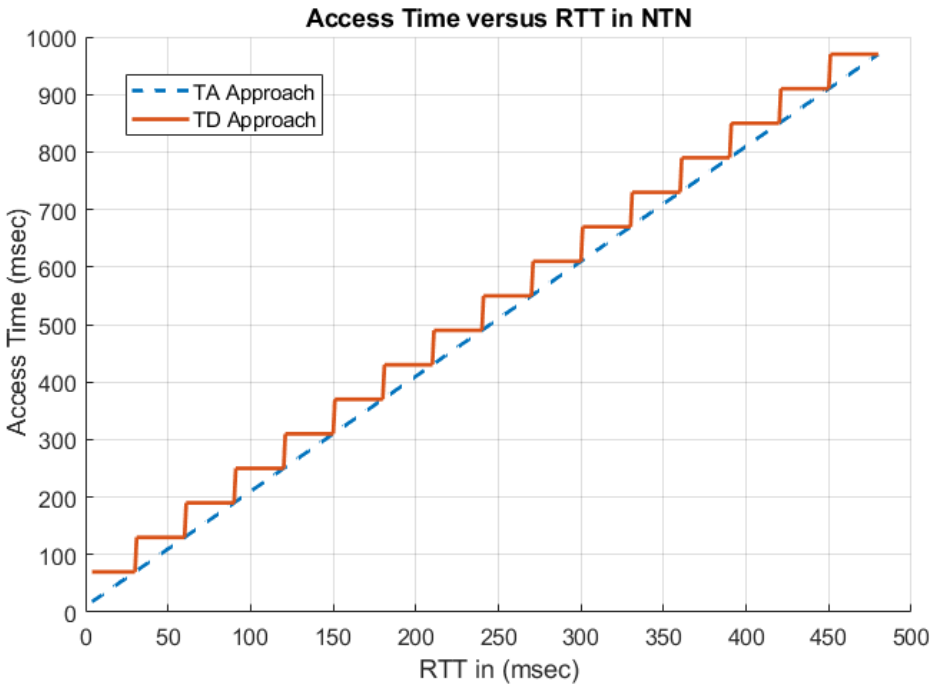

Figure 5.15: Single User Access Time (no collision)

single user to access the network under different values of RTTs, illustrated in Figure 5.15. As it can be seen, the TD approach results in a step-function behaviour because there are discrete values of the RAR window size and contention resolution timers reported by the BS to the UE (see Equation (4)). In our experiment, we add 16 more values (extra 4 bits) to the already existing ones, covering the NTN delays. In the TA approach we assume a perfect estimation of the TA by the UE, thus updating the RAR window size and contention resolution timer accordingly. Please note that we do not consider any extra time for the GNSS estimate since this process can be done in parallel with obtaining PSS/SSS synchronization. If it is done after, as shown in Figure 5.8, clearly the access time would be impacted. This is something we cannot measure in our experiment.

In a terrestrial-network case, the main delay bottleneck is caused by the processing time at the BS and UE. For LTE, such processing delay is around 4 ms, resulting in an access delay of around 12 ms in ideal channel conditions and without preamble collisions.

In an NTN case, the delay in the communication link becomes a driving factor in deciding the overall time the user needs for acquiring (re-acquiring) access to the serving BS. As it can be observed from Figure 5.15, the access time for a single user can be as high as 970 msec in the worst case scenario of a GEO satellite with transparent payload. Clearly, these

results represent only a lower bound since a single user is utilized for the experiment and represents a case where no collisions occurs. In a scenario where many user will try to access the network simultaneously, the presence of collisions in the RA procedure will naturally lead to a further increase in the user access times. This is something we are not able to measure in the current experimental setup due to hardware limitations. Nevertheless, the obtained results are a big step forward towards NTN systems. Through this work, we are able to demonstrate a successful RA procedure even in extreme values of delays experienced over a GEO satellite and measure the single user access time, which will act as a lower bound for future work in this direction.

5.4 Conclusions

In this chapter, we considered the RA procedure, which is a highly crucial mechanism in several standards, such as LTE, NB-IoT and NR, mainly utilized by the users to obtain uplink synchronization in the network. We analyzed the challenges imposed by the increased delay in an NTN channel into the RA procedure, and came up with novel practical solutions for the challenges identified. To test the proposed solutions, we designed a testbed based on OAI implementation for the 3GPP users and base station, and HW implementation for the NTN channel emulating the signal propagation delay. The laboratory test-bed built in this work enabled us to identify novel challenges not previously treated in the literature, demonstrate a successful RA procedure over NTN, and measure the single-user access times for various values of RTTs. The work shown in this chapter increases the technology readiness level (TRL) of NTN-based cellular systems, demonstrating over a laboratory environment a successful RA procedure even in extreme values of delays experienced in a GEO satellite.

Chapter 6

Conclusions and Future Work

In this chapter, the main conclusions of the thesis are summarized, and the future research directions are emphasized and discussed. The principal objective of this thesis has been the investigation of the challenges induced by the satellite channel impairments into the PHY and MAC layer procedures of the NB-IoT protocol, and the development of new communication algorithms capable of counteracting them. More specifically, the focus of this work has been to propose techniques that require minimal adaptations in the current standard, in order to have a fully functional NB-IoT network, either terrestrial or satellite-based.

In the first part, the data phase of a satellite-based NB-IoT system has been considered, with the assumption of having a successful access phase. The differential Doppler problem impacting the uplink data transmission over a LEO satellite has been identified and a novel user scheduling strategy that mitigates the level of the differential Doppler down to a supported limit has been proposed. The advantage of this approach is that it does not raise the complexity at the user side since the new algorithm has to be performed by the base station. This is particularly favourable for NB-IoT user terminals where the low complexity and the long battery lifetime are of utmost importance. Moreover, a link budget analysis has been performed with the purpose of deriving the space segment requirement from the power perspective with the condition of having the same user terminal specifications as in a terrestrial NB-IoT infrastructure. Last but not least, a novel resource allocation algorithm has been proposed which not only counteracts the differential Doppler problem, but also takes into account the dynamicity of the whole system by incorporating the distinct channel conditions and the various data demands coming from the on-ground users. This was an untreated problem in the literature and the methodology proposed in this thesis can act as a

framework for future works in the area of resource allocation strategies, particularly designed for LEO satellite-based NB-IoT systems.

The second part of the thesis has been devoted to the access phase, which is handled by the RA procedure. The impact of the increased delay over a non-terrestrial channel into the RA procedure has been thoroughly analysed and novel solutions to mitigate the induced challenges has been proposed. To broaden the scope of applicability, the analysis has been done in a general context targeting 4G, 5G and NB-IoT systems since the RA procedure is quasi-identical among these 3GPP technologies. The proposed solutions have been validated through an experimental setup utilising the OpenAir interface for the implementation of the 3GPP user equipment and base station, connected through the satellite channel emulator implemented in hardware. The laboratory test-bed that has been built in this part of the thesis, not only has enabled us to validate various solutions, but also has played a crucial role in identifying the novel challenges not previously treated in the literature. The technology readiness level of satellite-based NB-IoT systems has been increased by this work, demonstrating over a laboratory environment a successful RA procedure even in extreme values of delays experienced in a GEO satellite.

6.1 Future Work

The work carried out in this thesis can be extended in several directions. The main issues left for future work are discussed below:

- **User mobility scenario**: In this thesis, we assume users with a fixed location on Earth and no mobility is foreseen for them. Therefore, the user scheduling and the resource allocation strategies are only possible if the base station has prior knowledge of the user location which is static over time. When the users are free to move in the coverage area of the satellite, new mechanisms are needed to continuously inform the base station regarding the updated location, so as to maintain the functionality of the proposed strategies for the NB-IoT data phase and avoid any extra computation load at the user terminals. In this context, further analysis is required to evaluate the impact of the increased amount of data that has to be exchanged between the users and the base station into the NB-IoT protocol. Not only this, but such information becomes now critical and has a major impact on the resource allocation algorithms where outdated

parameters may compromise their efficiency. This is an important problem to be tackled in future work.

- **Joint design of access and data phase**: Another important assumption in the resource allocation strategy proposed in this thesis was the separation in time of the access and data phases. If this condition is not guaranteed by the NB-IoT protocol specifications and a frequency multiplexing of data and access channels is allowed, our proposed algorithm and its ability to mitigate the differential Doppler problem is directly compromised. Alternatively, a joint design is needed which mitigates the differential Doppler problem in both, access and data phase. One solution would be to utilize a group-based RA approach, similar to the technique we propose for the data phase. However, this requires further investigation and analysis.

- **Multi-user scenario**: The work performed in the second part of the thesis has been base on a single-user scenario trying to access the network. A possible extension of the work is to consider a multi-user scenario and to study the impact that this will have on the user access time. This is highly crucial especially for LEO satellite-based systems where the satellite coverage time is very limited, and the access time should occupy only a small portion of it in order to allow enough time for the data phase.

- **Non orthogonal multiple access techniques**: Maintaining the orthogonality, both in time and frequency, for the NB-IoT communications and all the other 3GPP technologies in general, is a critical precondition that should be satisfied. This becomes even more crucial for the access phase where the data transmission is not controlled by the base station, but is randomly initiated by the on-ground users. Besides, violating the orthogonality in the access phase would result in a higher number of collisions and unsuccessful attempts, thus extending the user access time. In this context, exploring alternative techniques relying on non-orthogonal multiple access schemes is a highly attractive direction for future research.

- **System level design**: Most of the IoT applications are based on periodic updates into the network with a low amount of data to be transmitted. As a result, continuous network coverage might not be needed since the demand coming from the users is mainly driven by the tremendous number of devices, rather than by the single-user demand. An interesting line of future work is to perform a system-level design from the space-segment

perspective (e.g. number of satellites, orbital parameters etc.) based on realistic user distribution on Earth, and realistic user demand for various IoT applications.

Bibliography

[1] Statista, "Internet of Things (IoT) connected devices installed base worldwide from 2015 to 2025," https://www.statista.com/statistics/471264/iot-number-of-connected-devices-worldwide/, [Online; accessed 07-July-2021].

[2] A. Ali, W. Hamouda, and M. Uysal, "Next generation m2m cellular networks: challenges and practical considerations," *IEEE Communications Magazine*, vol. 53, no. 9, pp. 18–24, 2015.

[3] A. Al-Fuqaha, M. Guizani, M. Mohammadi, M. Aledhari, and M. Ayyash, "Internet of things: A survey on enabling technologies, protocols, and applications," *IEEE Communications Surveys Tutorials*, vol. 17, no. 4, pp. 2347–2376, 2015.

[4] M. R. Palattella, M. Dohler, A. Grieco, G. Rizzo, J. Torsner, T. Engel, and L. Ladid, "Internet of things in the 5g era: Enablers, architecture, and business models," *IEEE Journal on Selected Areas in Communications*, vol. 34, no. 3, pp. 510–527, 2016.

[5] Y.-P. E. Wang, X. Lin, A. Adhikary, A. Grovlen, Y. Sui, Y. Blankenship, J. Bergman, and H. S. Razaghi, "A primer on 3gpp narrowband internet of things," *IEEE Communications Magazine*, vol. 55, no. 3, pp. 117–123, 2017.

[6] S. A. Gbadamosi, G. P. Hancke, and A. M. Abu-Mahfouz, "Building upon nb-iot networks: A roadmap towards 5g new radio networks," *IEEE Access*, vol. 8, pp. 188 641–188 672, 2020.

[7] L. Vangelista, A. Zanella, and M. Zorzi, "Long-range iot technologies: The dawn of lora™," in *Future Access Enablers for Ubiquitous and Intelligent Infrastructures*, V. Atanasovski and A. Leon-Garcia, Eds. Cham: Springer International Publishing, 2015, pp. 51–58.

[8] Sigfox, "Technical overview," https://www.huawei.com/en/news/2020/7/3gpp-itu-imt-2020-5g-standard, [Online; accessed 09-July-2021].

[9] K. Mekki, E. Bajic, F. Chaxel, and F. Meyer, "A comparative study of lpwan technologies for large-scale iot deployment," *ICT Express*, vol. 5, no. 1, pp. 1–7, 2019. [Online]. Available: https://www.sciencedirect.com/science/article/pii/S2405959517302953

[10] 3GPP, https://www.3gpp.org/, [Online; accessed 09-July-2021].

[11] M. Kanj, V. Savaux, and M. Le Guen, "A tutorial on nb-iot physical layer design," *IEEE Communications Surveys Tutorials*, vol. 22, no. 4, pp. 2408–2446, 2020.

[12] Huawei, "3gpp 5g formally endorsed as itu imt-2020 5g standard," https://www.huawei.com/en/news/2020/7/3gpp-itu-imt-2020-5g-standard, [Online; accessed 09-July-2021].

[13] G. Barb, M. Otesteanu, F. Alexa, and F. Danuti, "Ofdm multi-numerology for future 5g new radio communication systems," in *2020 International Conference on Software, Telecommunications and Computer Networks (SoftCOM)*, 2020, pp. 1–3.

[14] H. Mroue, A. Nasser, S. Hamrioui, B. Parrein, E. Motta-Cruz, and G. Rouyer, "Mac layer-based evaluation of iot technologies: Lora, sigfox and nb-iot," in *2018 IEEE Middle East and North Africa Communications Conference (MENACOMM)*, 2018, pp. 1–5.

[15] N. Mangalvedhe, R. Ratasuk, and A. Ghosh, "Nb-iot deployment study for low power wide area cellular iot," in *2016 IEEE 27th Annual International Symposium on Personal, Indoor, and Mobile Radio Communications (PIMRC)*, 2016, pp. 1–6.

[16] O. Georgiou and U. Raza, "Low power wide area network analysis: Can lora scale?" *IEEE Wireless Communications Letters*, vol. 6, no. 2, pp. 162–165, 2017.

[17] M. Chiani and A. Elzanaty, "On the lora modulation for iot: Waveform properties and spectral analysis," *IEEE Internet of Things Journal*, vol. 6, no. 5, pp. 8463–8470, 2019.

[18] F. Adelantado, X. Vilajosana, P. Tuset-Peiro, B. Martinez, J. Melia-Segui, and T. Watteyne, "Understanding the limits of lorawan," *IEEE Communications Magazine*, vol. 55, no. 9, pp. 34–40, 2017.

[19] K. A. Daudov, A. M. Patrusova, and V. V. Nadrshin, "Analysis of narrowband data transfer technologies on the internet of things (IoT)," *IOP Conference Series: Materials Science and Engineering*, vol. 1111, no. 1, p. 012016, mar 2021. [Online]. Available: https://doi.org/10.1088/1757-899x/1111/1/012016

[20] Ericson, "Breaking new ground with nb-iot in rural areas," https://www.ericsson.com/en/blog/2020/7/groundbreaking-nb-iot-in-rural-areas, [Online; accessed 10-July-2021].

[21] 3GPP TR 38.913, "5G; Study on scenarios and requirements for next generation access technologies (3GPP TR 38.913 version 16.0.0 Release 16) ," Tech. Rep., July 2020.

[22] O. Kodheli, E. Lagunas, N. Maturo, S. K. Sharma, B. Shankar, J. F. M. Montoya, J. C. M. Duncan, D. Spano, S. Chatzinotas, S. Kisseleff, J. Querol, L. Lei, T. X. Vu, and G. Goussetis, "Satellite communications in the new space era: A survey and future challenges," *IEEE Communications Surveys Tutorials*, vol. 23, no. 1, pp. 70–109, 2021.

[23] S. Cioni, R. De Gaudenzi, O. Del Rio Herrero, and N. Girault, "On the satellite role in the era of 5g massive machine type communications," *IEEE Network*, vol. 32, no. 5, pp. 54–61, 2018.

[24] B. Soret, I. Leyva-Mayorga, S. Cioni, and P. Popovski, "5g satellite networks for internet of things: Offloading and backhauling," *International Journal of Satellite Communications and Networking*, vol. 39, no. 4, pp. 431–444, 2021. [Online]. Available: https://onlinelibrary.wiley.com/doi/abs/10.1002/sat.1394

[25] N. Alagha, "Satellite air interface evolutions in the 5g and iot era," *SIGMETRICS Perform. Eval. Rev.*, vol. 46, no. 3, p. 93–95, Jan. 2019. [Online]. Available: https://doi.org/10.1145/3308897.3308941

[26] 3GPP TR 22.822, "Technical Specification Group Services and System Aspects; Study on using Satellite Access in 5G; Stage 1 (Release 16) ," Tech. Rep., June 2018.

[27] 3GPP TR 38.811, "Technical Specification Group Radio Access Network; Study on New Radio (NR) to support non-terrestrial networks (Release 15) ," Tech. Rep., September 2020.

[28] O. Technology, https://www.oqtec.space/, [Online; accessed 10-July-2021].

[29] ——, "Successful launch of tiger-2 satellite aboard spacex transporter-2 mission," https://www.oqtec.space/news/successful-launch-of-tiger-2-satellite-aboard-spacex-transporter-2-mission, [Online; accessed 10-July-2021].

[30] Sateliot, https://sateliot.space/, [Online; accessed 10-July-2021].

[31] OSateliot, "Sateliot & spanish mod promotes first nanosatellite constellation for secure iot and data exchange," https://sateliot.space/sateliot-spanish-mod-promotes-first-nanosatellite-constellation-for-secure-iot-and-data-exchange-2/, [Online; accessed 10-July-2021].

[32] GateHouse, "5g compliant nb-iot ntn solution," https://gatehouse.com/satcom/satellite-iot-and-m2m-connectivity/5g-satellite-nb-iot/, [Online; accessed 10-July-2021].

[33] Mediatek, https://www.mediatek.com/, [Online; accessed 10-July-2021].

[34] ——, "Mediatek conduct world's first public test of 5g satellite iot data connection with inmarsat," https://corp.mediatek.com/news-events/press-releases/mediatek-conduct-worlds-first-public-test-of-5g-satellite-iot-data-connection-with-inmarsat, [Online; accessed 10-July-2021].

[35] M. Centenaro, C. E. Costa, F. Granelli, C. Sacchi, and L. Vangelista, "A survey on technologies, standards and open challenges in satellite iot," *IEEE Communications Surveys Tutorials*, pp. 1–1, 2021.

[36] S. Scalise, C. P. Niebla, R. De Gaudenzi, O. Del Rio Herrero, D. Finocchiaro, and A. Arcidiacono, "S-mim: a novel radio interface for efficient messaging services over satellite," *IEEE Communications Magazine*, vol. 51, no. 3, pp. 119–125, 2013.

[37] R. De Gaudenzi, O. Del Rio Herrero, G. Gallinaro, S. Cioni, and P.-D. Arapoglou, "Random access schemes for satellite networks, from vsat to m2m: a survey," *International Journal of Satellite Communications and Networking*, vol. 36, no. 1, pp. 66–107, 2018. [Online]. Available: https://onlinelibrary.wiley.com/doi/abs/10.1002/sat.1204

[38] S. Cluzel, M. Dervin, J. Radzik, S. Cazalens, C. Baudoin, and D. Dragomirescu, "Physical layer abstraction for performance evaluation of leo satellite systems for iot using time-frequency aloha scheme," in *2018 IEEE Global Conference on Signal and Information Processing (GlobalSIP)*, 2018, pp. 1076–1080.

[39] M. Krondorf, M. Goblirsch, R. de Gaudenzi, G. Cocco, N. Toptsidis, and G. Acar, "Towards the implementation of advanced random access schemes for satellite iot," *International Journal of Satellite Communications and Networking*, vol. 38, no. 2, pp. 177–199, 2020. [Online]. Available: https://onlinelibrary.wiley.com/doi/abs/10.1002/sat.1331

[40] O. Del Rio Herrero and R. De Gaudenzi, "High efficiency satellite multiple access scheme for machine-to-machine communications," *IEEE Transactions on Aerospace and Electronic Systems*, vol. 48, no. 4, pp. 2961–2989, 2012.

[41] E. Casini, R. De Gaudenzi, and O. Del Rio Herrero, "Contention resolution diversity slotted aloha (crdsa): An enhanced random access schemefor satellite access packet networks," *IEEE Transactions on Wireless Communications*, vol. 6, no. 4, pp. 1408–1419, 2007.

[42] J.-B. Doré and V. Berg, "Turbo-fsk: A 5g nb-iot evolution for leo satellite networks," in *2018 IEEE Global Conference on Signal and Information Processing (GlobalSIP)*, 2018, pp. 1040–1044.

[43] R. Ratasuk, B. Vejlgaard, N. Mangalvedhe, and A. Ghosh, "Nb-iot system for m2m communication," in *2016 IEEE Wireless Communications and Networking Conference Workshops (WCNCW)*, 2016, pp. 428–432.

[44] 3GPP TR 45.820, "Technical Specification Group GSM/EDGE Radio Access Network; Cellular system support for ultra-low complexity and low throughput Internet of Things (CIoT) (Release 13) ," Tech. Rep., November 2015.

[45] 3GPP TS 36.211, "Technical Specification Group Radio Access Network; Evolved Universal Terrestrial Radio Access (E-UTRA); Physical channels and modulation (Release 16) ," Tech. Rep., June 2021.

[46] X. Lin, A. Adhikary, and Y.-P. Eric Wang, "Random access preamble design and detection for 3gpp narrowband iot systems," *IEEE Wireless Communications Letters*, vol. 5, no. 6, pp. 640–643, 2016.

[47] R. Ratasuk, N. Mangalvedhe, Y. Zhang, M. Robert, and J.-P. Koskinen, "Overview of narrowband iot in lte rel-13," in *2016 IEEE Conference on Standards for Communications and Networking (CSCN)*, 2016, pp. 1–7.

[48] Rohde & Schwarz, "Narrowband Internet of Things Measurements," https://scdn.rohde-schwarz.com/ur/pws/dl_downloads/dl_application/application_notes/1ma296/1MA296_2e_NB-IoT_Measurements.pdf, [Online; accessed 07-July-2021].

[49] L. Feltrin, G. Tsoukaneri, M. Condoluci, C. Buratti, T. Mahmoodi, M. Dohler, and R. Verdone, "Narrowband iot: A survey on downlink and uplink perspectives," *IEEE Wireless Communications*, vol. 26, no. 1, pp. 78–86, 2019.

[50] 3GPP TS 36.213, "Technical Specification Group Radio Access Network; Evolved Universal Terrestrial Radio Access (E-UTRA); Physical layer procedures (Release 16) ," Tech. Rep., June 2021.

[51] I. Ali, N. Al-Dhahir, and J. Hershey, "Doppler characterization for leo satellites," *IEEE Transactions on Communications*, vol. 46, no. 3, pp. 309–313, 1998.

[52] O. Kodheli *et al.*, *Chapter 2: Narrowband IoT technologies for smart city applications*. IET, 2021, https://digital-library.theiet.org/content/books/10.1049/pbte090e_ch2(visited 17/07/2021).

[53] ETSI TR 102 443, "Satellite Earth Stations and Systems (SES); Satellite Component of UMTS/IMT-2000; Evaluation of the OFDM as a Satellite Radio Interface ," Tech. Rep., August 2008.

[54] 3GPP TS 38.213, "Technical Specification Group Radio Access Network; NR; Physical layer procedures for control (Release 16) ," Tech. Rep., June 2021.

[55] 3GPP TS 38.821, "Technical Specification Group Radio Access Network; Solutions for NR to support non-terrestrial networks (NTN) (Release 16) ," Tech. Rep., May 2021.

[56] H. Wang, H. Zhao, W. Wu, J. Xiong, D. Ma, and J. Wei, "Deployment algorithms of flying base stations: 5g and beyond with uavs," *IEEE Internet of Things Journal*, vol. 6, no. 6, pp. 10 009–10 027, 2019.

[57] 3GPP TR 36.763, "Technical Specification Group Radio Access Network; Study on Narrow-Band Internet of Things (NB-IoT) / enhanced Machine Type Communication (eMTC) support for Non-Terrestrial Networks (NTN) (Release 17) ," Tech. Rep., April 2021.

[58] B. G. Evans, "The role of satellites in 5g," in *2014 7th Advanced Satellite Multimedia Systems Conference and the 13th Signal Processing for Space Communications Workshop (ASMS/SPSC)*, 2014, pp. 197–202.

[59] K. Liolis, A. Geurtz, R. Sperber, D. Schulz, S. Watts, G. Poziopoulou, B. Evans, N. Wang, O. Vidal, B. Tiomela Jou, M. Fitch, S. Diaz Sendra, P. Sayyad Khodashenas, and N. Chuberre, "Use cases and scenarios of 5g integrated satellite-terrestrial networks for enhanced mobile broadband: The sat5g approach," *International Journal of Satellite Communications and Networking*, vol. 37, no. 2, pp. 91–112, 2019. [Online]. Available: https://onlinelibrary.wiley.com/doi/abs/10.1002/sat.1245

[60] A. Guidotti, A. Vanelli-Coralli, M. Caus, J. Bas, G. Colavolpe, T. Foggi, S. Cioni, A. Modenini, and D. Tarchi, "Satellite-enabled lte systems in leo constellations," in *2017 IEEE International Conference on Communications Workshops (ICC Workshops)*, 2017, pp. 876–881.

[61] A. Guidotti, A. Vanelli-Coralli, M. Conti, S. Andrenacci, S. Chatzinotas, N. Maturo, B. Evans, A. Awoseyila, A. Ugolini, T. Foggi, L. Gaudio, N. Alagha, and S. Cioni, "Architectures and key technical challenges for 5g systems incorporating satellites," *IEEE Transactions on Vehicular Technology*, vol. 68, no. 3, pp. 2624–2639, 2019.

[62] E. Corbel, I. Buret, J.-D. Gayrard, G. E. Corazza, and A. Bolea-Alamanac, "Hybrid satellite amp; terrestrial mobile network for 4g : Candidate architecture and space segment dimensioning," in *2008 4th Advanced Satellite Mobile Systems*, 2008, pp. 162–166.

[63] O. Kodheli, A. Guidotti, and A. Vanelli-Coralli, "Integration of satellites in 5g through leo constellations," in *GLOBECOM 2017 - 2017 IEEE Global Communications Conference*, 2017, pp. 1–6.

[64] X. Lin, S. Rommer, S. Euler, E. A. Yavuz, and R. S. Karlsson, "5G from Space: An Overview of 3GPP Non-Terrestrial Networks," *arXiv*, 2021. [Online]. Available: https://arxiv.org/ftp/arxiv/papers/2103/2103.09156.pdf

[65] O. Liberg, S. E. Löwenmark, S. Euler, B. Hofström, T. Khan, X. Lin, and J. Sedin, "Narrowband Internet of Things for Non-Terrestrial Networks," *IEEE Communications Standards Magazine*, vol. 4, no. 4, pp. 49–55, 2020.

[66] G. Charbit, A. Medles, P. Jose, D. Lin, X. Zhu, and I.-K. Fu, "Satellite and cellular networks integration - a system overview," in *2021 Joint European Conference on Networks and Communications 6G Summit (EuCNC/6G Summit)*, 2021, pp. 118–123.

[67] J. Lin, Z. Hou, Y. Zhou, L. Tian, and J. Shi, "Map estimation based on doppler characterization in broadband and mobile leo satellite communications," in *2016 IEEE 83rd Vehicular Technology Conference (VTC Spring)*, 2016, pp. 1–5.

[68] J. Li, Y. Zhang, Y. Zhang, W. Xiong, Y. Huang, and Z. Wang, "Fast tracking doppler compensation for ofdm-based leo satellite data transmission," in *2016 2nd IEEE International Conference on Computer and Communications (ICCC)*, 2016, pp. 1814–1817.

[69] M. Conti, S. Andrenacci, N. Maturo, S. Chatzinotas, and A. Vanelli-Coralli, "Doppler impact analysis for nb-iot and satellite systems integration," in *ICC 2020 - 2020 IEEE International Conference on Communications (ICC)*, 2020, pp. 1–7.

[70] J.-B. Doré and V. Berg, "Turbo-fsk: A 5g nb-iot evolution for leo satellite networks," in *2018 IEEE Global Conference on Signal and Information Processing (GlobalSIP)*, 2018, pp. 1040–1044.

[71] F. Bastia et al., "LTE Adaptation for Mobile Broadband Satellite Networks," *EURASIP Journal on Wireless Communications and Networking*, November 2009.

[72] G. Araniti, M. Condoluci, and A. Petrolino, "Efficient resource allocation for multicast transmissions in Satellite-LTE networks," in *2013 IEEE Global Communications Conference (GLOBECOM)*, Dec 2013, pp. 3023–3028.

[73] H. Saarnisaari, A. O. Laiyemo, and C. H. M. de Lima, "Random access process analysis of 5g new radio based satellite links," in *2019 IEEE 2nd 5G World Forum (5GWF)*, 2019, pp. 654–658.

[74] A. Guidotti, "Beam Size Design for New Radio Satellite Communications Systems," *IEEE Transactions on Vehicular Technology*, vol. 68, no. 11, pp. 11 379–11 383, 2019.

[75] L. Zhen, T. Sun, G. Lu, K. Yu, and R. Ding, "Preamble design and detection for 5g enabled satellite random access," *IEEE Access*, vol. 8, pp. 49 873–49 884, 2020.

[76] R. Barbau, V. Deslandes, G. Jakllari, J. Tronc, J.-F. Chouteau, and A.-L. Beylot, "Nb-iot over geo satellite: Performance analysis," in *2020 10th Advanced Satellite Multimedia Systems Conference and the 16th Signal Processing for Space Communications Workshop (ASMS/SPSC)*, 2020, pp. 1–8.

[77] I. del Portillo Barrios, B. Cameron, and E. Crawley, "A technical comparison of three low earth orbit satellite constellation systems to provide global broadband," *Acta Astronautica*, vol. 159, 03 2019.

[78] E. Juan, M. Lauridsen, J. Wigard, and P. E. Mogensen, "5g new radio mobility performance in leo-based non-terrestrial networks," in *2020 IEEE Globecom Workshops (GC Wkshps*, 2020, pp. 1–6.

[79] P.-D. Arapoglou, S. Cioni, E. Re, and A. Ginesi, "Direct access to 5g new radio user equipment from ngso satellites in millimeter waves," in *2020 10th Advanced Satellite Multimedia Systems Conference and the 16th Signal Processing for Space Communications Workshop (ASMS/SPSC)*, 2020, pp. 1–8.

[80] O. Kodheli, S. Andrenacci, N. Maturo, S. Chatzinotas, and F. Zimmer, "Resource allocation approach for differential doppler reduction in nb-iot over leo satellite," in *2018 9th Advanced Satellite Multimedia Systems Conference and the 15th Signal Processing for Space Communications Workshop (ASMS/SPSC)*, 2018, pp. 1–8.

[81] ——, "An uplink ue group-based scheduling technique for 5g mmtc systems over leo satellite," *IEEE Access*, vol. 7, pp. 67 413–67 427, 2019.

[82] O. Kodheli, N. Maturo, S. Andrenacci, S. Chatzinotas, and F. Zimmer, "Link budget analysis for satellite-based narrowband iot systems," in *Ad-Hoc, Mobile, and Wireless*

Networks, M. R. Palattella, S. Scanzio, and S. Coleri Ergen, Eds. Cham: Springer International Publishing, 2019, pp. 259–271.

[83] J. Lee and J. Lee, "Prediction-Based Energy Saving Mechanism in 3GPP NB-IoT Networks," *Sensors*, vol. 17, no. 9, 2017. [Online]. Available: https://www.mdpi.com/1424-8220/17/9/2008

[84] H. Malik *et al.*, "Radio Resource Management Scheme in NB-IoT Systems," *IEEE Access*, vol. 6, pp. 15 051–15 064, 2018.

[85] C. Yu *et al.*, "Uplink Scheduling and Link Adaptation for Narrowband Internet of Things Systems," *IEEE Access*, vol. 5, pp. 1724–1734, 2017.

[86] Y. Yu and J. Wang, "Uplink resource allocation for narrowband internet of things (nb-iot) cellular networks," in *2018 Asia-Pacific Signal and Information Processing Association Annual Summit and Conference (APSIPA ASC)*, 2018, pp. 466–471.

[87] A. Azari *et al.*, "On the Latency-Energy Performance of NB-IoT Systems in Providing Wide-Area IoT Connectivity," *IEEE Transactions on Green Communications and Networking*, vol. 4, no. 1, pp. 57–68, 2020.

[88] O. Kodheli, N. Maturo, S. Chatzinotas, S. Andrenacci, and F. Zimmer, "Nb-iot via leo satellites: An efficient resource allocation strategy for uplink data transmission," *IEEE Internet of Things*, 2021.

[89] ——, "On the random access procedure of nb-iot non-terrestrial networks," in *2020 10th Advanced Satellite Multimedia Systems Conference and the 16th Signal Processing for Space Communications Workshop (ASMS/SPSC)*, 2020, pp. 1–8.

[90] O. Kodheli *et al.*, "Random access procedure over non-terrestrial networks: From theory to practice," *IEEE Access*, 2021.

[91] N. Mangalvedhe, R. Ratasuk, and A. Ghosh, "Nb-iot deployment study for low power wide area cellular iot," in *2016 IEEE 27th Annual International Symposium on Personal, Indoor, and Mobile Radio Communications (PIMRC)*, 2016, pp. 1–6.

[92] J. Li, Y. Zhang, Y. Zhang, W. Xiong, Y. Huang, and Z. Wang, "Fast tracking doppler compensation for ofdm-based leo satellite data transmission," in *2016 2nd IEEE International Conference on Computer and Communications (ICCC)*, 2016, pp. 1814–1817.

[93] 3GPP TR 25.913, "Technical Specification Group Radio Access Network; Requirements for Evolved UTRA (E-UTRA) and Evolved UTRAN (E-UTRAN) (Release 9) ," Tech. Rep., December 2009.

[94] 3GPP TR 24.301, "3rd Generation Partnership Project; Technical Specification Group Core Network and Terminals; Non-Access-Stratum (NAS) protocol for Evolved Packet System (EPS); Stage 3 (Release 17)) ," Tech. Rep., June 2021.

[95] A. Hoglund, X. Lin, O. Liberg, A. Behravan, E. A. Yavuz, M. Van Der Zee, Y. Sui, T. Tirronen, A. Ratilainen, and D. Eriksson, "Overview of 3gpp release 14 enhanced nb-iot," *IEEE Network*, vol. 31, no. 6, pp. 16–22, 2017.

[96] 3GPP TR 36.212, "Technical Specification Group Radio Access Network; Evolved Universal Terrestrial Radio Access (E-UTRA); Multiplexing and channel coding (Release 16) ," Tech. Rep., June 2021.

[97] MATLAB NB-IoT modelling toolbox, "Nb-iot npusch block error rate simulation." [Online]. Available: https://nl.mathworks.com/help/lte/examples/nb-iot-npusch-block-error-rate-simulation.html

[98] J. E. Beasley, "An exact two-dimensional non-guillotine cutting tree search procedure," *Operations Research*, vol. 33, no. 1, pp. 49–64, 1985. [Online]. Available: http://www.jstor.org/stable/170866

[99] N. Christofides and E. Hadjiconstantinou, "An exact algorithm for orthogonal 2-d cutting problems using guillotine cuts," *European Journal of Operational Research*, vol. 83, no. 1, pp. 21 – 38, 1995. [Online]. Available: http://www.sciencedirect.com/science/article/pii/0377221793E02775

[100] S. P. Fekete, J. Schepers, and J. C. van der Veen, "An Exact Algorithm for Higher-Dimensional Orthogonal Packing," *Operations Research*, vol. 55, no. 3, pp. 569–587, 2007. [Online]. Available: https://doi.org/10.1287/opre.1060.0369

[101] D. Pisinger, "An exact algorithm for large multiple knapsack problems," *European Journal of Operational Research*, vol. 114, no. 3, pp. 528 – 541, 1999. [Online]. Available: http://www.sciencedirect.com/science/article/pii/S0377221798001209

[102] S. Martello and P. Toth, *Knapsack Problems: Algorithms and Computer Implementations*. USA: John Wiley & Sons, Inc., 1990.

[103] 3GPP TR 38.211, "Technical Specification Group Radio Access Network; NR; Physical channels and modulation (Release 16) ," Tech. Rep., June 2021.

[104] 3GPP TS 36.321, "Technical Specification Group Radio Access Network; Evolved Universal Terrestrial Radio Access (E-UTRA); Medium Access Control (MAC) protocol specification (Release 16) ," Tech. Rep., April 2021.

[105] 3GPP TS 38.321, "Technical Specification Group Radio Access Network; NR; Medium Access Control (MAC) protocol specification (Release 16) ," Tech. Rep., March 2021.

[106] 3GPP TS 36.331, "Technical Specification Group Radio Access Network; Evolved Universal Terrestrial Radio Access (E-UTRA); Radio Resource Control (RRC); Protocol specification (Release 16) ," Tech. Rep., March 2021.

[107] 3GPP TS 38.331, "Technical Specification Group Radio Access Network; NR; Radio Resource Control (RRC) protocol specification (Release 16) ," Tech. Rep., March 2021.

[108] 3GPP TS 38.213, "Technical Specification Group Radio Access Network; NR; Physical layer procedures for control (Release 16) ," Tech. Rep., March 2021.

[109] (OSA) OpenAirInterface Software Alliance, "Openairinterface — 5g software alliance for democratising wireless innovation." [Online]. Available: https://openairinterface.org

[110] F. Kaltenberger, G. d. Souza, R. Knopp, and H. Wang, "The OpenAirInterface 5G New Radio Implementation: Current Status and Roadmap," in *WSA 2019; 23rd International ITG Workshop on Smart Antennas*, 2019, pp. 1–5.